DEVELOPMENT OF AN ANTIRHEUMATIC DRUG

A thesis submitted to the University of Cape Town
in fulfilment of the requirements for the degree of

DOCTOR OF PHILOSOPHY

by

Kuku Vinolia Vuyelwa Voyi B.Sc.(Fort Hare) M.Sc.(U.C.T.)

Department of Inorganic Chemistry
University of Cape Town
Rondebosch
South Africa

March 1988

To my Mom, Boons and Fonko

Lowo woyisayo ndomhlalisa nam

Njengoko Nam ndoyisayo

Ndahlala noBawo

ACKNOWLEDGEMENTS

Sincere thanks are expressed to:

Dr. G.E. Jackson, my supervisor, for his friendship and support throughout this project.

Mr Campbell for his useful comments.

The CSIR and AECI for financial support.

ABSTRACT

The diamino-diamide ligands have been investigated in an attempt to develop an antirheumatic drug.

The ligands N,N'-di-(2-dimethylamino)ethyloxamide and N,N'-di-(2-diethylamino)ethyloxamide were synthesised and characterised using the physical techniques, NMR, mass- and infrared spectrometry.

The stability constants of the complexes of Mg, Ca, Zn and several first transition metal-ions with the ligands were determined potentiometrically. The solution conformation of the CuII complexes were determined using visible spectrophotometry.

Finally the physico-chemical studies were carried out. Firstly by studying the interaction of the copper complex with albumin at the physiological pH 7.4 using visible spectrophotometry. Secondly by determining the superoxide dismutase activity of the ligand by reduction of nitrobluetetrazolium using visible spectrophotometry. Lastly the ligands and the CaII, CuII, MgII and ZnII metal-ions were monitored in vitro using the computer blood plasma model.

GLOSSARY OF SYMBOLS

BSA	bovine serum albumin
β_{pqr}	overall formation constant, p = metal, q = ligand, r = proton
DEO	N,N'-di-(2-diethylamino)ethyloxamide
DMO	N,N'-di-(2-dimethylamino)ethyloxamide
I	ionic strength
I_gG	immunoglobin
I_{50}	50% inhibition of nitrobluetetrazolium reduction
K	stepwise formation constant
m/e	mass divided by charge
$\bar{n}$	formation function for the ligand subsystem
NSAID	non-steroidal antiinflammatory drug
pA	negative logarithm of ligand concentration
pGE_2	prostaglandin E_2
pKa	negative logarithm of acid dissociation constant
$\bar{Q}$	deprotonation constant
RA	rheumatoid arthritis
SAARD	slow acting anti-rheumatic drug
SOD	superoxide dismutase
$\bar{z}$	average number of ligands bound per metal ion
T_H	total hydrogen concentration
T_L	total ligand concentration
T_M	total metal concentration

CONTENTS

CONTENTS(contd)

CONTENTS (contd)

CHAPTER 1
INTRODUCTION

1.1 Rheumatoid arthritis - molecular review

1.1.1 Inflamed tissue analysis

Rheumatoid arthritis (RA) is a disease that afflicts mainly synovial joints. It manifests itself by chronic inflammation, fibrosis and tissue degradation. The nature of the disease is so complex that RA is said to be an autoimmune disease [1, 2]. It has also been postulated that stress (physical, emotional, hormonal, environmental) [3] triggers the inflammatory response resulting in overcorrection due to failure to switch off response when correction is done. However, a number of physiological disorders have been identified and implicated in RA patients.

These are hypohistinaemia [3-5], this implies low concentration levels of the amino acid, histidine in blood plasma, alteration of immunoglobulin (IgG) [1, 6-8] thus forming an antibody which is called the Rheumatoid factor, RF, and the generation of superoxide by synovial fluids, which is higher than normal [8-12]: this is the overcorrection process as discussed later.

Furthermore, in the damaged tissue areas the chondrocytes and phagocytes release hydrolytic lysosomal enzymes [13, 14] that result in the digestion of the cartilage, especially collagen. The pain and joint swelling has been associated

with prostanoids, particularly the PGE_2 (prostaglandin E_2) [15].

T lymphocytes which induce class II antigen cells [16], interleukin I (IL-1) [15] a particular type of monokinase has also been implicated.

The list of metabolites implicated in RA is legion, some of these being chain reaction products of the above mentioned processes.

1.1.2 Copper complexes

Long before the extensive biochemical studies of the affected tissues, copper was already associated with RA. It is noted that copper homeostasis in biofluids is disturbed in RA sufferers, this results in elevated levels of copper [6, 17-22]. However, copper is not present in free ionic state in RA [3, 23].

Copper and its complexes can have a dual nature. The copper amino acid complex of glycine has been found to be an irritant [21] - a response which is observed in copper salts and metallic copper [9, 24]. Fortunately the beneficial effects of copper supercedes the adverse side, more especially that copper does not exist in any significant amount in free ionic state.

Low molecular weight complexes of copper have been found to collectively have the following healing effects in RA treatment. The stabilisation of human gammaglobulin of antimicrobial activity and of lysosomal enzymes is observed. They are also found to have superoxide dismutase activity by controlling the hydroxide and superoxide radical levels in blood plasma. The activity of the metalloenzyme, lysyl oxidase, which is needed for collagen and elastin synthesis is induced by the copper complexes. In the modulation of T lymphocyte responses and of prostaglandin synthesis which regulate the autoimmune response copper complexes have been implicated [129].

Copper is among the essential metals of the body. The concentration of copper in human plasma is reported to be 1μg per cm^3 [20, 25,26]. Most is firmly bound to ceruloplasmin i.e. 93-95%. The remainder is bound to albumin, 4%, which is labile, and also a readily exchangeable low molecular weight fraction bound to amino acids [21]. This fraction is considered to be the immediate transport form of copper [25, 27-31].

The liver, brain, heart and kidney are the organs which contain the highest concentration of copper with the liver accounting for 10% of the total [20, 32, 33]. The liver is found to have an increased requirement of copper in RA [5].

1.2 Treatment

As much as the disease is complex, the approach to the treatment has also proved to be just as complex. In the trial and error process to get to the relevant drug, two classes of drugs have been identified. The non-steroidal antiinflammatory drugs (sometimes called the non-specific antiinflammatory drugs) and the slow acting anti-rheumatoid drugs (sometimes called the specific anti-rheumatoid agents). The mode of action on RA differentiates between these drugs - either by suppressing certain compounds of the inflammatory response or in reducing symptoms and signs associated with inflammation.

The NSAIDs have not been shown to alter the course of the disease [34], although they do induce antiinflammatory activity. Generally they have been found to have the capacity to inhibit cyclooxygenase activity [35]. This results in lowering of PGE_2 concentration in synovial fluid [36, 38]. Therefore the NSAIDs have analgesic activity or are pain killers since PGE_2 is known to be associated with pain (see Section 1.1.1).

Notwithstanding their activity, the NSAIDs have several side effects. These include gastrointestinal toxicity [39], and development of renal toxicity in patients since PGE_2 has an important renal function [40]. Also in patients using

anticoagulants, gastrointestinal bleeding may be caused [41].

Of the SAARDs, the most used and well studied is D-penicillamine [42, 43]. It has been found to be very effective in altering the course of the disease. This could be due to its resemblance to one of the amino acids, cysteine, [34]. Its mode of action is thought to be via its ability to bind firmly to plasma proteins, including albumin, α-globulins and ceruloplasmin via the disulfide linkages [44].

Like all other drugs that are being currently used it has its side effects. Collectively these are optic nuritis, proteinuria, marrow aplasia, rashes, nausea, loss of taste acuity [5, 45, 46] and increase in histidine levels [5].

A combination of drugs is sometimes used and seems effective, particularly in the reduction of side effects. One example of this is D-penicillamine and hydroxychloroquine (an antimalarial) [46]. D-penicillamine increases the levels of histidine while hydroxychloroquine stabilises the level.

The noticeable fact about the above drugs is that, given on their own, they can be toxic over long-term administration. However, copper complexes of both the NSAIDs and the SAARDs

are less toxic or have improved activity than the parent drug on its own [6, 47-52].

There are very few low molecular weight complexes that have been found to be irritants resembling the copper ions [24, 47].

None of the above drugs were designed specifically for RA [3, 15, 34, 53-55]. They were discovered either accidentally or by trial and error. That a drug specific for RA has not been designed to date is understandable when considering the complexity of the disease (see Section 1.1.1).

1.3 Drug design

1.3.1 Requirements

Drug designing per se is a complicated issue. There are quite a number of approaches to the method. No single route can be considered as the best. For instance, biological fluids, being an equilibrium system, the presence of added exogenous ligand or metal ion will result in a new equilibrium distribution [56]. The prerequisite for rational drug designing is the knowledge of the various metabolic reactions in the biofluids [55, 57]. Derived from this will be the ability to distinguish between a physiologically healthy and disease condition at the molecular level [58]. From the molecular structure, the design will be restricted to functional structure [57].

In RA the metabolites have been studied bearing copper ion involvement in mind (see Section 1.1). The metal binding sites on the protein have been identified and well studied [3, 15, 28, 29, 59-61]. Another approach has been the investigation of the mode of action of the present drugs. This was to help the researchers understand the disease better [6, 15, 34, 45].

Armed with the above information, drug design could seem to be long overdue. There are, however, a number of limitations which need to be considered when designing a

drug. First and foremost, drug availability on the inflamed site has to be considered. Pharmacologically a drug is considered to be distributed in two different fractions in blood plasma [62]:

(a) bound to proteins

(b) free form likely to penetrate the tissues

Varied serum binding of the drug to the biofluid species can affect pharmacokinetics and pharmacodynamics of the drug. This can in turn cause different tissue levels of the drug, hence toxicity [60]. The mode of uptake of the drug will also be restricted by cells other than those the drug's action is intended for [59].

The free form of the drug will have its activity governed by its electrical neutrality. For diffusion into tissues, the drug has to be electrically neutral [56, 62, 63]. Stability and solubility of the drug in the different media of the body, at different pHs, is also essential. In acidic medium, the stomach, some insoluble compounds can be dissolved [47] possibly resulting in alteration of the basic structure or active core. Therefore gastrointestinal absorption is considered first in bioavailability of a drug [64]. Metalloactive drugs have to be specific for that particular ion. It has been found that drugs may interact

with trace elements [62, 65] thus disturbing the metal ion homeostasis in biofluids.

1.3.2 Drug modification

Drug modification has been proved beneficiary in agents that have been found to be active but suffer the above mentioned disadvantages.

Synthetic polymers as drug carriers have been synthesised and investigated [59]. The synthesised oligopeptide linkages should be resistant to degradation on transportation to the cell. This will enable the polymer drug complex to remain intact and stable during its journey in the plasma. This approach is with the assumption that the drug core is the active form required to treat the disease.

Sometimes it can be difficult to design a metabolism-safe drug that is likely to keep its pharmacological activity. Two methods of modifying the drug have been investigated - the analogue and the prodrug approach [57]. The analogue approach has been found to suffer from major structure change in the drug, that often has negative effects on the pharmacological behaviour of the compound. Bioreversible derivatives of known pharmacologically active compounds are

produced in the prodrug approach. The latter approach gives rise to three possibilities:

1) prodrugs aiming at enhanced absorption and bioavailability

2) prodrugs aiming at prolonged duration of effect of the parent compound

3) site specific prodrugs which will preferentially convert to active drug via the action of unique enzymes present in the target organ or tissue

Metal chelates of the parent compound can be made which are not susceptible to enzyme degradation [66]. By this, bioavailability of the active ingredient is increased as compared to that of the compound alone.

The multiple interrelated cellular and molecular process of RA is borne in mind. It would seem that any drug which interrupts a sequence in the self-perpetuating inflammatory process may be beneficial.

1.4 Proposed research

Based on the above evidence, it is therefore sensible to design a drug that is copper chelating. Jackson et al.[58] have schematically summarised the approach that the copper chelator can take. The present research bears this in mind in the design of a drug.

It is well and good to design the structure of the active compound, but it will have to be tested for its pharmacological activities with respect to biofluids. The low molecular weight fraction of metal ion complexes cannot be monitored in vivo by instrumental techniques. This is due to the concentrations which are several orders of magnitude below those identifiable by research equipment. For this reason a computer model of blood plasma has been developed [26]. This model has been used widely and upgrading occurs at regular intervals in accordance with more information about biofluids being obtained. A series of computer programmes can be used to study and give structure of target protein, also to determine stability constants of the designed ligand-metal complex and model the ligand-metal complex behaviour in blood plasma.

The results from the latter can be integrated to predict the efficacy of metal binding in plasma. This takes into account changes in the ligand concentration with time. If

the drug's pharmacological tests are promising, the results from integration can help in deciding the delay in treatments for animal screening.

In this research the study of structure of the target proteins will not be undertaken. Literature search provided for this first step (Section 1.1). It is partly from the data above that the following structure has been based:

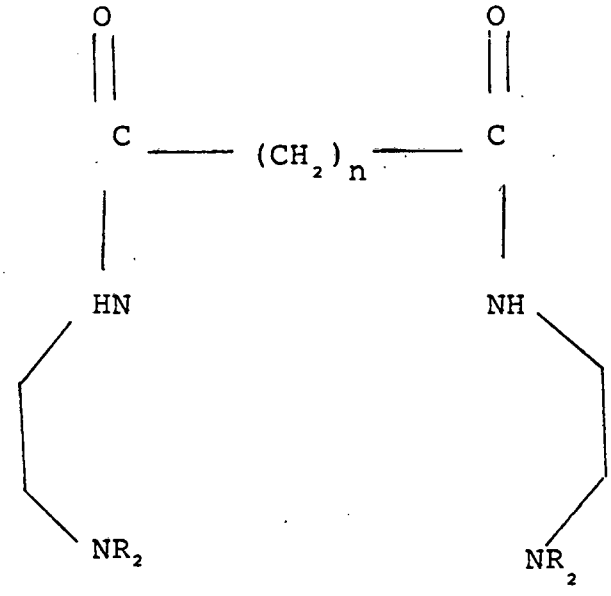

where n is 0

R is either $-CH_3$ or $-CH_2-CH_3$.

The aim of the research is to:

- synthesise the series of the ligands

CHAPTER 2

DIAMINO-DIAMIDE LIGANDS

2.1 Introduction

N,N'-di-(2-dimethylamino) ethyloxamide (DMO) and N,N'-di-(2-diethylamino) ethyloxamide (DEO) fall into the diamino-diamide ligands category.

There is a wide variety of these ligands which have been studied from linear to macrocyclic structures [68-78]. These ligands have been found to resemble peptide chains which are associated with copper binding in the body.

In all the studies carried out, it has been found that the amide protons are displaced by the metal ion, this is a unique situation. These protons are not easily removed since the charge is depicted as:

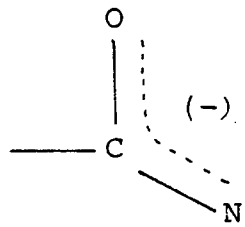

thus making it difficult to remove the proton that balances the charge.

Previous studies with regard to RA have shown that a ligand which is more likely to mobilise copper [84] and also show superoxide dismutase (SOD) activity [86] should have the structure:

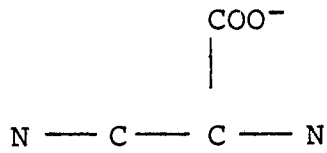

Structures which are based on this core have been studied [84, 85].

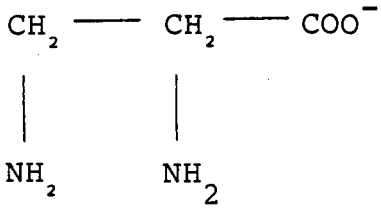

I

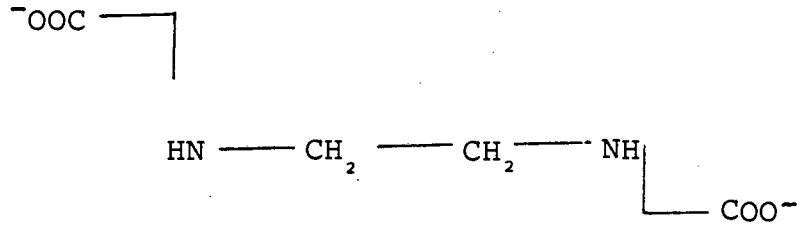

II

I 2,3 diaminopropionate (DPA) and II ethylene-diamine diacetic acid (EDDA). They have been found to form neutral complexes and also mobilise protein-bound copper. However, DPA does not possess sufficient structural advantage over naturally occurring ligands to make it a better copper chelator. EDDA is non-specific, zinc and calcium have been found to compete with copper and effective copper complexation is lost in blood plasma. [84]

Other variations of the core structure above have been studied generally [77]. These also do not exhibit any specificity.

The diamino-diamides were studied with respect to their ability to bind divalent metal ions especially the first transition elements.

Trien which has been widely studied as well as in Wilson's disease [79, 80] for its copper binding served as the core structure of the present research. This choice is based on the findings that the amino groups are the stabilising factor in the metal complexes formed with diamino-diamides [70]. It was apparent therefore that in order for the ligand to be selective towards copper, the amide should have all four nitrogens available for binding.

The choice of the site of the amide carbonyl group (-c=0) came about by studying work done previously [68, 76, 81]. Liu and Chung in their study showed that addition of a polar group -OH in their case improved reactivity. The addition of an alkyl group reduced reactivity. Kodoma and Kimura have studied other similar ligands with respect to cation selectivity of macrocyclic tetramines as found in macrocyclic hexaethers. They found that stability of the copper complexes increased with amide macrocycle and reached maximum stability with a 5,6,5,6 ring cluster.

A characteristic of the diamino-diamides is that they form a cluster of rings with the metal ion in the centre. The

effect of the ring size has also been studied [79-83]. The general agreement is that the five-six-five structure:

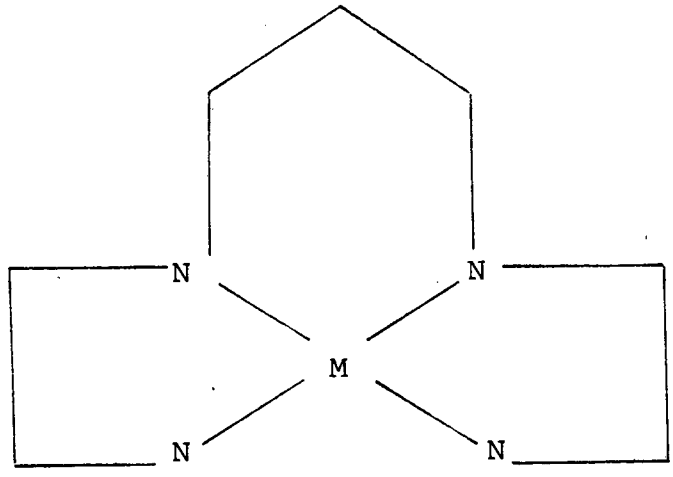

is the most reactive and most stable. Moreover with regard to copper complexes the macrocycle:

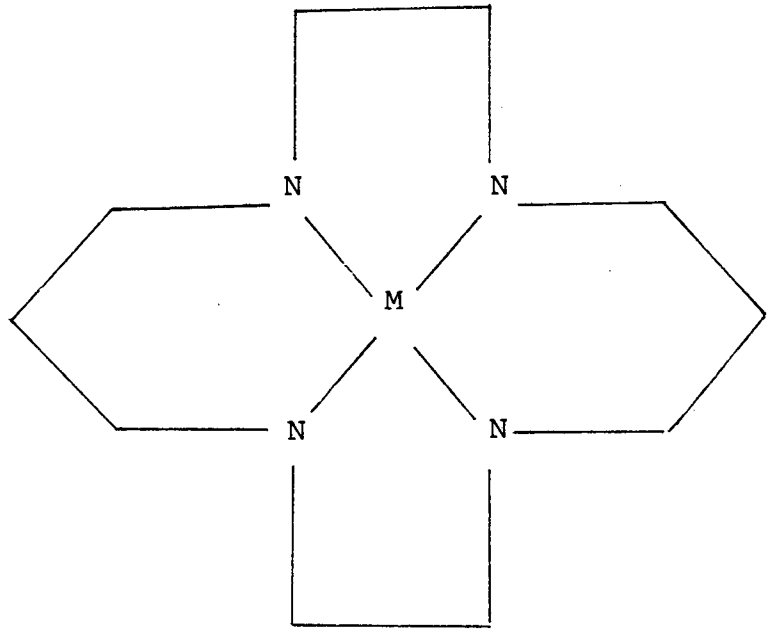

has been found to have a higher formation constant for the neutral species $CuH_{-2}L$ [68]. However, copper has a small

ionic radius, same as nickel [87] and therefore the five-five-five structure:

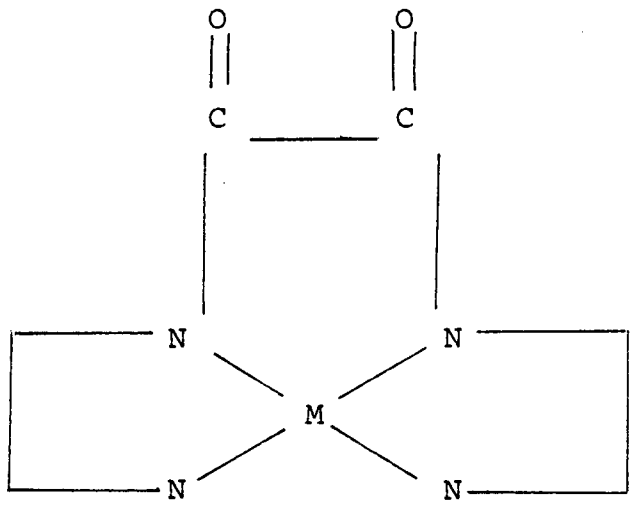

would be an appropriate choice. This structure looks somehow strained but it has been suggested that the cis conformation is most stable [82] with no distortion in the bond angles. A similar structure has been found for nickel [76].

Armed with the above information the ligands chosen were:

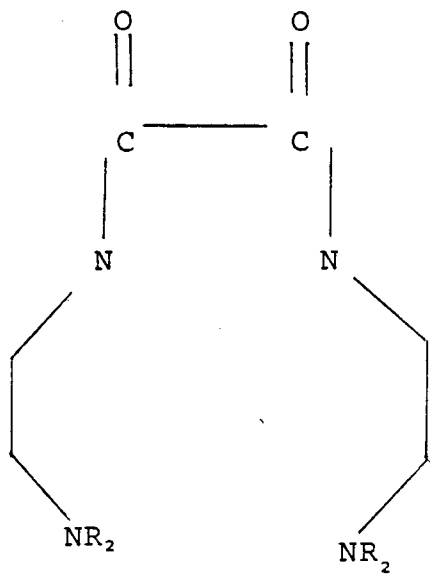

with R an alkyl group CH_3 or CH_2-CH_3. The alkyl groups replacing the hydrogens in the previously mentioned ligands should provide rigidity to the structure thus mimicking the macrocycles.

The alkyl groups were also a result of a comparison with the macrocycle [68] which showed improvement on the complexation.

Rigidity of the structure would also limit the ring opening effect thus allowing only smaller ions inside the cage. The alkyl groups have to be small to avoid bulkiness and hence crowding which would limit the transfer of copper ion to the relevant tissue in vivo.

2.2 Synthesis of DEO and DMO

2.2.1 Preparation of compounds

The reagents used were all from Aldrich chemicals and were used without further purification. The solvents used were tetrahydrofuran (THF) dried over sodium wire and absolute ethanol (EtOH) dried over molecular sieve.

Method

The reaction was carried out under dry nitrogen and in an ice bath to slow down the reaction.

Into a dry two necked round bottom flask the required mole equivalent of the amine was poured. About 20cm^3 THF was added. The required mole equivalent of the oxalyl chloride in THF was added slowly while stirring. A white precipitate formed immediately. The reaction was allowed to complete.

The mixture was filtered and the precipitate washed with THF. The latter was allowed to dry at room temperature, further recrystallised from hot ethanol and then stored in a desiccator over silica gel. The product was the hydrochloride form of the ligands. The percentage yield was 80% for DEO and 82% for DMO.

2.2.2 Analysis of ligands

For microanalysis, the Heraueus CHN-rapid analyser was used while the Reichert Thermovar was used to determine the melting point.

TABLE 1

microanalysis	calculated			found		
	% C	H	N	C	H	N
(a) DMO $C_{10}H_{24}N_4O_2Cl_2$	39.61	7.97	18.48	39.2	7.4	18.35
(b) DEO $C_{14}H_{32}N_4O_2Cl_2$	46.79	8.97	15.59	46.8	8.9	15.60

melting point: DMO 264°C

DEO 244-246°C

2.3 Spectroscopy

2.3.1 Nuclear magnetic resonance (NMR)

The Varian VXR 200 Spectrometer was used to obtain the spectra of DMO and DEO, shown in Figures 1 and 2 respectively. Table 2 represents the identified peaks. The solvent used in NMR studies was D_2O.

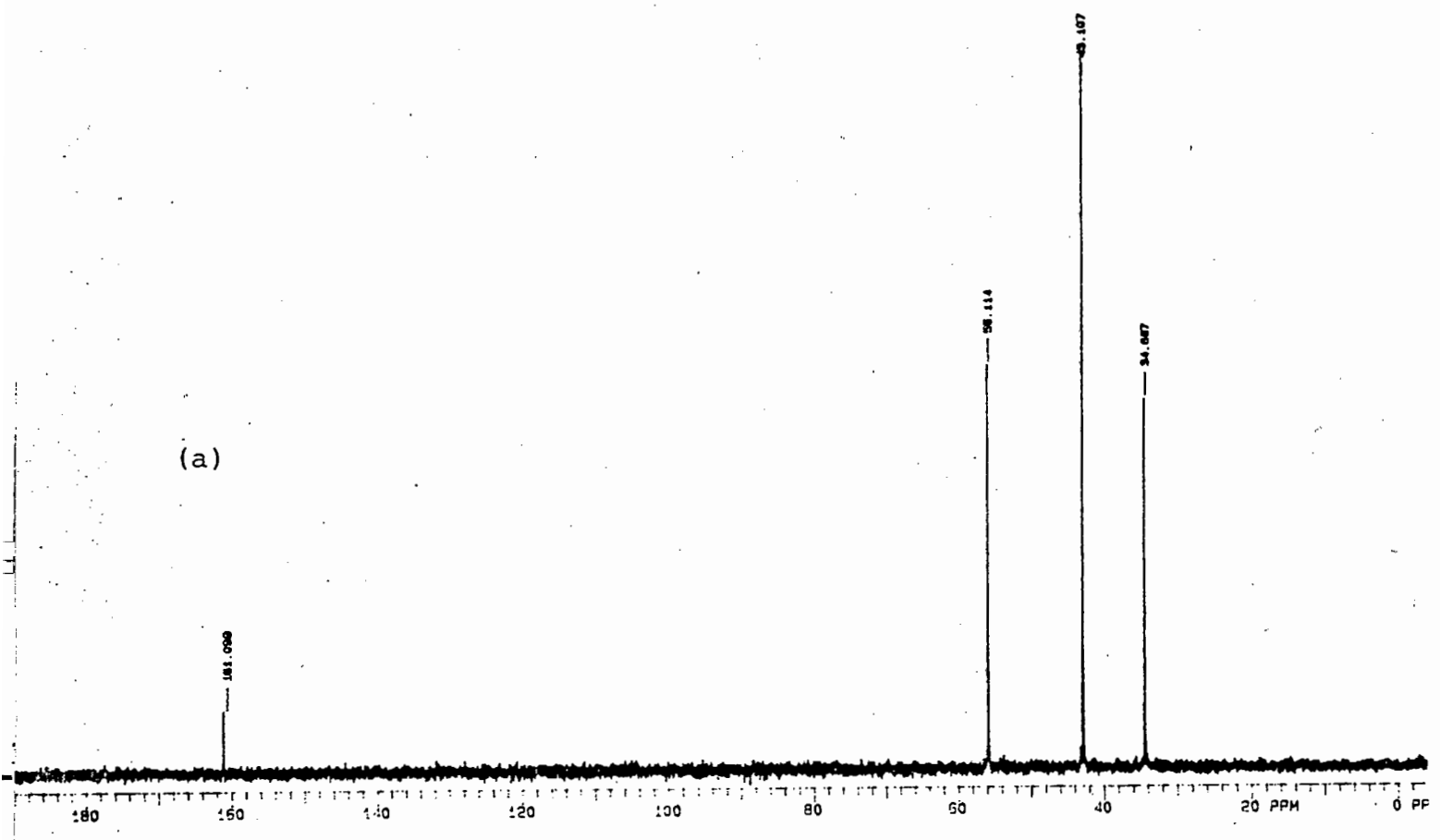

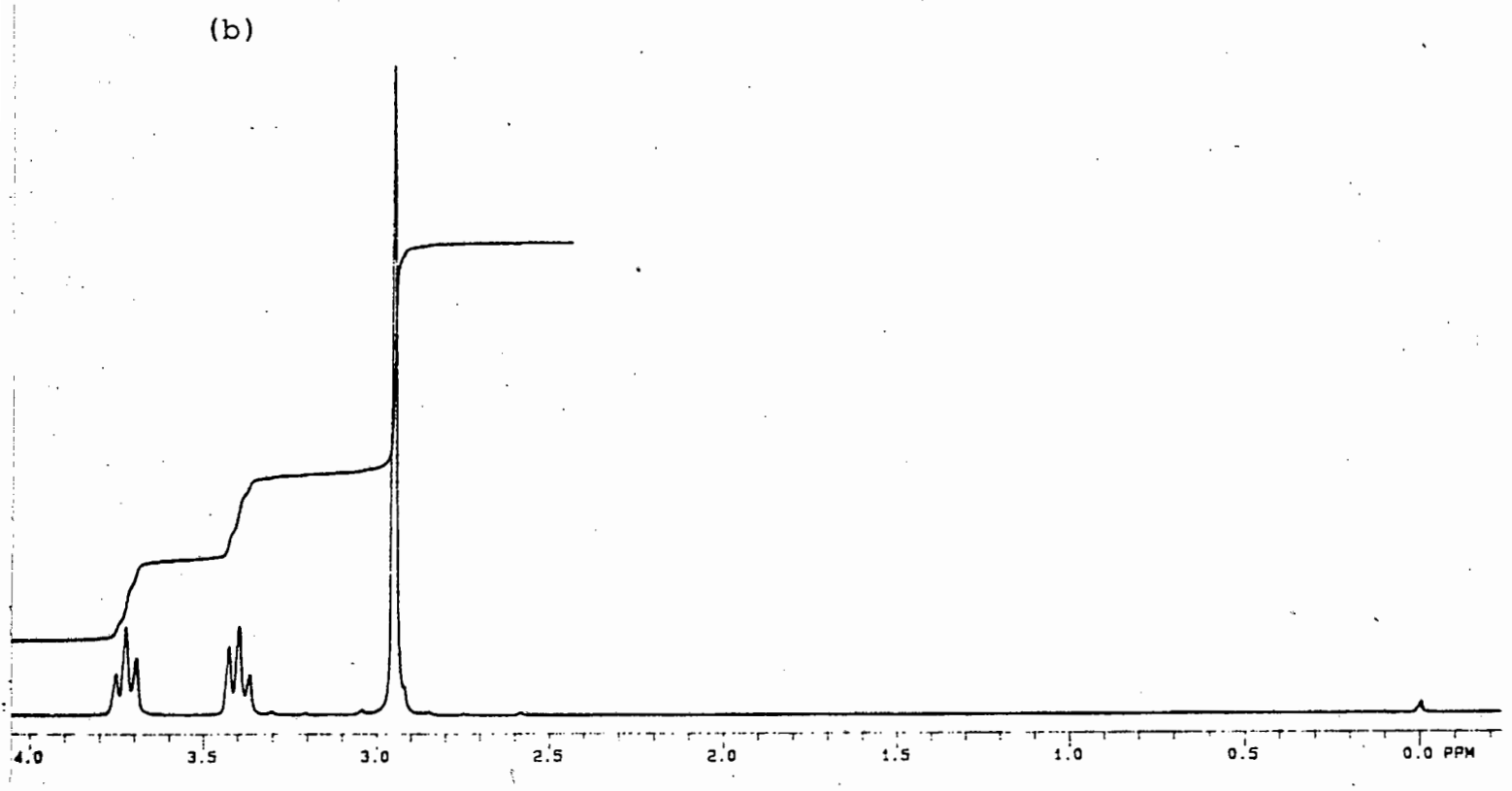

FIGURE 1 : (a) ^{13}C and (b) ^{1}H nuclear magnetic resonance spectra of DMO

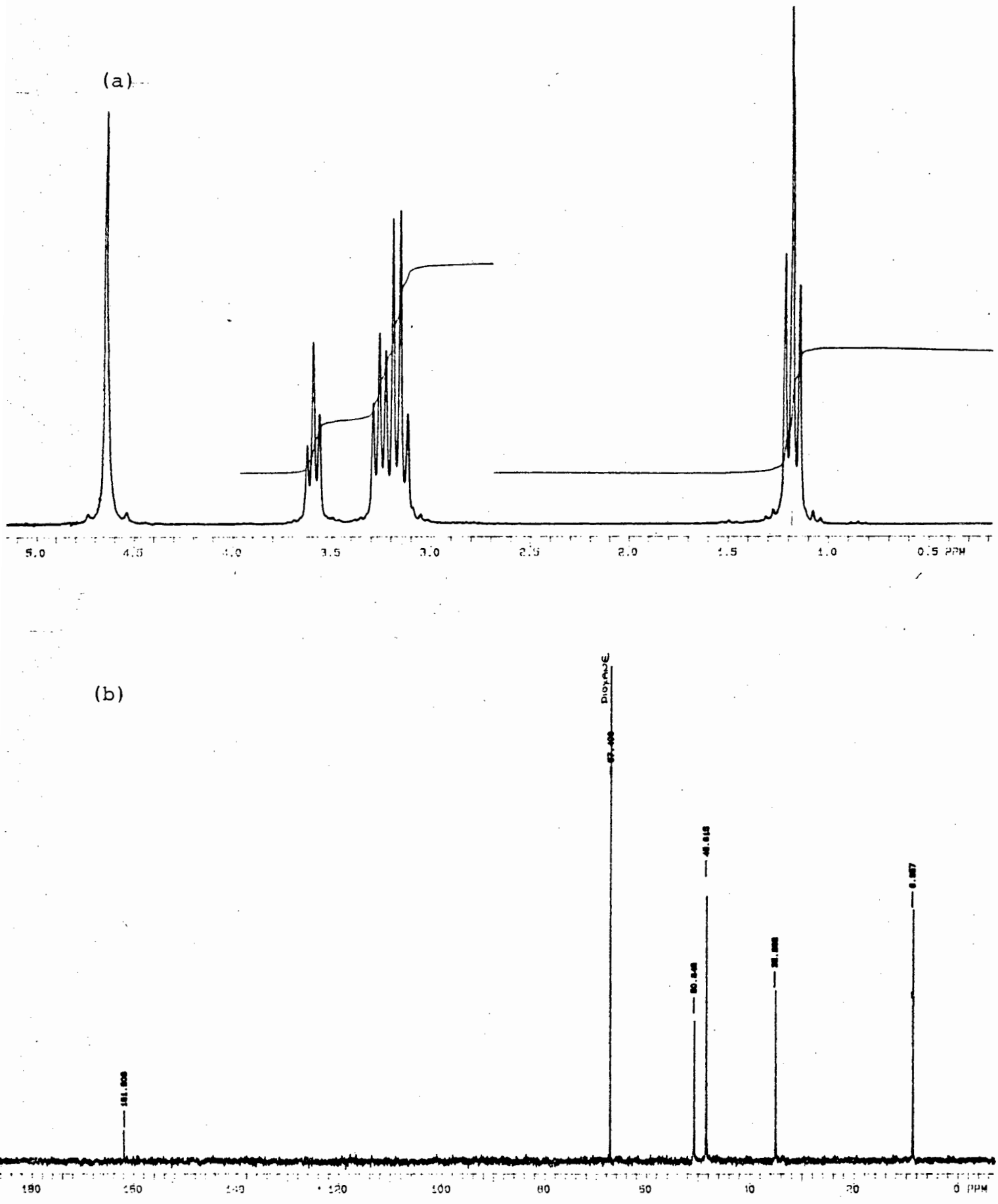

FIGURE 2 : (a) ^{1}H and (b) ^{13}C nuclear magnetic resonance spectra of DEO

TABLE 2

ligand	nucleus	δ(ppm)	rel integration(cm)	type peak	assignt	no of protons
DMO	^{1}H	2.95	6	s	$N(CH_3)_2$	12
		3.4	2	t	$H_2C-N(CH_3)_2$	4
		3.72	2	t	$O=C-N-CH_2$	4
	^{13}C	34.69	-	s	$N(CH_3)_2$	-
		43.11	-	s	$CH_2-N<$	
		56.11	-	s	$-HN-CH_2$	
		161.09	-	s	$O=C-N$	
DEO	^{1}H	1.2		t	$N(CH_3)_2$	12
		3.18		q	$N(CH_2-)_2$	8
		3.26		t	CH_2-N	4
		3.6		t	$OCN-CH_2$	4
	^{13}C	8.96		s	$N(CH_3)_2$	
		35.27			$N(CH_2-)_2$	
		48.62			CH_2-N	
		50.85			$N-CH_2$	
		161.91			$O=C-N$	

s = singlet, t = triplet, Q = quartet

^{1}H NMR relative to DSS

^{13}C NMR dioxane as internal standard

2.3.2 Mass spectrometry

The VG Micromass 16F mass spectrometer in tandem with Carlo Erba gas chromatograph was used to analyse DMO and DEO.

The fragmentation pattern for DMO can be represented in the following scheme, with initial loss of 2HCl, m/e = 230

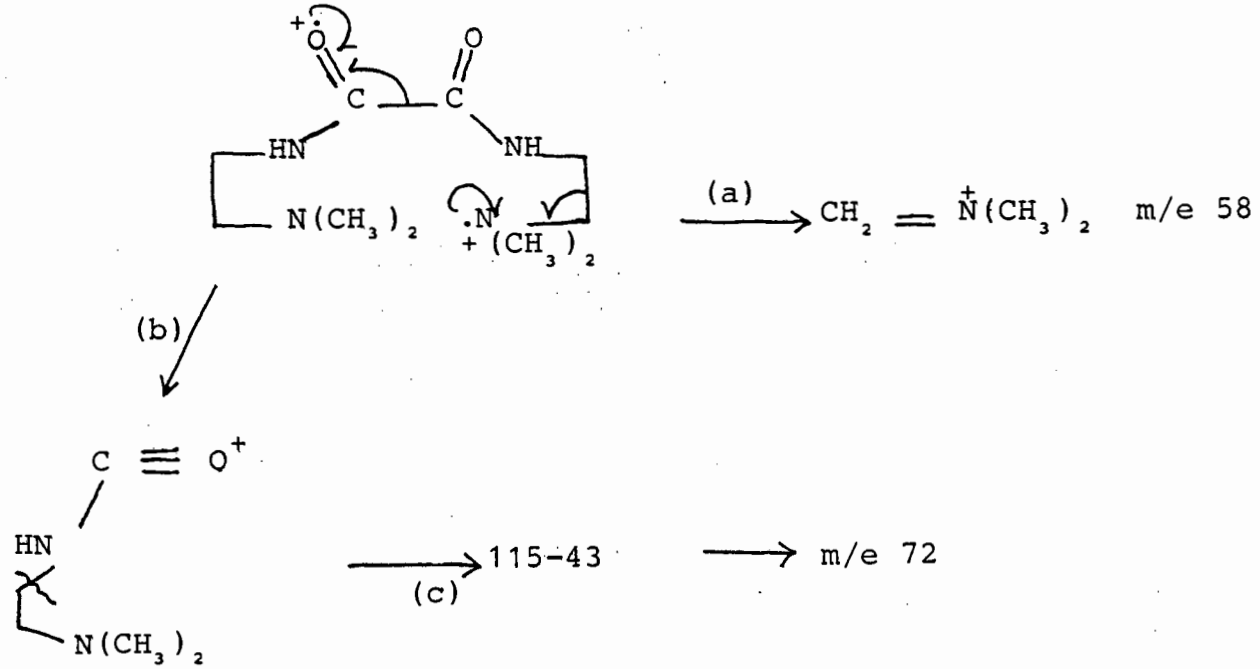

For DEO, after initial loss of 2HCl : m/e 286

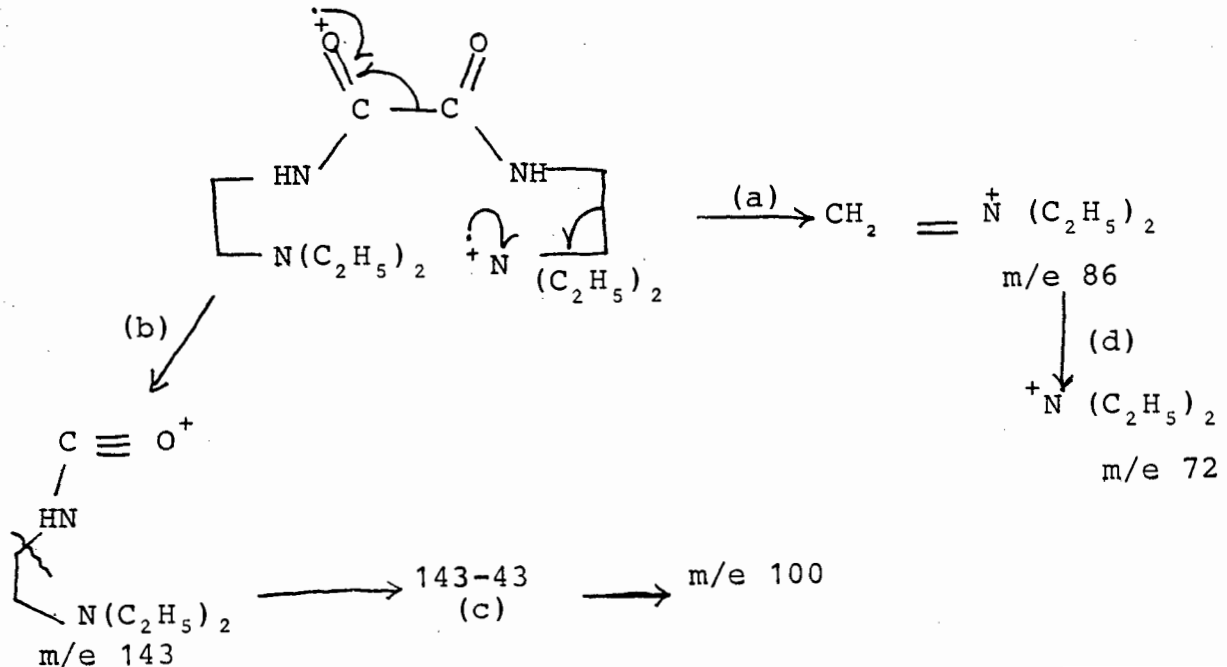

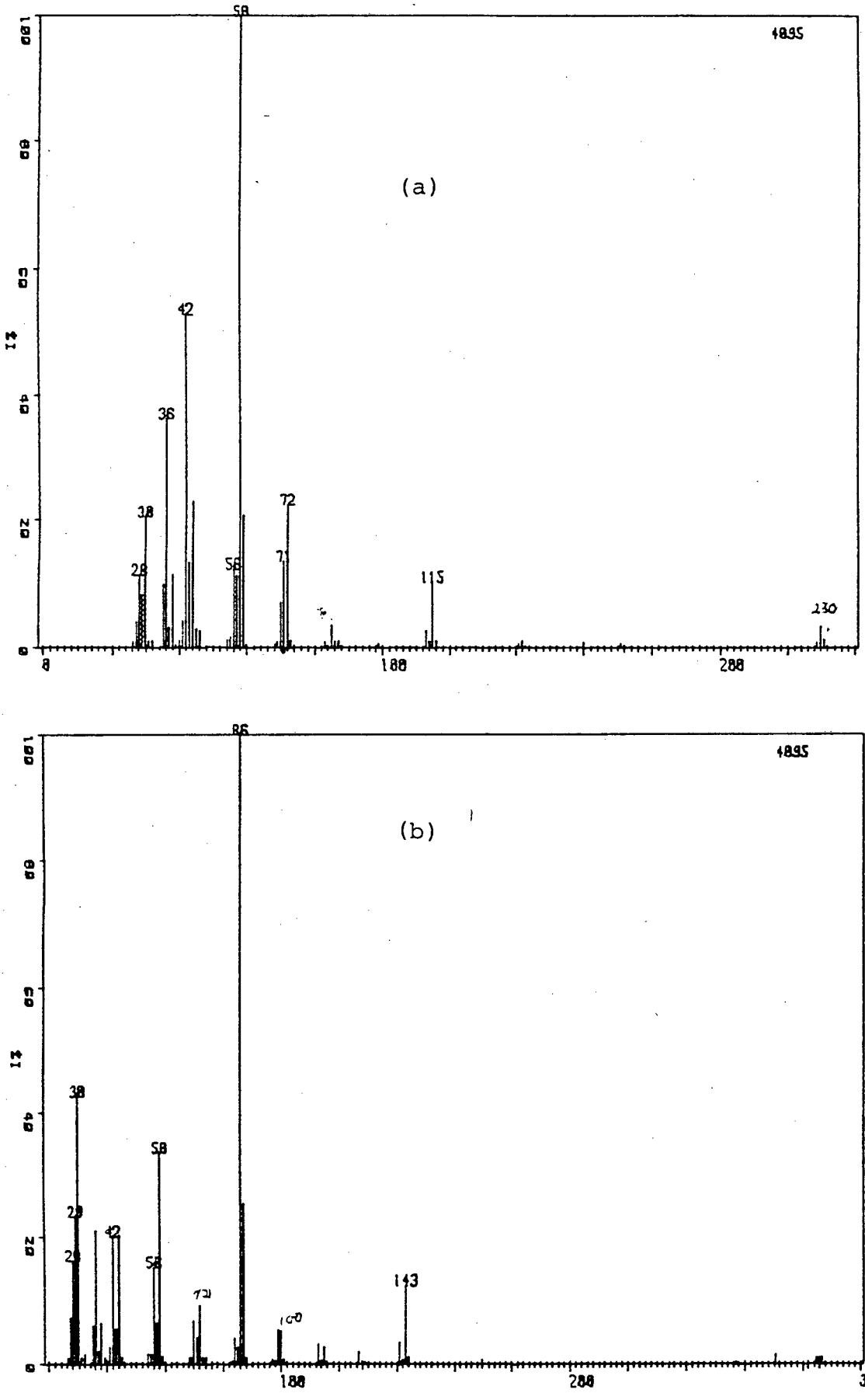

FIGURE 3 : Mass spectra of (a) DMO and (b) DEO

These ligands behave in a peculiar manner. As can be seen from the mass spectra and in the proposed fragmentation pattern in Scheme 1, they behave as amines. Peaks of highest intensity are those of pathway (a) in both cases. The confirmation of the hydrochloride is observed in peak m/e 36 for HCl which is in the expected isotope ratio.

2.3.3 Infrared spectroscopy

The Perkin Elmer 983 Infrared spectrophotometer was used for the characterisation of DMO and DEO. The samples were analysed as Nujol mulls.

The infrared spectra of DMO and DEO are shown in figures 4(a) and (b) respectively.

As these ligands have both characteristics of amides and amines they should present some interesting study.

Properties that are known to be characteristic of amides are the following, they have amide I band due to C=O and amide II band due to NH. The amide I band has its position being determined by the degree of H-bonding and the physical state of the compound. Also multiple bands are observed in the

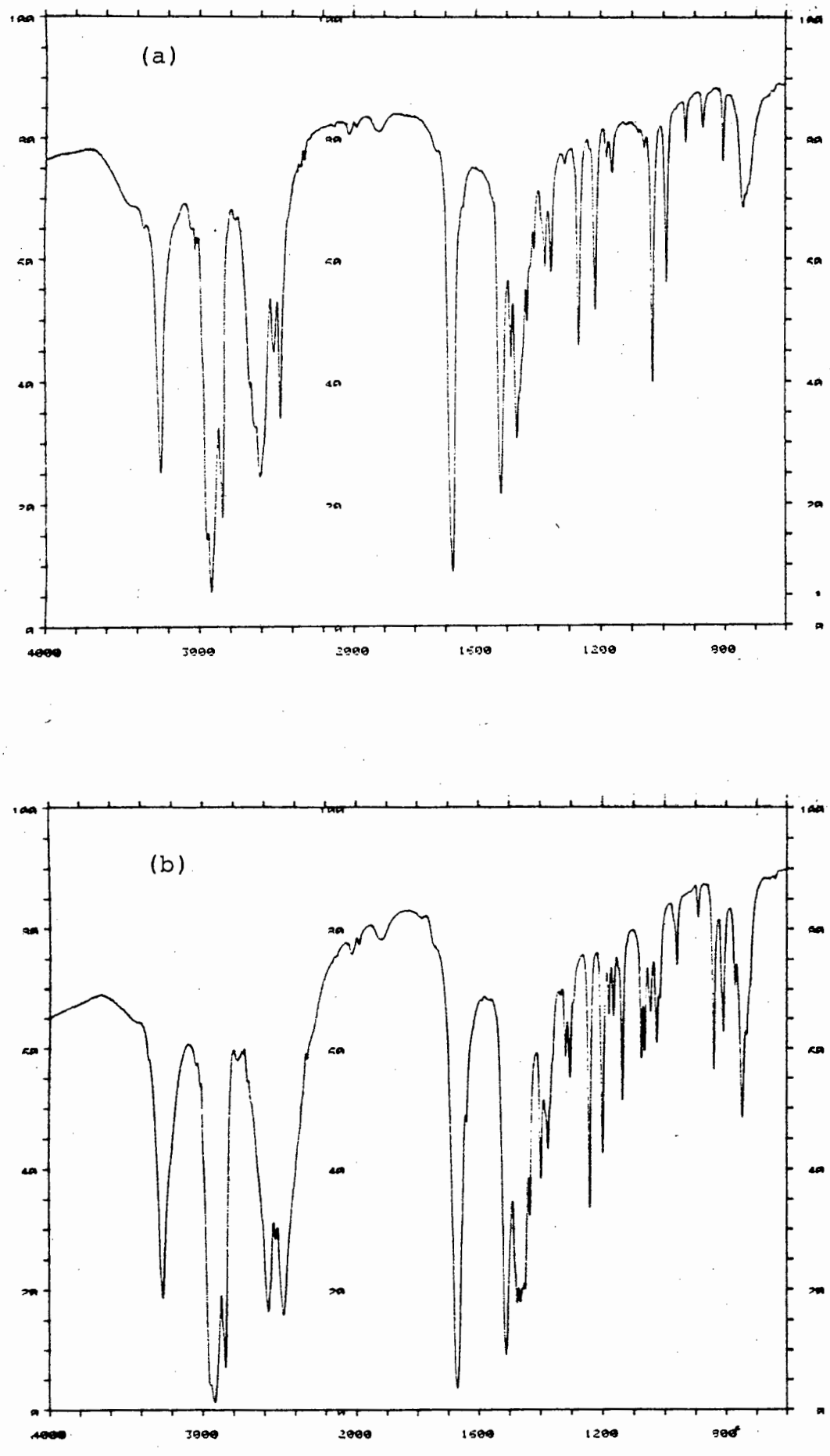

FIGURE 4 : Infrared spectra of (a) DMO and (b) DEO

spectra since amide groups can bond to produce dimers [88] the

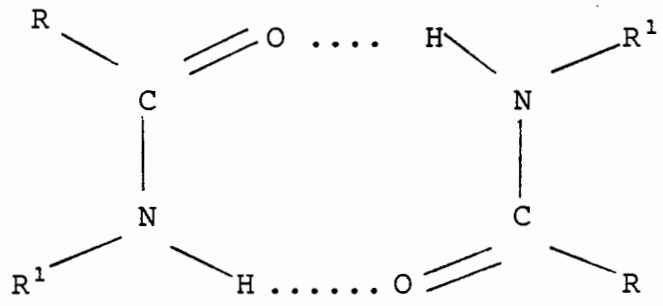

cis

and

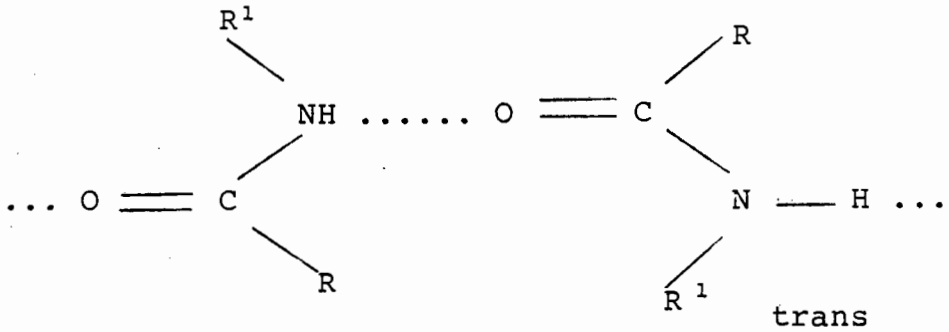

trans

conformations

- the C=O absorption of amides occurs at longer wavelengths than "normal" carbonyl absorption due to the resonance effect

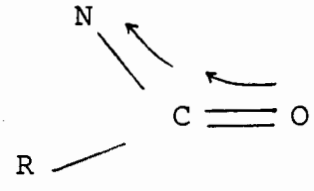

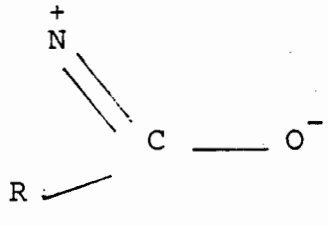

In characterising the spectra only bands due to either the amide or amine groups will be reported as the fingerprint of the ligands.

Figure 4 shows the infrared spectra of (a) DMO and (b) DEO.

TABLE 3

Frequency cm^{-1}		Assignment
DEO	DMO	
3257	3251	NH and CH stretch in amide
2576-2477	2612-2476	tertiary amine salt absorption band
1671	1676	amide I band due to C=O
1512	1518	NH amide II band
1434	1433	CN stretch of amide
1200-1045	1215-1033	CN stretch of amines
809-747	806-742	out of plane NH wagging

CHAPTER 3
POTENTIOMETRY

3.1 Introduction

In principle, as the basis for determining stability constants, any property which varies with the degree of complex formation can be used. However, quantitative relationship between the property and nature of the species present is essential. Broadly the experimental methods for determining stability constants fall into two categories. These are the spectroscopic and electrochemical methods where the observable property is proportional to the number of molecules and activity respectively.

Potentiometry has been, and still is, the most popular method for the determination of formation constants. This is due to its high accuracy and precision [90]. With the advent of sophisticated computer programs [91-93] the precision of data interpretation has been improved considerably.

The glass electrode has a wide applicability and is dependent on the hydrogen ion activity. However, below pH 2 and above pH 12 this is no longer applicable. In these regions ion concentration is predominant and recalibration of the electrode is necessary to maintain linearity of the Nernst equation.

$$E = E^{\circ} + \frac{RT}{zF} \ln \frac{\{M^{(m-z)+}\}}{\{m^{z+}\}}$$

3.2 Theory

Consider a metal M, and ligand L, in solution. The activity of the complex formed is related to the activities of the reactants M and L thus:

$$\frac{\{ML\}}{K'} = \{M\}\{L\} \qquad \ldots \quad (i)$$

where K' is the thermodynamic stability constant

However, in practice mal analytical techniques yield concentrations rather than activities. In turn, activities are related to concentration by:

$$K' = \frac{\{ML\}}{\{M\}\{L\}} = \frac{[ML]}{[M][L]} \cdot \frac{\gamma_{ML}}{\gamma_M \gamma_L} \qquad \ldots \quad (ii)$$

where γ is the activity coefficient of the species.

The experimental determination of activity coefficients is very difficult. This problem is overcome by working at constant ionic strength. Under these conditions $\gamma_{ML}/\gamma_M \gamma_L$ is a constant and the equation reduces to $K = [M]/[M][L]$ where K is the stoichiometric stability constant.

The stepwise formation of a complex can be described by a set of stability constants:

$$M + L \rightleftharpoons ML \qquad K_1 = \frac{[ML]}{[M][L]} \qquad \ldots \quad (iii)$$

$$ML_{n-1} + L \rightleftharpoons ML_n \qquad K_n = \frac{[ML_n]}{[ML_{n-1}][L]} \qquad \ldots \quad (iv)$$

where $K_1 \ldots K_n$ are stepwise stability constants.

The above stability constants can be represented by the overall stability constants, β , where:

$$\beta_1 = K_1 = \frac{[ML]}{[M][L]} \qquad \ldots \quad (v)$$

$$\beta_n = K_1 K_2 \ldots K_n = \frac{[ML_n]}{[M][L]^n} \qquad \ldots \quad (vi)$$

generally written as:

$$\beta_n = \prod_{i=1}^{n} K_i \qquad \ldots \quad (vii)$$

The possibility of formation of protonated, hydroxo or oligonuclear complexes can be taken into account by subscripts, for example $M_pL_qH_r$, hence:

$$\beta_{pqr} = \frac{[M_pL_qH_r]}{[M]^p[L]^q[H]^r} \qquad \ldots \quad (viii)$$

There are a number of secondary functions that are used in the determination of stability constants. The ones used in this study are the $\bar{Z}$ functions [93], which can take the form:

$$\bar{Z}_H = \frac{T_H - H + OH}{T_{Lig}} \qquad \ldots \quad (ix)$$

for ligand protonation studies and:

$$\bar{Z}_M = \frac{T_L - A\left(1 + \Sigma_n \beta_{LH_n} H^n\right)}{T_M} \qquad \ldots \quad (x)$$

for metal complexation studies. A plot of $\bar{Z}_H$ against pH and $\bar{Z}_M$ against pA is used to evaluate the experimental and calculated functions from E_K^{obs} and E_K^{calc} respectively. Another function is $\bar{Q}$, the deprotonation function. It is only defined for the binary (MLH) and ternary (MLXH) systems:

$$\bar{Q} = \frac{\left(T_{H*} - T_H\right)}{T_M} \qquad \ldots \quad (xi)$$

where T_{H*} is calculated total concentration of protons in the system at the experimental pH ignoring the presence of all metal complexes. In the plot of $\bar{Q}$ against pH the formation function for the ligand subsystem $\bar{n}$, is plotted as a solid line (see Figure 1).

$$\bar{n} = \frac{\left(T_{H^*} - H + OH\right)}{T_L} \qquad \ldots \quad (xii)$$

$\bar{Q}$ is the average number of protons, per metal-ion, displaced by complexation, while $\bar{n}$ is the average number of protons bound to the ligand in the absence of any metal-ion. For example, if $\bar{Z} \doteq 1$, $\bar{Q} \doteq 2$ and $\bar{n} = 1$. This implies the presence of the species MLH_{-1}. On the other hand, if $\bar{Z} = 2$ with still $\bar{Q} = 2$ and $\bar{n} = 1$, then the species ML_2 is indicated.

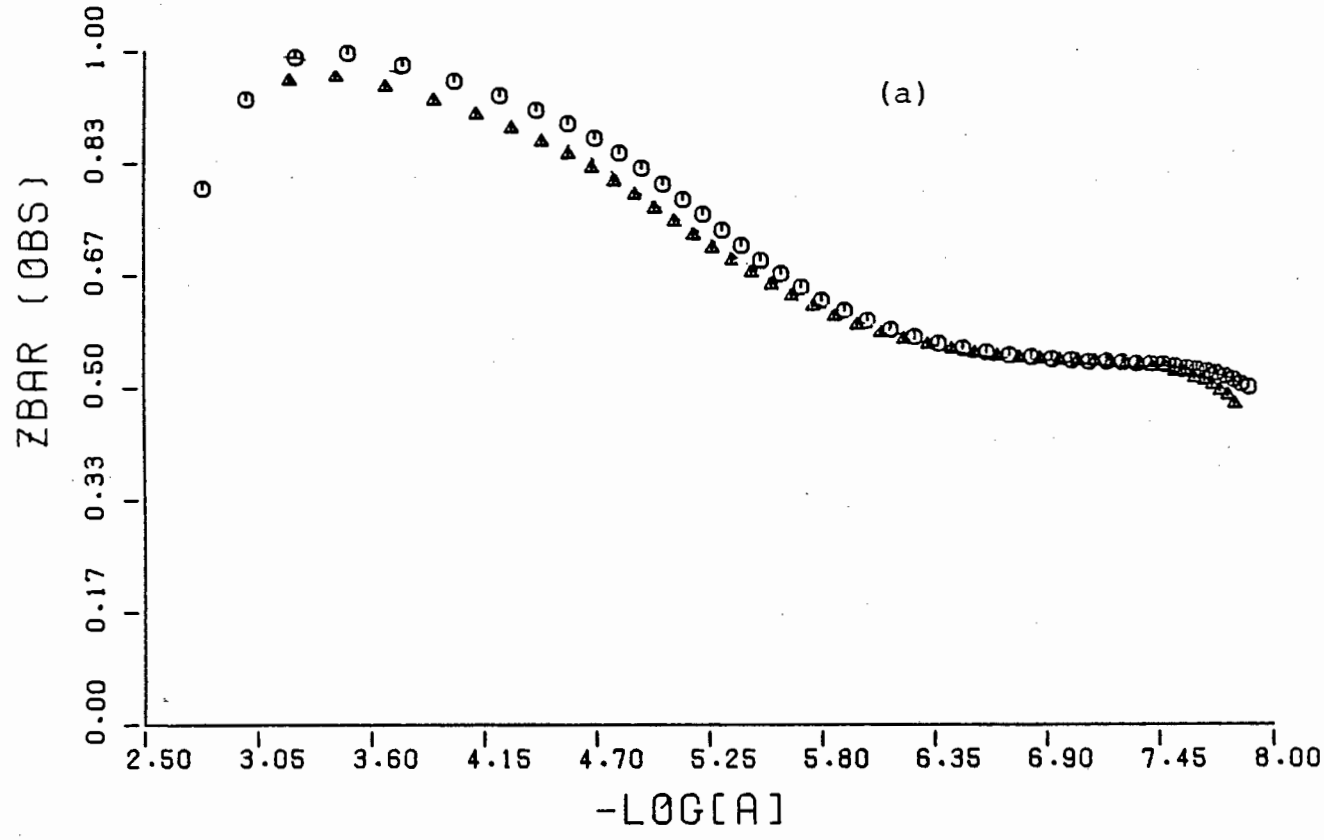

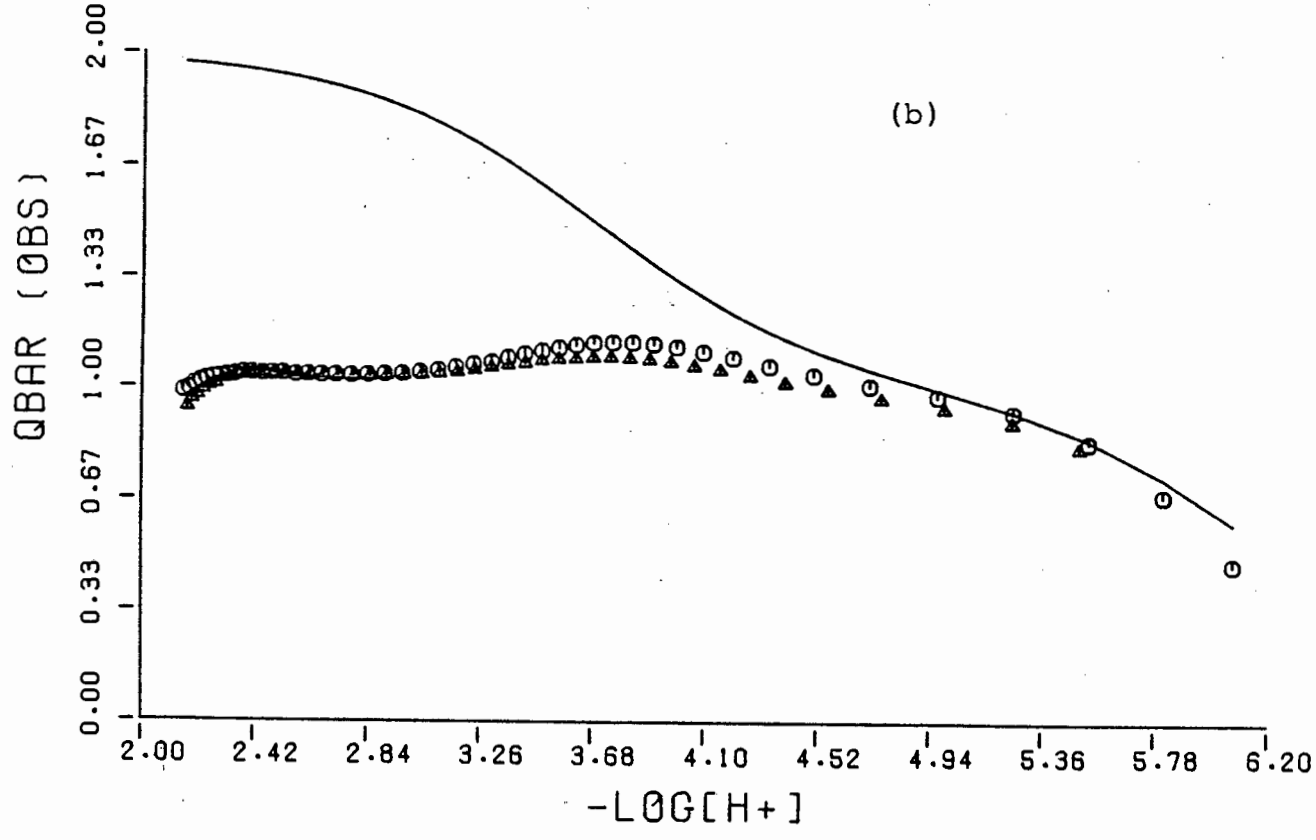

FIGURE 1 : The (a) formation and (b) deprotonation curves

3.3 Computing

ESTA [93] a computer program library which performs calculations concerned with competitive aqueous solution equilibria, was used in the analysis of the potentiometric data.

The overall analysis is performed via two major modules, the simulation (ESTA 1) and the optimisation (ESTA 2) module. Simulation of theoretical data and curves can be carried out using the ESTA 1 module. The two functions that play a major role are the $\bar{Q}$ and $\bar{Z}$ functions. The $\bar{Q}$ is a unique function that helps or supports the interpretations of the $\bar{Z}$ function curves. To show this consider the formation curves of a particular system (Figure 1(a)). Looking at the curves the interpretation can be that these curves show a stepwise formation of either protonation of a complex or the formation of ML_2 species. The fanning out at the high pH region could indicate the presence of a hydroxyl species or deprotonated species in the solution. The $\bar{Z}$ function on its own is not easy to interpret and typically so in this case. The $\bar{Q}$ function (Figure 1(b)) shows the following: at the beginning of the titration $\bar{n}$ is level at $\bar{n} = 2$ and the $\bar{Q}$ function at $\bar{Q} = 1.0$. In this region the predominant species is the MLH species, because the ligand has two protons and it has lost one due to complexation. Beyond pH 5 the two curves are superimposable indicating the presence of a ML

species. As stated, the interpretation of the system is easier when using both the $\bar{Z}$ and $\bar{Q}$ functions.

The $\bar{Q}$ function is also useful combined with the optimisation module ESTA 2. Modelling of the system can be carried out with confidence. An example of this combination is observed in Figures 2 and 3. Figure 2 shows a large discrepancy between the observed and the calculated $\bar{Q}$ function values. If the other titrations in the system agree with the proposed model, then usually refining the E° and acid in the vessel of this particular titration in Figure 2 would result in a more acceptable model. This is shown in Figure 3, which is result of the optimisation of the E°.

The optimisation module has an interesting feature in that it can be used to simultaneously optimise the formation constants and other titration parameters such as concentrations, initial volumes, electrode slope and intercept. Optimisation of formation constants together with other parameters has been shown to significantly reduce the effect of systematic errors in the data (Figure 4). [97] The data used is not experimental data but simulated data.

```
CONC
VESL IVOL      25.000   0 0
VESL MN+2      .0030000 0 0
VESL DMD2      .0052000 0 0
VESL H +1      .0104000 0 0
VESL NA+1      .1370000 0 0
VESL CL-1      .1530000 0 0
BUR1 H +1     -.1030000 0 0
BUR1 NA+1      .1530000 0 0
BUR1 CL-1      .0500000 0 0
ELEC
ZERO H +1     350.350   0
GRAD H +1      59.160   0
ISTR H +1        .150   0
DATA
```

EMF OBS	PH OBS	NBAR CALC	ZBAR(H) OBS	ZBAR(H) CALC	ZBAR(H) RESID	QBAR OBS	QBAR CALC	QBAR RESID
104.700	4.152	1.98	1.99	1.96	.023	.00	.04	-.040
67.000	4.790	1.93	1.92	1.86	.061	.03	.14	-.106
49.300	5.089	1.88	1.84	1.74	.100	.06	.23	-.172
37.700	5.285	1.81	1.76	1.63	.132	.09	[illegible]	-.229
28.500	5.440	1.75	1.68	1.52	.163	.11	.40	-.283
21.200	5.564	1.68	1.60	1.42	.185	.14	[illegible]	-.321
14.800	5.672	1.62	1.52	1.32	.203	.16	[illegible]	-.353
9.200	5.767	1.55	1.45	1.23	.215	.19	.56	-.372
3.600	5.861	1.48	1.37	1.14	.230	.20	.60	-.398
-1.200	5.942	1.42	1.29	1.05	.233	.23	.63	-.404
-5.900	6.022	1.35	1.21	[illegible]	.235	.25	.66	-.407
-10.500	6.100	1.28	1.13	.89	.235	.27	.67	-.407
-14.900	6.174	1.21	1.05	.82	.230	.29	[illegible]	-.399
-19.400	6.250	1.14	.97	.74	.226	.30	.69	-.392
-23.800	6.324	1.07	.89	.67	.218	.32	[illegible]	-.378
-27.700	6.390	1.01	.81	.61	.200	.34	.69	-.347
-32.300	6.468	.93	.73	[illegible]	.192	.35	[illegible]	-.332
-37.100	6.549	.86	.65	.47	.183	.35	[illegible]	-.318
-41.900	6.630	.78	.57	.40	.173	.36	.66	-.299
-47.000	6.717	.70	.49	[illegible]	.163	.36	.64	-.283
-52.800	6.815	.62	.42	[illegible]	.161	.35	.63	-.278
-58.900	6.918	.53	.34	.18	.158	.34	.62	-.275
-65.400	7.028	.45	.26	.10	.158	.33	.61	-.274
-72.700	7.151	.37	.18	[illegible]	.163	.33	.61	-.282
-80.100	7.276	.29	.10	-.07	.164	.34	[illegible]	-.284
-86.600	7.386	.24	.02	-.13	.151	.38	.64	-.261
-91.800	7.474	.20	-.06	-.18	.122	.45	.66	-.211

H +1 COEFF. FOR	1:1	1:2	1:3	MN+2: DMD2 2:1	2:2
	2.0	4.0	6.0	2.0	4.0
	1.9	3.8	5.8	1.9	3.8
	1.8	3.7	5.6	1.8	3.6
	1.7	3.5	5.4	1.8	3.4
	1.6	3.4	5.1	1.5	3.3
	1.5	3.2	4.9	1.4	3.1
	1.5	3.1	4.7	1.3	2.9
	1.4	2.9	4.5	1.2	2.7
	1.3	2.8	4.2	1.1	2.6
	1.2	2.6	4.0	1.0	2.4
	1.1	2.5	3.8	.9	2.2
	1.0	2.3	3.6	.7	2.0
	.9	2.1	3.4	.6	1.9
	.8	2.0	3.1	.5	1.7
	.8	1.8	2.9	.4	1.5
	.7	1.7	2.7	.3	1.3
	.6	1.5	2.5	.2	1.2
	.5	1.4	2.2	.1	1.0
	.4	1.2	2.0	.1	.8
	.3	1.0	1.7	.0	.7
	.3	.9	1.5	-.1	.5
	.2	.7	1.3	-.1	.4
	.1	.6	1.0	-.2	.2
	.0	.4	.8	-.3	.1
	.0	.2	.5	-.4	-.1
	-.1	.1	.3	-.5	-.3
	-.3	.0	.2	-.7	-.5

FIGURE 2 : A printout of the $\bar{Q}$ function showing the high error between observed and calculated values of $\bar{Q}$ and $\bar{Z}_H$

```
CONC
VESL IVOL      25.000   0 0
VESL MN+2      .0030000 0 0
VESL DMD2      .0052000 0 0
VESL H +1      .0104000 0 0
VESL NA+1      .1370000 0 0
VESL CL-1      .1530000 0 0
BUR1 H +1     -.1030000 0 0
BUR1 NA+1      .1530000 0 0
BUR1 CL-1      .0500000 0 0
ELEC
ZERO H +1    336.350    0
GRAD H +1     59.160    0
ISTR H +1       .150    0
DATA
```

EMF OBS	PH OBS	NBAR CALC	ZBAR(H) OBS	ZBAR(H) CALC	ZBAR(H) RESID	QBAR OBS	QBAR CALC	QBAR RESID
104.700	3.916	1.99	1.98	1.98	-.002	.02	.02	.003
67.000	4.553	1.96	1.92	1.91	.003	.08	.08	-.005
49.300	4.852	1.93	1.84	1.84	.002	.15	.15	-.003
37.700	5.048	1.89	1.76	1.76	.000	.22	.22	-.001
28.500	5.204	1.84	1.68	1.68	.002	.28	.28	-.004
21.200	5.327	1.80	1.60	1.60	.001	.34	.34	-.001
14.800	5.435	1.75	1.52	1.52	.000	.39	.39	.000
9.200	5.530	1.70	1.44	1.45	-.003	.45	.44	.006
3.600	5.625	1.65	1.37	1.37	.000	.49	.49	.000
-1.200	5.706	1.60	1.29	1.29	-.004	.54	.53	.006
-5.900	5.785	1.54	1.21	1.21	-.006	.58	.57	.010
-10.500	5.863	1.48	1.13	1.14	-.008	.61	.60	.013
-14.900	5.937	1.42	1.05	1.06	-.011	.65	.64	.020
-19.400	6.013	1.36	.97	.98	-.013	.67	.65	.022
-23.800	6.088	1.29	.89	.91	-.016	.70	.67	.028
-27.700	6.154	1.23	.81	.84	-.029	.73	.68	.050
-32.300	6.231	1.16	.73	.76	-.031	.74	.70	.054
-37.100	6.313	1.08	.65	.68	-.032	.75	.69	.055
-41.900	6.394	1.01	.57	.61	-.035	.75	.69	.061
-47.000	6.480	.92	.49	.55	-.036	.74	.68	.063
-52.800	6.578	.83	.42	.45	-.030	.72	.67	.052
-58.900	6.681	.74	.34	.36	-.024	.69	.65	.042
-65.400	6.791	.64	.26	.27	-.016	.66	.63	.028
-72.700	6.914	.54	.18	.18	-.003	.62	.62	.005
-80.100	7.039	.44	.10	.07	.007	.59	.61	-.013
-86.600	7.149	.37	.02	.02	.003	.60	.61	-.005
-91.800	7.237	.32	-.06	-.04	-.019	.65	.62	.034

H +1 COEFF. FOR MN+2:DMD2 STOIC

1:1	1:2	1:3	2:1	2:2
2.0	4.0	5.9	1.9	3.9
1.9	3.8	5.8	1.8	3.8
1.8	3.7	5.6	1.6	3.6
1.7	3.6	5.4	1.5	3.3
1.6	3.4	5.2	1.3	3.1
1.5	3.3	5.1	1.1	2.9
1.4	3.1	4.9	1.0	2.7
1.3	3.0	4.7	.8	2.5
1.2	2.8	4.5	.7	2.3
1.1	2.7	4.3	.5	2.1
1.0	2.5	4.0	.4	1.9
.9	2.4	3.8	.3	1.7
.8	2.2	3.6	.1	1.5
.7	2.0	3.4	.0	1.4
.6	1.9	3.2	-.1	1.2
.5	1.7	3.0	-.2	1.0
.4	1.6	2.7	-.3	.8
.3	1.4	2.5	-.4	.7
.2	1.3	2.3	-.5	.5
.2	1.1	2.0	-.6	.4
.1	.9	1.8	-.6	.2
.0	.8	1.5	-.6	.1
.0	.6	1.3	-.7	.0
-.1	.5	1.0	-.7	-.2
-.2	.3	.7	-.7	-.3
-.2	.1	.5	-.8	-.5
-.3	.0	.3	-1.0	-.7

FIGURE 3 : A printout of the $\bar{Q}$ function showing the good agreement between the observed and calculated $\bar{Q}$ and $\bar{Z}_H$ after refining the value of E°

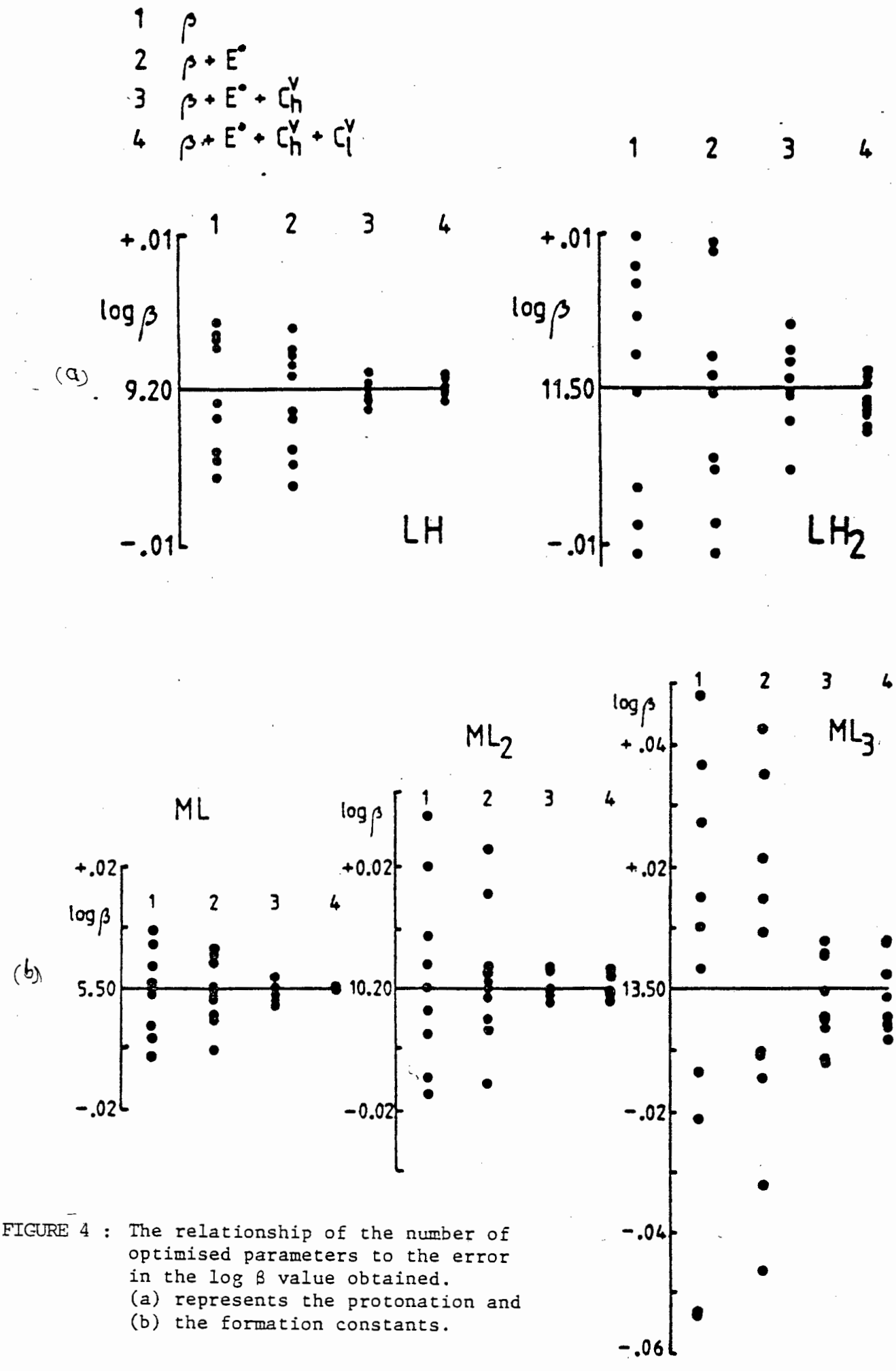

FIGURE 4 : The relationship of the number of optimised parameters to the error in the log β value obtained.
(a) represents the protonation and
(b) the formation constants.

The optimisation is performed by minimising an objective function, U.

$$U = (N-np)^{-1} \sum_{n=1}^{N} n_o^{-1} \sum_{i=1}^{N_o} W_{ni} \left(Y^o_{ni} - Y^c_{ni} \right)^2$$

using the Gauss-Newton method.

The weight at each titration point is calculated using

$$W_{ni} = \left(\sum_{p} \left(\delta \left(Y^o_{ni} - Y^c_{ni} \right) / \delta p \right)^2 \cdot \sigma p^2 \right)^{-1}$$

the Hamilton R-factor is given by:

$$R = \sqrt{U \Big/ \sum_{n=1}^{N} n_o^{-1} \sum_{i=1}^{n_o} W_{ni} \left(Y^o_{ni} \right)^2}$$

and the R limit,

$$R_{lim} = \sqrt{\frac{N}{\sum_{n=1}^{N} n_o^{-1} \sum_{i=1}^{n_o} W_{ni} \left(Y^o_{ni} \right)^2}}$$

A schematic flow diagram of the route followed when using the ESTA library for analysing data in this research is shown in Scheme 1. The dotted line box in the scheme represents the ESTA 1 module.

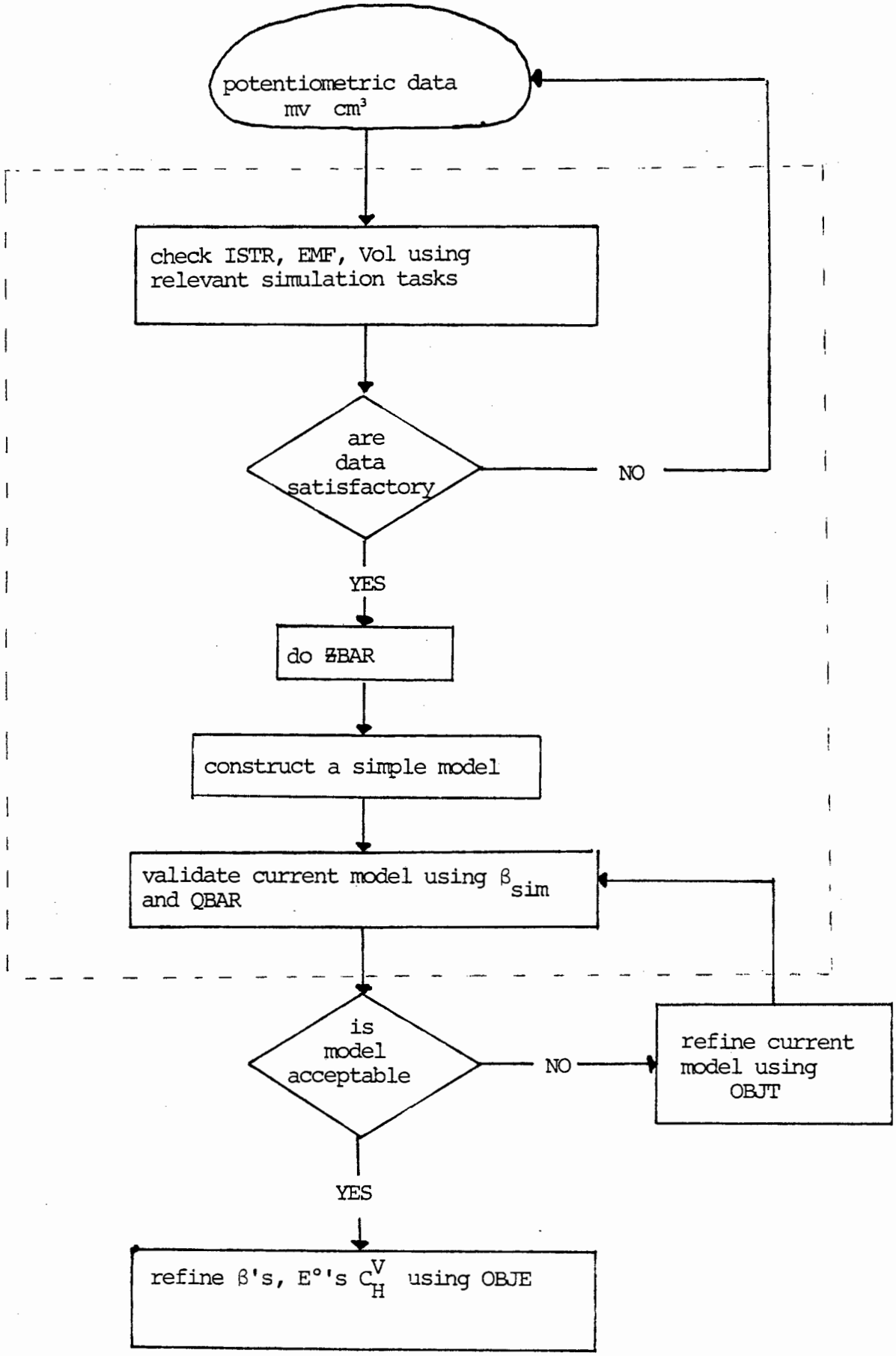

FIGURE 5 : Schematic flow diagram of the ESTA library used in the data analysis

3.4 Experimental

All solutions were prepared using glass distilled deionised and degassed water. All titrations were done under high quality grade nitrogen (Air Products) and passed through:

1) 15% 1,2,3 trihydroxy benzene in 30% KOH to remove O_2

2) 50% KOH to remove CO_2

3) 150mmol.dm^{-3} NaCl to humidify the gas

To control the ionic strength, all solutions were maintained at a chloride concentration of 150mmol.dm^{-3} by the addition of sodium chloride (SAARCHEM ANALAR).

All the metal ion solutions were prepared from their chloride salts (SAARCHEM ANALAR) and standardised by complexometric titration using EDTA [95] and by Gran plot [96] for hydrogen ion concentration. Sodium hydroxide solution (100mmol.dm^{-3}) was prepared freshly and weekly from Merck concentrated ampoules, under nitrogen and standardised using potassium hydrogen phthalate [95]. Hydrochloric acid for calibrating the electrode (10mmol.dm^{-3}) and also that for titration (100mmol.dm^{-3}) was prepared from BDH standard concentrated acid and standardised by Gran plot. Stock

solutions of the ligands were prepared and standardised potentiometrically.

All solutions that were in use in one particular time were kept under nitrogen in polyethylene bottles. Storage of other solutions was also in polyethylene vessels with exchangeable tops with the titration vessels.

The titrations were performed in a double walled vessel (Metrohm) thermostatted at 25 $\pm$ 0.1 °C by circulating water (Heto thermostat). The emf reading was measured with a Radiometer PHM 84 research pH meter equipped with a Metrohm glass electrode and an Ag/AgCl reference electrode (Metrohm) with a renewable liquid junction of 150mmol.dm^{-3} chloride concentration. The titrating solution and all other reagents except ligands were added from a piston-burette. The titrations were automated (UCT electronics) and data stored on floppy disc.

Due to the complexity of the potentiometry, which was plagued by precipitation, the date were analysed using the scheme outlined below. The precipitate was analysed and found to be the hydrolysed metal.

A number of approaches have been tried in attempting to analyse the metal-ligand titration data:

a) Editing where the precipitate started and concentrate only on a shorter section of the titration

b) Performing the titration in both directions i.e. from high to low pH and from low to high pH

c) Splitting the data into two sections, one at high pH and the other at low pH which could then be analysed separately

The first approach (a) was limited in that only the protonated species could be analysed for, although it gave good statistics on refinement. The region was also far from the physiological pH of 7.4, which is of interest in this study. The second approach (b) had its shortcoming in that because of the limitations of the available computer programs the number of dissociable protons of the ligand had to be changed. High arbitrary values for the protonation constants had to be created to allow for LH_3 and LH_4 ligand species. Finally the approach (c) had the disadvantages that when combining the separate refined sections convergence could not be obtained.

The final solution was to repeat the titrations at very low concentrations of both the metal and the ligand and to analyse the data over the entire pH range.

the consequence of high standard deviations on the β values of the order of 0.05. This had been found to reflect the "true" species present in the solution although being hampered by the presence of small amounts of precipitate. Sometimes the precipitate could not be seen, but on data analysis it could be detected.

In most of the data analysis the approach suggested by May and Murray and outlined in the theory section has been adopted. This entailed simultaneous optimisation of the values, the E° and the concentration of the acid in the vessel.

3.5 Analysis of Data

3.5.1 Protonation studies (H -DMO and H -DEO systems)

Figures 6(a) and 6(b) show the protonation curves of DMO and DEO respectively. The symbols represent different ligand concentrations while the solid lines represent the theoretical curves calculated using the constants given in Table 1. Although there are two amine nitrogens, the titration curves show only one inflection. This is because the pKa values of the two amines are so close they are titrated virtually simultaneously. Table 1 shows the final protonation constants together with the relevant statistics. From these statistics and Figure 6(a) and (b) it can be seen that the agreement between theory and experiment is good.

Both these ligands are more acidic than the trien on whose structure they are based. Trien has pKa values of 10.09 and 9.31 [101]. The difference in the pKa values can be interpreted by considering the following concepts. Generally it is known that the base strength in nitrogen donor ligands depends on the availability of the nitrogen lone pairs of electrons. Consider NH_3, in water it is a weak base. In this state the nitrogen atom is experiencing the inductive effects of the hydrogen atoms and is therefore partially negatively charged. On replacing the hydrogen with an electron withdrawing group results in decreased

basicity e.g. pKa NH_3 = 9.26 and pKa NH_2OH = 6.03. Compare bis-(2-N,N'-aminoethyl)oxamide (BAO)

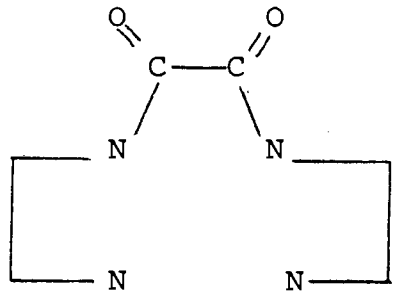

which has pKa values of 9.31 and 8.43 with trien whose pKa values are 10.09 and 9.31. This decrease in the pKa can be attributed to the introduction of the amide groups to the trien structure.

Alkyl groups are more electrondonating than hydrogen atoms therefore replacing the hydrogen atoms with an alkyl group will result in increased basicity which is caused by an increase in electron density on the nitrogen atom. Increasing the number of alkyl substituents on the nitrogen also results in increase in the basicity, however, not as much effect as the initial substitution. The tertiary substituted alkylamines are less basic than their primary substituted counterparts. This anomaly has been explained by the solvation effect [99]. Hydrogen-bonding solvation tends to increase the apparent strength of amines. In the positively charged ammonium ions solvation occurs more than in the uncharged amine, resulting in enhanced basicity of the amine.

basicity e.g. pKa NH_3 = 9.26 and pKa NH_2OH = 6.03. Compare bis-(2-N,N'-amonoethyl)oxamide (BAO)

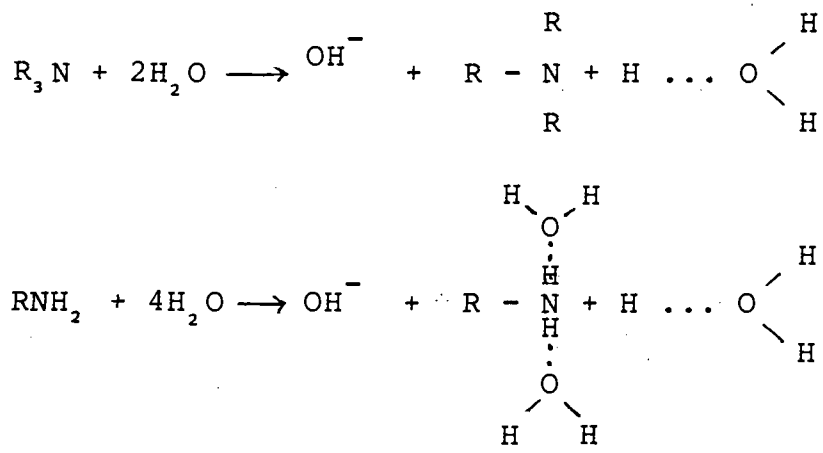

Therefore based on the above arguments, it follows that the decrease in basicity of trien on going to DMO and DEO is due to both factors discussed above. The electronwithdrawing amide group on the central ethylene group and also the less solvated tertiary amine groups. The difference in the pKa values of DMO and DEO can be attributed to the inductive effect of the alkyl groups increasing the electron cloud around the amine nitrogen e.g.

$Me_3N = 9.72$*

$Et_3N = 10.72$

which is electrondonating substitution. Therefore DMO and DEO do succumb to the rules of the nitrogen donor ligands.

---

* Ref [99] Me = methyl group; Et = ethyl group

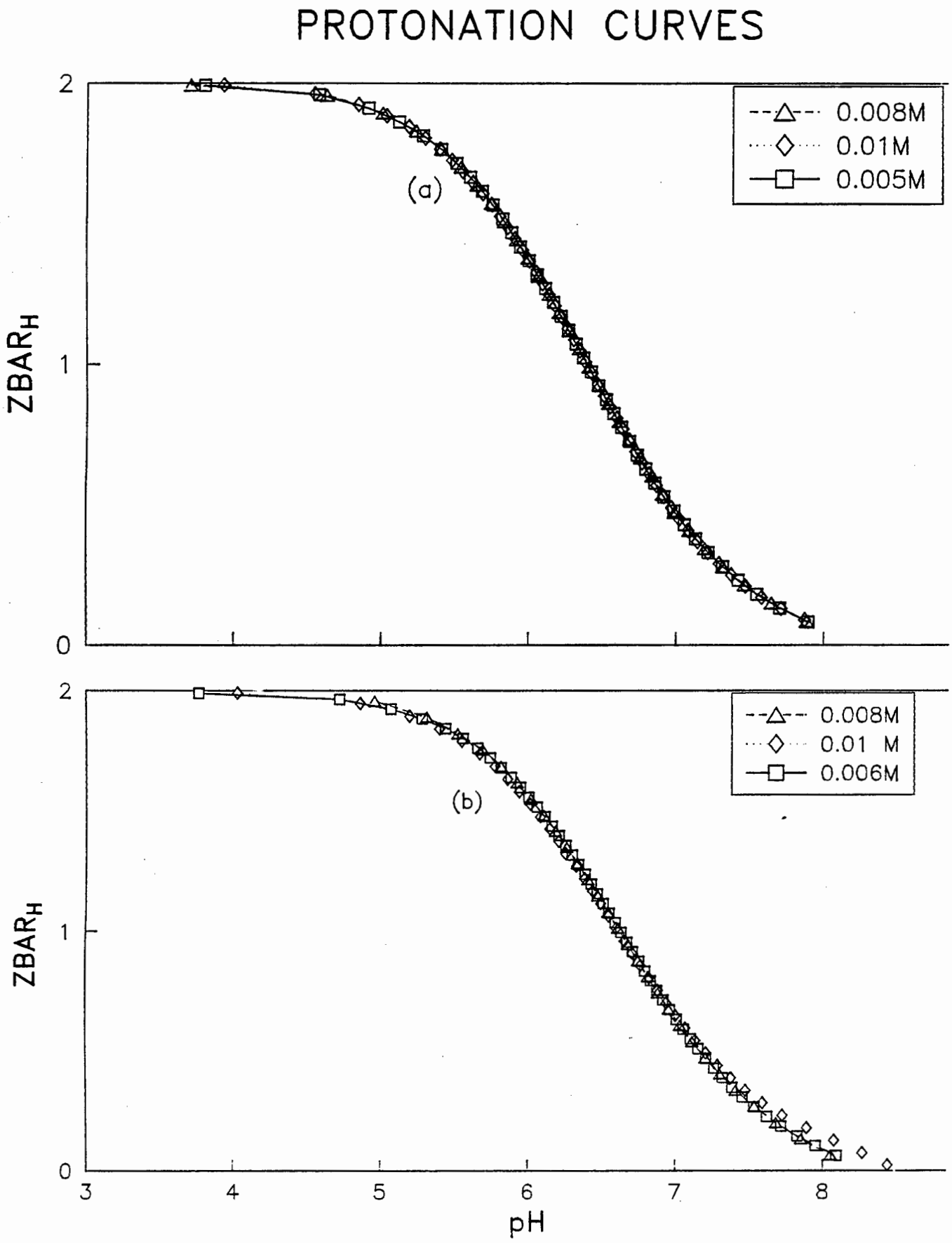

FIGURE 6 : Protonation curves for (a) DMO and (b) DEO

TABLE 1

Logarithms of the overall formation constants, β_{pqr} for the H -DMO and -DEO systems, determined in this study at 25°C and 0.15 mol.dm^{-3} Na[Cl]

Pkw used = 13.59

ligand	pqr	β_{pqr}	U	R	pH range
DMO	011	6.848 ± 0.0001	16.2	0.01	3 - 9
	012	12.80 ± 0.001			
DEO	011	7.04 ± 0.002	18	0.01	
	012	13.256 ± 0.001			

3.5.2 Copper

Figures 7 and 8 show the formation curves for the Cu-DMO and -DEO systems respectively. The symbols represent different metal to ligand concentrations. The curves are superimposable showing no existence of polynuclear species. At the beginning of the titrations the protonated species hump is observed, but the theoretical curves 7(b) and 8(b), plotted using the formation constants in Table 2 do not show any agreement in this region. This region, however, is also a high error region as shown by the big jump in the emf value from the first titration point to the second. However, on removing the MLH species from the refining process the statistics are very high and convergence is not achieved. In the species distribution curves, Figures 11 and 12, it can be observed that at the start of the titration about 20% and 40% of Cu in Cu-DEO and Cu-DMO systems respectively has been complexed. Continuing with the titration it can be seen that the curves show a typical step-wise formation sequence up to $\bar{Z}$ value of one. In the low pA region deprotonation is seen to take place. This is shown by the "backward fanning" of the titration curves.

Table 2 shows the formation constants of the Cu-DMO and Cu-DEO systems. There is [illegible] agreement in the observed and theoretical results as seen from Figures 7(b) and 8(b). The objective functions, U, are much lower than 100, which shows

that the true values are approached [100]. The two systems are similar.

The Cu-DEO system has formation constants lower than those of the Cu-DMO system with the average difference of about 0.2 log units. This is in accordance with the pKa values of DEO being higher than those of DMO. Therefore, the lowered metal complex stability could be attributed to the inductive effect of the groups on the amine nitrogen.

For the DMO equilibrium

$$MLH \rightleftharpoons ML + H$$

it can be seen that the pKa is 3.0 which is lower than pKa_1 6.85. A similar effect is shown by DEO, 3.4 and 7.04 for deprotonation of the complex and ligand respectively. This decrease in pKa upon coordination of the metal ion cannot be due to an inductive effect of the Cu^{2+}, as coordination is occurring at one end of the molecule and deprotonation is occurring at the other end.

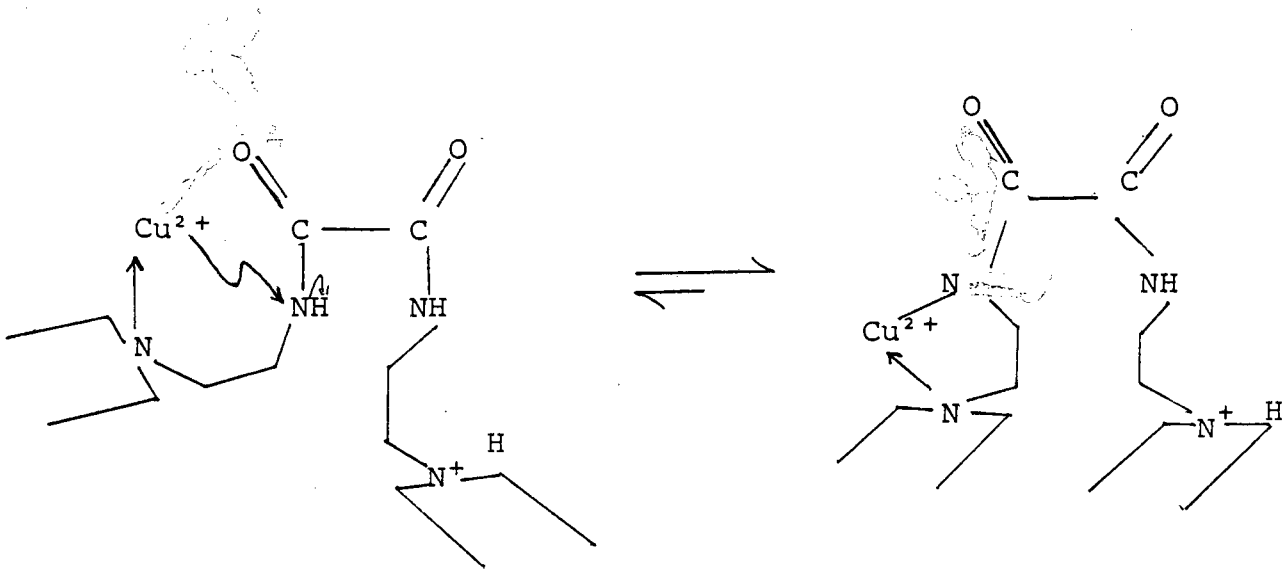

On the other hand, if the postulated structure is accepted, then it can be seen that it is not the protonated amine that becomes deprotonated but the amide nitrogen. This would account for the pKa values obtained.

The relationship between the Cu-DMO and -DEO can be further interpreted by considering the substituted amine's complexation constants, Table 3 [101].

The monodentate ligands show a decrease in the ML formation constant with increase in the number of alkyl substituents on the nitrogen. The same trend is observed with BAO and DMO. A similar trend is envisaged for the DEO system. The difference in the stability of the ML species between the two sets of ligands is in their structure. Trimethylamine is a monodentate ligand while BAO, DMO and DEO are potentially multidentate. Two possible structures for the ML species are shown: [110]

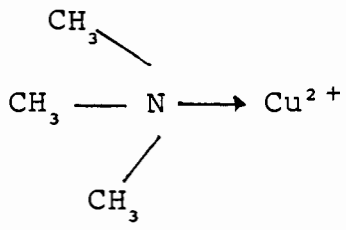

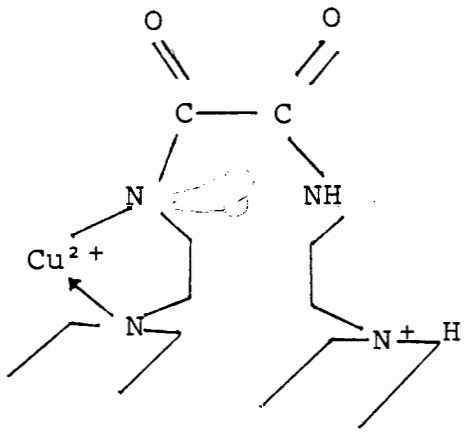

For the MLH_{-1} and MLH_{-2} species more steric hinderance is expected with the diethyl than the dimethyl substituent leading to a lower stability. However, the difference in the formation constants of the MLH_{-2} of the DMO and that of the DEO is minimal. A solution to this problem and that of the DEO is ethylene groups which could possibly create a hydrophobic end of the structure.

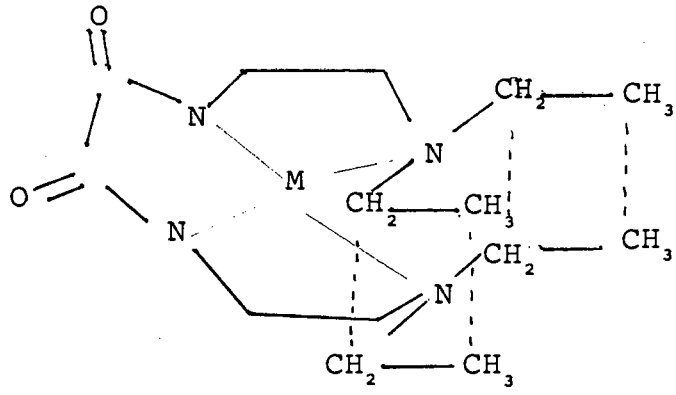

Figures 9 and 10 show the deprotonation function Q of the Cu-DMO and Cu-DEO systems respectively. The overall number of protons that the ligand is capable of losing during complexation is four, but only two protons are titrated during protonation, the other two being amide protons. With reference to the Cu-DEO system, it can be seen that at pH 3.0, $\bar{Q} = 0,8$ which means that one proton has already been lost although n is still at 2. This is acceptable in the light of the previous explanation. At this stage "three" protons are still on the ligand. At pH 5, $\bar{Q} = 2$ and $\bar{n} = 2$ which means that two protons have been displaced by complex

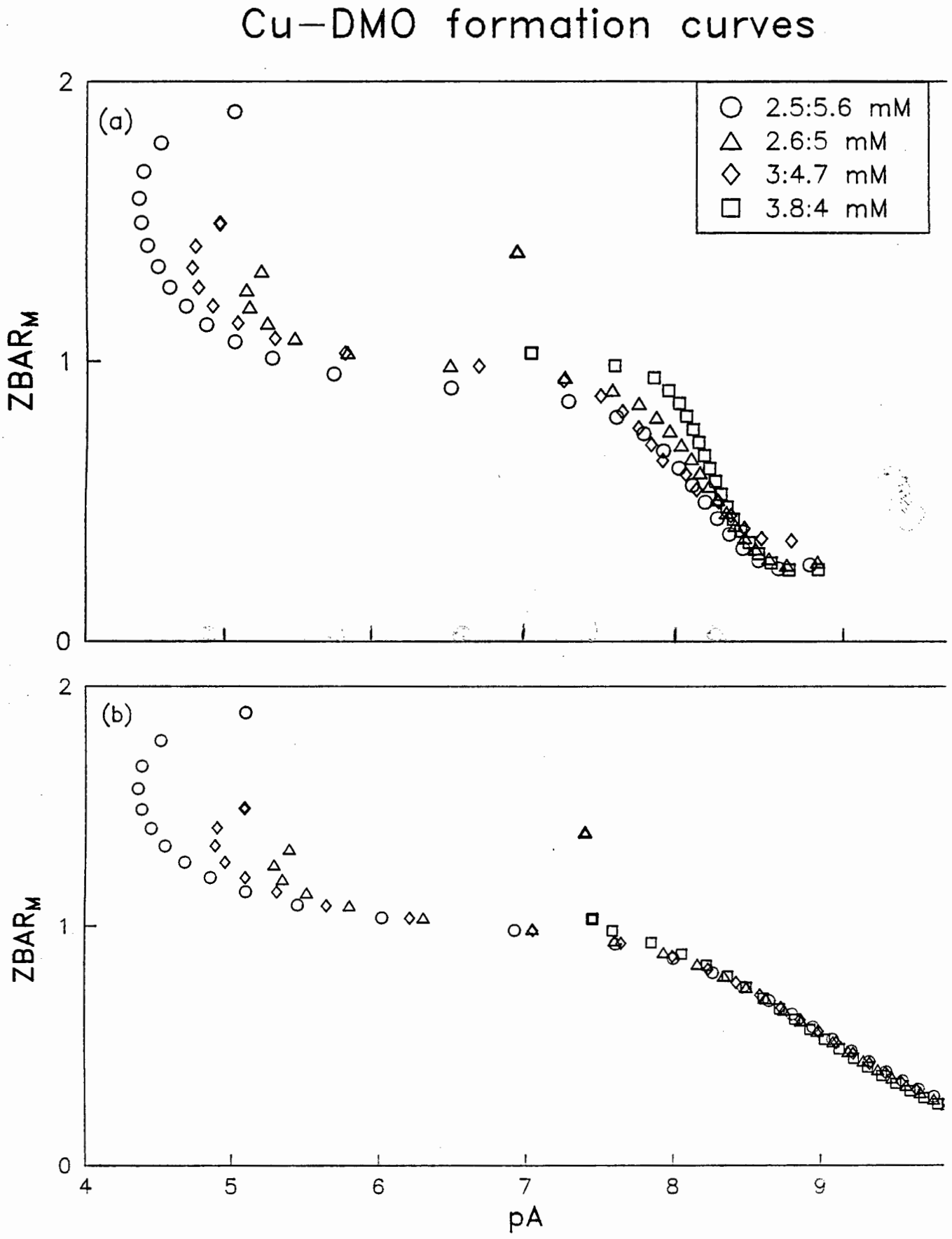

FIGURE 7 : Experimental (a) and theoretical (b) curves for the Cu-DMO system at 25°C and 0.15M (Na) Cl

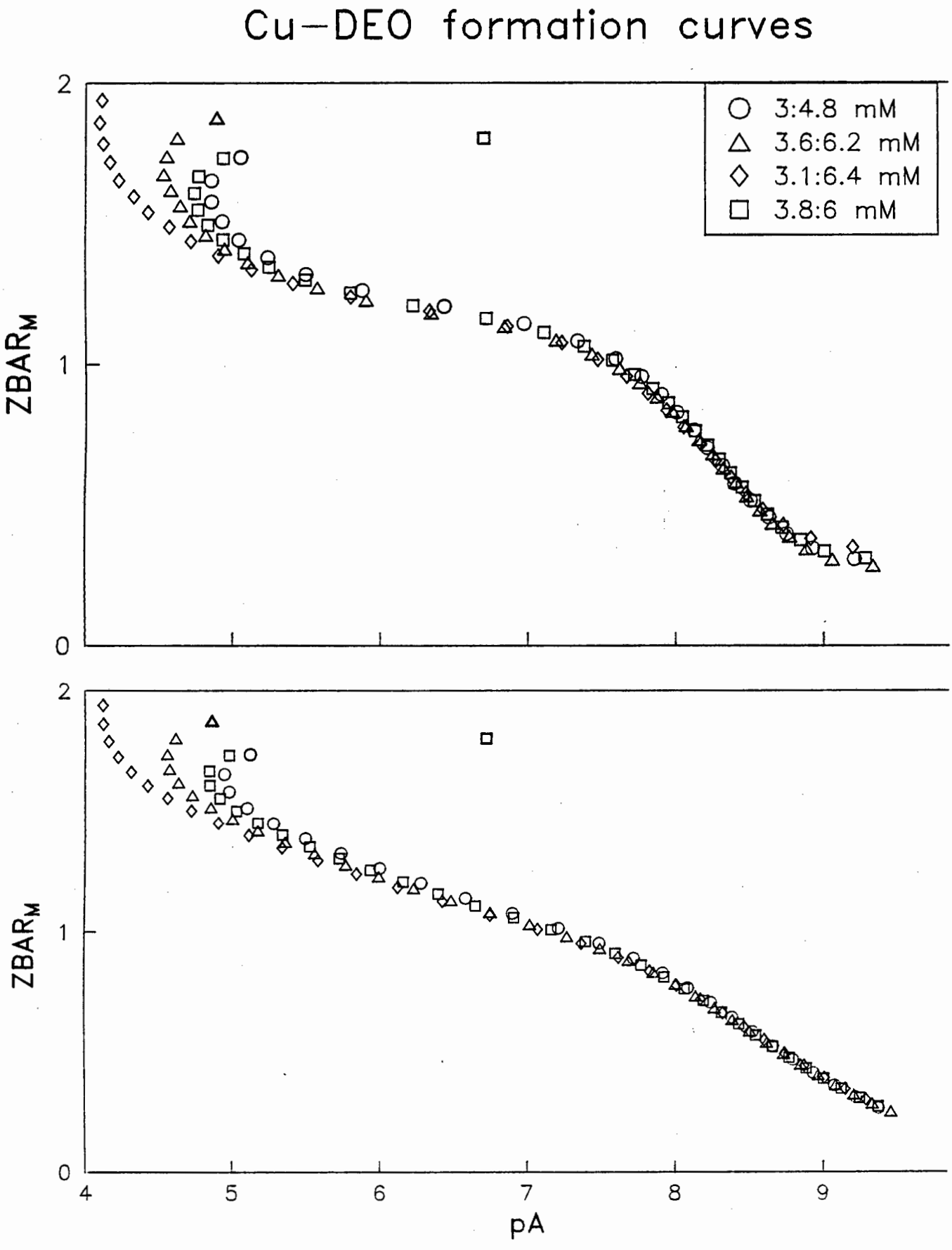

FIGURE 8 : Experimental (a) and theoretical (b) curves for the Cu-DEO system at 25°C and 0.15M (Na) Cl

TABLE 2

Logarithms of the overall formation constants, β_{pqr} for the Cu-DMO and -DEO systems, determined in this study at 25°C and 0.15 mol.dm^{-3} Na[Cl]

Pkw used = 13.59

ligand	pqr	β_{pqr}	U	R	pH range
DMO	111	12.24 ± 0.04	51	0.06	3 - 8
	110	9.2 ± 0.03			
	11-1	3.44 ± 0.04			
	11-2	-2.94 ± 0.03			
DEO	111	12.16 ± 0.04	76	0.05	3 - 8
	110	8.74 ± 0.02			
	11-1	3.74 ± 0.02			
	11-2	-2.98 ± 0.01			

TABLE 3

Logarithms of the 1:1 formation constants of H^+ and Cu with the substituted amines

ligand	metal ion	formation constant
NH_3	H^+	9.43
	Cu^{2+}	K_1 = 4.14
NMe_2	H^+	10.86
	Cu^{2+}	3.21
NMe_3	H^+	9.72
	Cu^{2+}	2.88
BAO	H^+	9.31
	Cu^{2+}	9.41
DMO	H^+	6.85
	Cu^{2+}	9.2
DEO	H^+	7.04
	Cu^{2+}	8.47

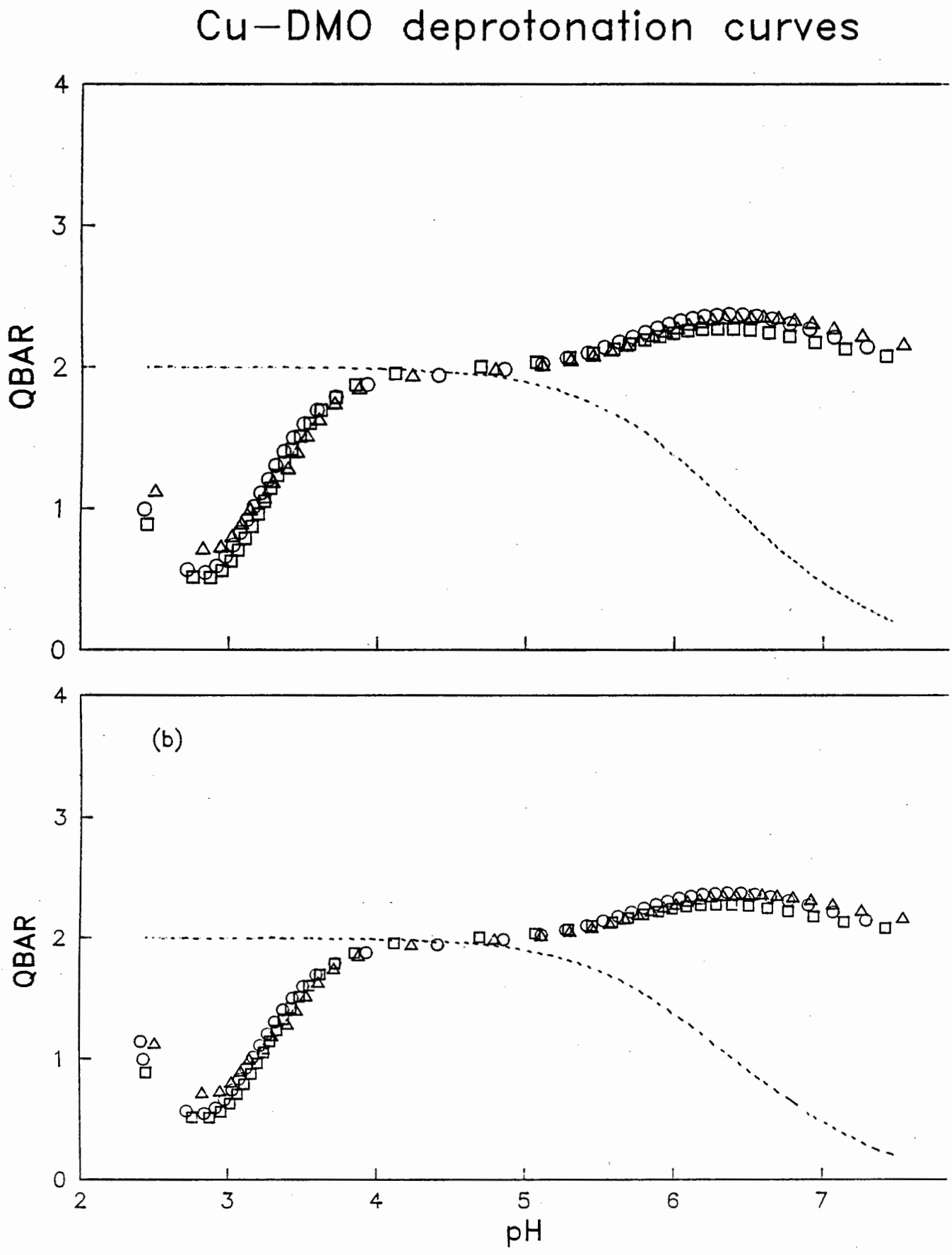

FIGURE 9 : The (a) experimental and (b) theoretical curves of $\bar{Q}$ vs pH for the Cu-DMO system at 25°C and 0.15M (Na) Cl ... = $\bar{n}$ vs pH

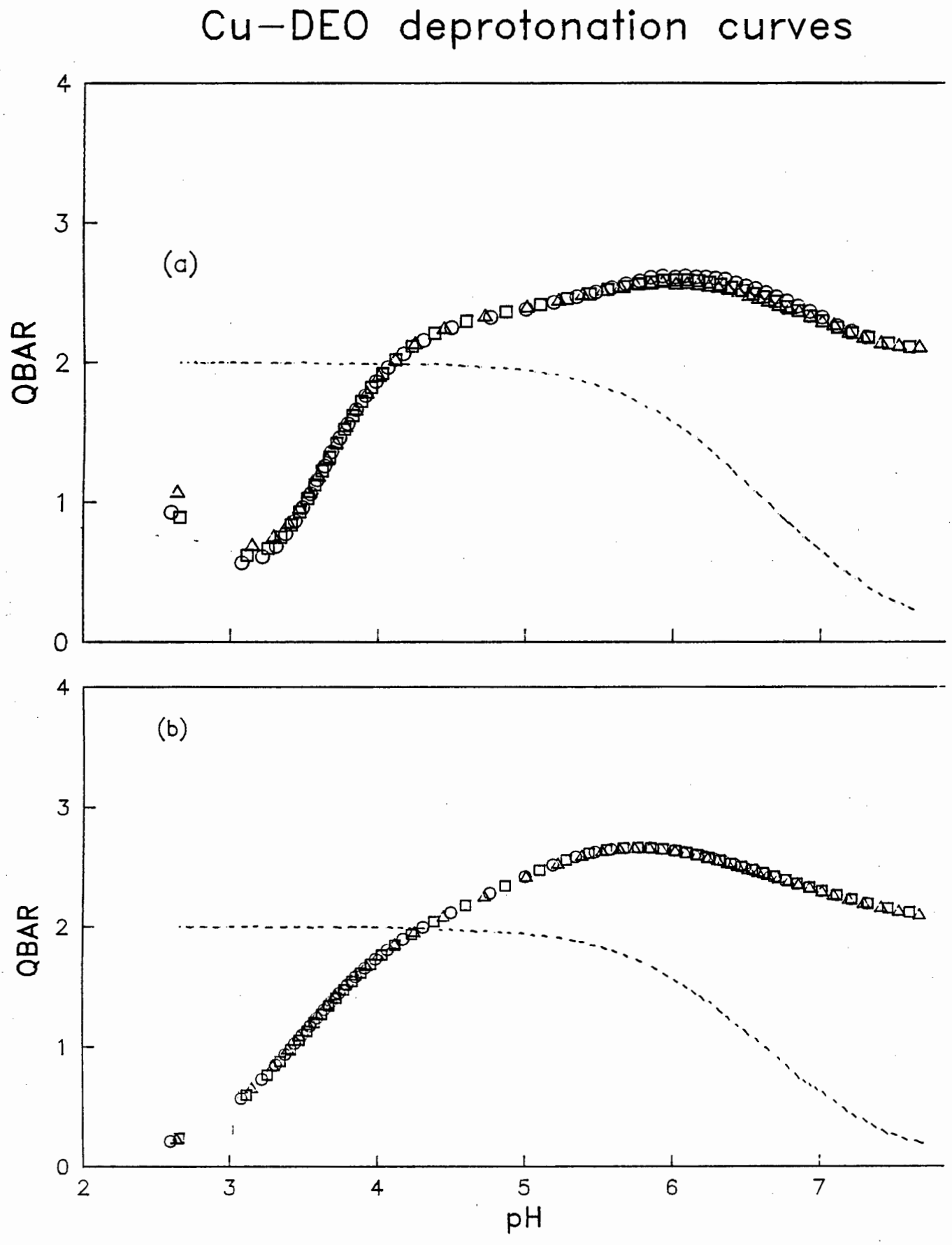

FIGURE 10 : The (a) experimental and (b) theoretical curves of $\bar{Q}$ vs pH for the Cu-DEO system at 25°C and 0.15M (Na) Cl . .. = n vs pH

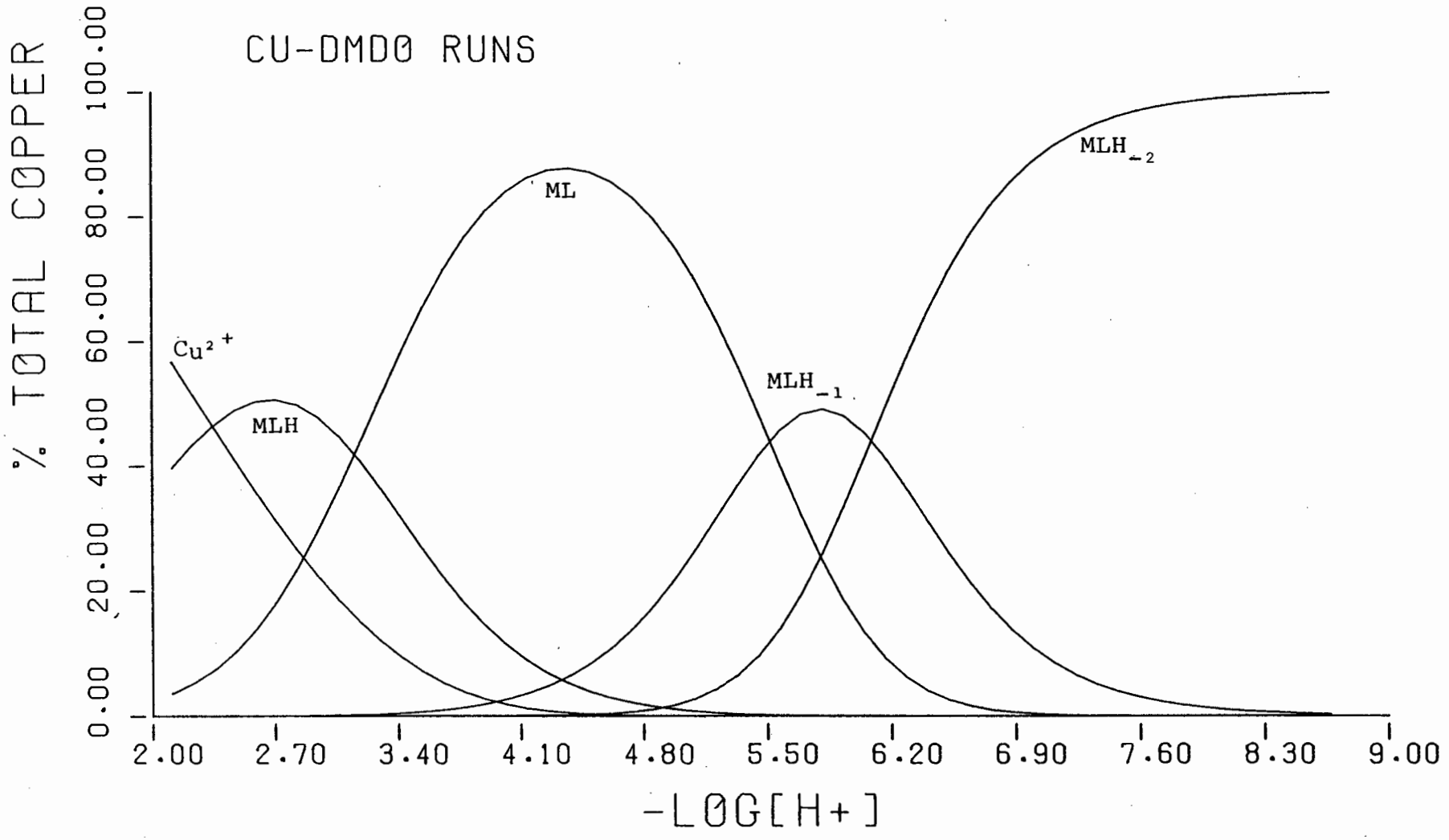

FIGURE 11 : The species distribution curves for the Cu-DMO system showing the percentage of copper in each species in 1 : 1 ligand-to-metal solution at a concentration of 4mM.

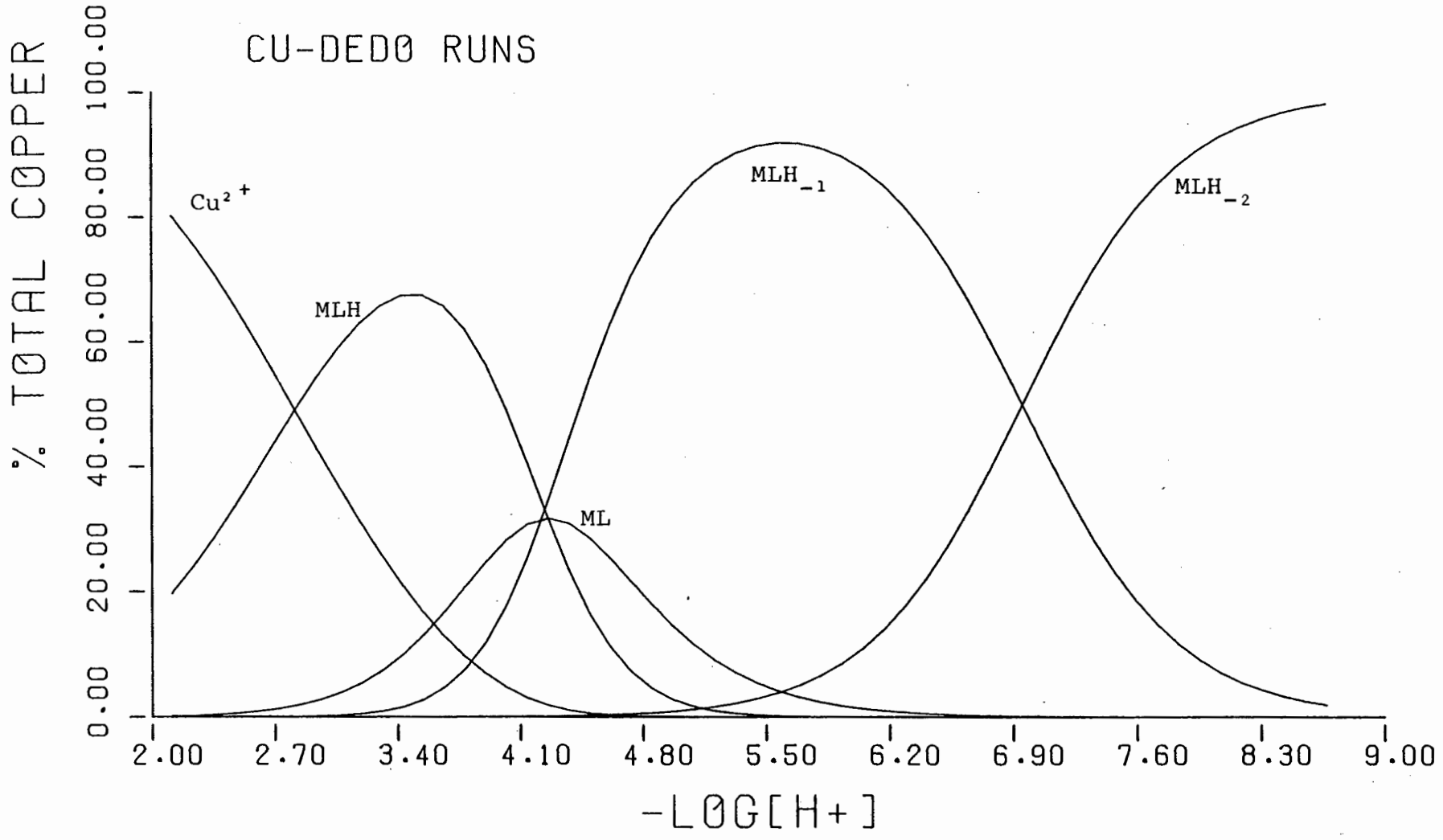

FIGURE 12 : The species distribution curves for the Cu-DEO system showing the percentage of copper in each species in 1.5 : 1 ligand-to-metal solution at a concentration of 4mM.

formation. Above pH 5 the complex continues to lose protons (Q increases), with $\bar{Q}$ = 3 and $\bar{n}$ = 1. This is the MLH_{-2} region.

At pH 8.25 complexation is complete with $\bar{Q}$ = 2 and $\bar{n}$ = 0 which means that a total of four protons have been lost and the MLH_{-2} species has been formed.

Figures 11 and 12 show the species distribution at different pH values. These represent the percentage of the Cu^{2+} ion present in each species. In agreement with the $\bar{Q}$ it can be seen that at the beginning of the titration 20% of the copper has been complexed in the form of MLH.

3.5.3 Zinc

Figures 13 and 14 show the formation curves for the Zn-DMO and -DEO systems respectively. The symbols represent different metal to ligand concentrations. An interesting feature arises from the ill-defined shape of the Zn-DEO formation curves. During the titrations gross precipitation occurred in both systems, but was excessive in the Zn-DEO system. In explaining the processes taking place in the solution, the following discussion has got to be introduced. Firstly, it is known that the ZnII ion does hydrolyse in acidic media, though sparingly, forming $ZnOH^{+}$ and Zn_2OH^{3+} and precipitation commences in the neutral region [102]. Secondly, solutions containing such small amounts of

hydrolysis species are poorly buffered. The Zn precipitate obtained in this study was taken for microanalysis which proved it to be the hydrolysed metal ion and not the Zn-DEO complex. Despite the difficulties encountered in the study, careful use of the data analysis scheme helped in obtaining the constants in Table 4 which were subsequently used to plot the theoretical curves in Figures 13(b)and 14(b). There is agreement in the shape of the curves of the theoretical and the observed systems.

The data analysis does not show any stepwise formation from $MLH \rightarrow ML + H^+$. There is a huge jump in the deprotonation process in that the protonated complex loses two protons of the total of "four" that the ligand is capable of losing, forming MLH_{-1}, which is the result of the loss of three protons. The ML species was included in the modelling of the species in the solution, however, on refining the formation constants it gave such high error that it was excluded. It was further assumed that if ML is there it is in very little amounts that are not significant or that it is an intermediate in the fast reaction

$$MLH \rightleftharpoons [ML + H] \rightleftharpoons MLH_{-1} + 2H^+$$

In the low pA region there is backward fanning which is indicative of the presence of hydroxy species i.e. deprotonation of the complex takes place.

Table 4 shows the formation constants of the Zn-DMO and Zn-DEO systems. There is good agreement in the observed and theoretical results despite the presence of precipitate. The objective function U is much lower than 100* showing that the true value under these conditions was approached.

As with the previous complexation studies of DMO and DEO with H^+ and Cu^{2+}, the inductive effect of the ethyl group over the DMO is obvious. The formation constant of the fully deprotonated complex for the Zn-DEO system is lower than that of the Zn-DMO system. However, the opposite is observed with the MLH and MLH_{-1} species. This could mean that because the DEO is more basic than DMO it is more inclined to form stable complexes with Zn. This cannot be explained in terms of the inductive effect. An explanation could be that the ethyl groups form a stable rigid hydrophobic end by packing on top of each other therefore limiting the amount of "sweep" of the alkyl groups around the nitrogen atom. Steric hinderance in the case of DMO could therefore result from the relatively free methyl groups that revolve around the nitrogen atom. In this way the methyl groups could be forcing the bond angles of the amine to open up causing more s character to be used in the bonding and more p character to be left in the lone pair [99] which is poorly suited for donation to an acid. This is called back,"B-strain".

Figures 15 and 16 show the deprotonation function $\bar{Q}$ of the Zn-DMO and -DEO systems. As was the case with the Cu systems, the curves show a total loss of four protons in the final MLH_{-2} species. At the beginning of the titration the $\bar{Q}$ shows a loss of one proton while $\bar{n} = 2$ showing that 2 protons are still attached to the ligand. With increase in pH there is loss of three protons with $\bar{Q} = 3$ and $\bar{n} = 1$ and finally, when $\bar{Q} = 2$ and $\bar{n} = 0$ there is a total loss of four protons.

Figures 17 and 18 show the species distribution at different pH values. These represent the percentage of the Zn^{2+} ion present in each species. In agreement with the $\bar{Q}$, at the beginning of the titration, the Zn has been used to form the MLH species. The MLH curve, however, does not follow a simple Gaussean curve. It shows the existence of another species under the curve, though not so marked in the Zn-DMO system. This shape implies that in this region the ML species is formed. The amount though is not as much as the curves formed by the dotted lines show. The ML species could possibly be not a stable species in this solution or its formation could be the rate determining step in the formation of the deprotonated species.

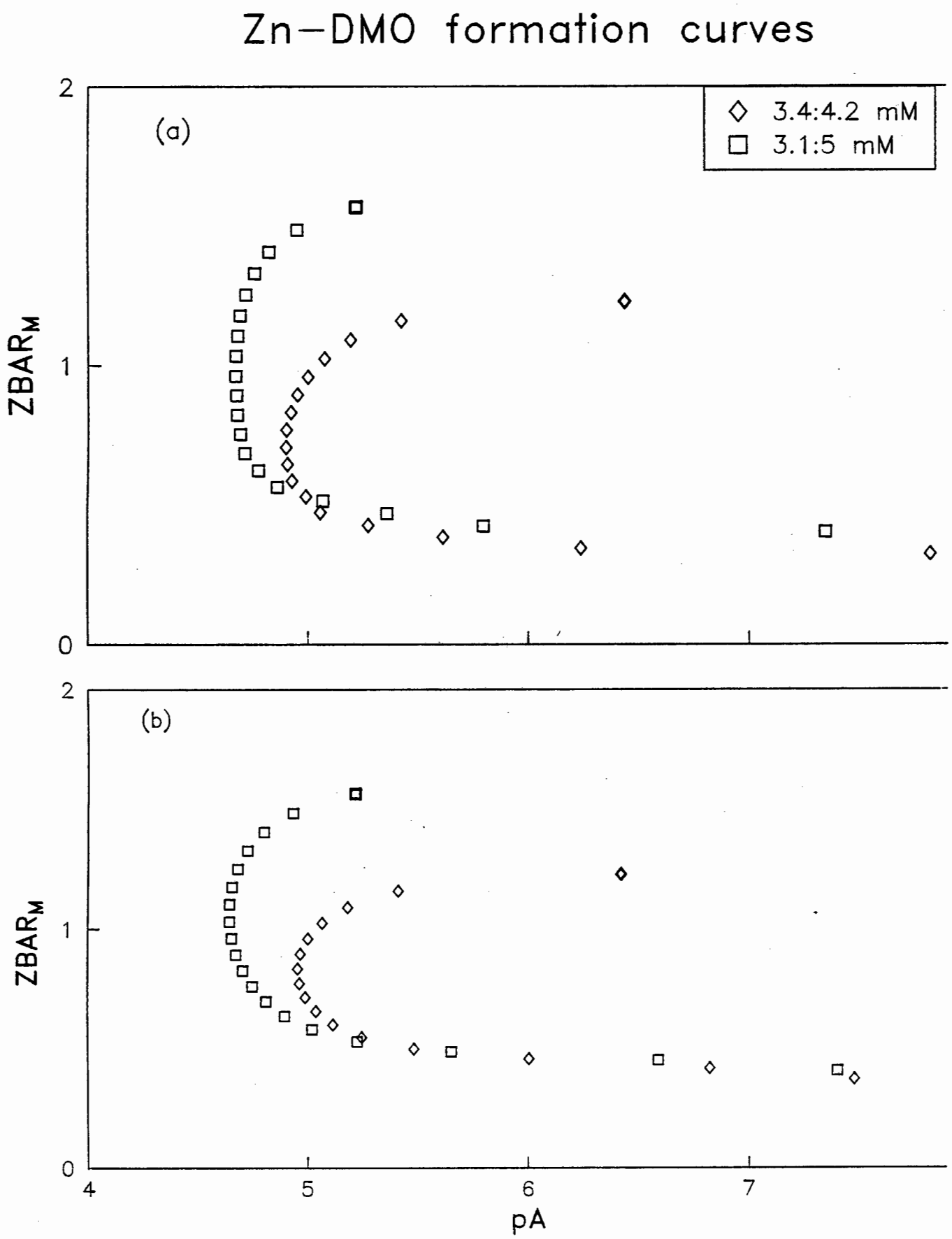

FIGURE 13 : Experimental (a) and theoretical (b) curves for the Zn-DMO system at 25°C and 0.15M (Na) Cl

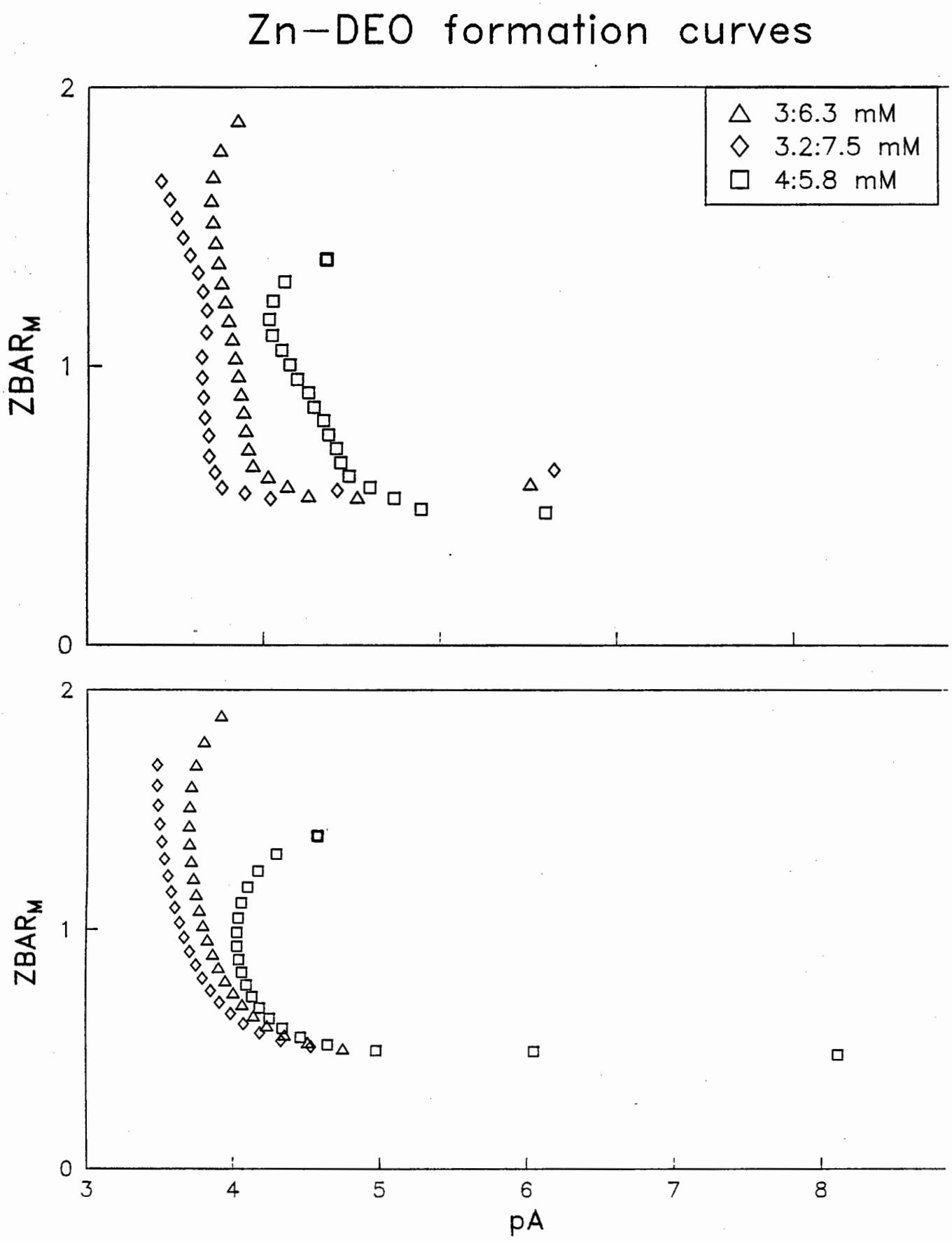

FIGURE 14 : Experimental (a) and theoretical (b) curves for the Zn-DEO system at 25°C and 0.15M (Na) Cl

TABLE 4

Logarithms of the overall formation constants, β_{pqr} for the Zn-DMO and -DEO systems, determined in this study at 25°C and 0.15 mol.dm^{-3} Na[Cl]

Pkw used = 13.59

ligand	pqr	β_{pqr}	U	R	pH range
DMO	111	12.12 ± 0.01	64.5	0.014	3 - 7.5
	11-1	-0.73 ± 0.03			
	11-2	-4.93 ± 0.01			
DEO	111	13.47 ± 0.02	79.9	0.17	3 - 8
	11-1	1.17 ± 0.02			
	11-2	-6.55 ± 0.06			

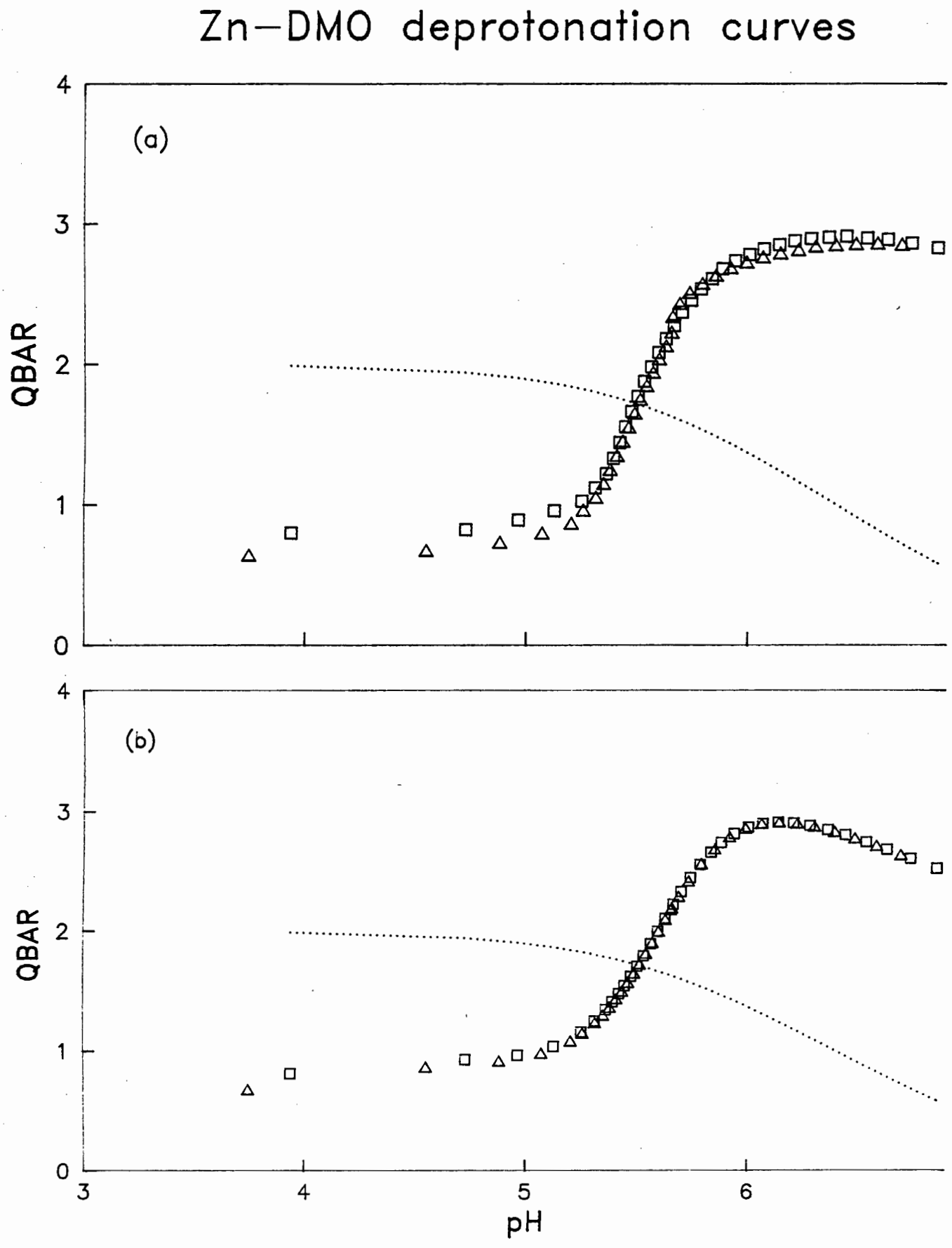

FIGURE 15 : The (a) experimental and (b) curves of $\bar{Q}$ vs pH for the Zn-DEO system at 25°C and 0.15M (Na) Cl
.... = n vs pH

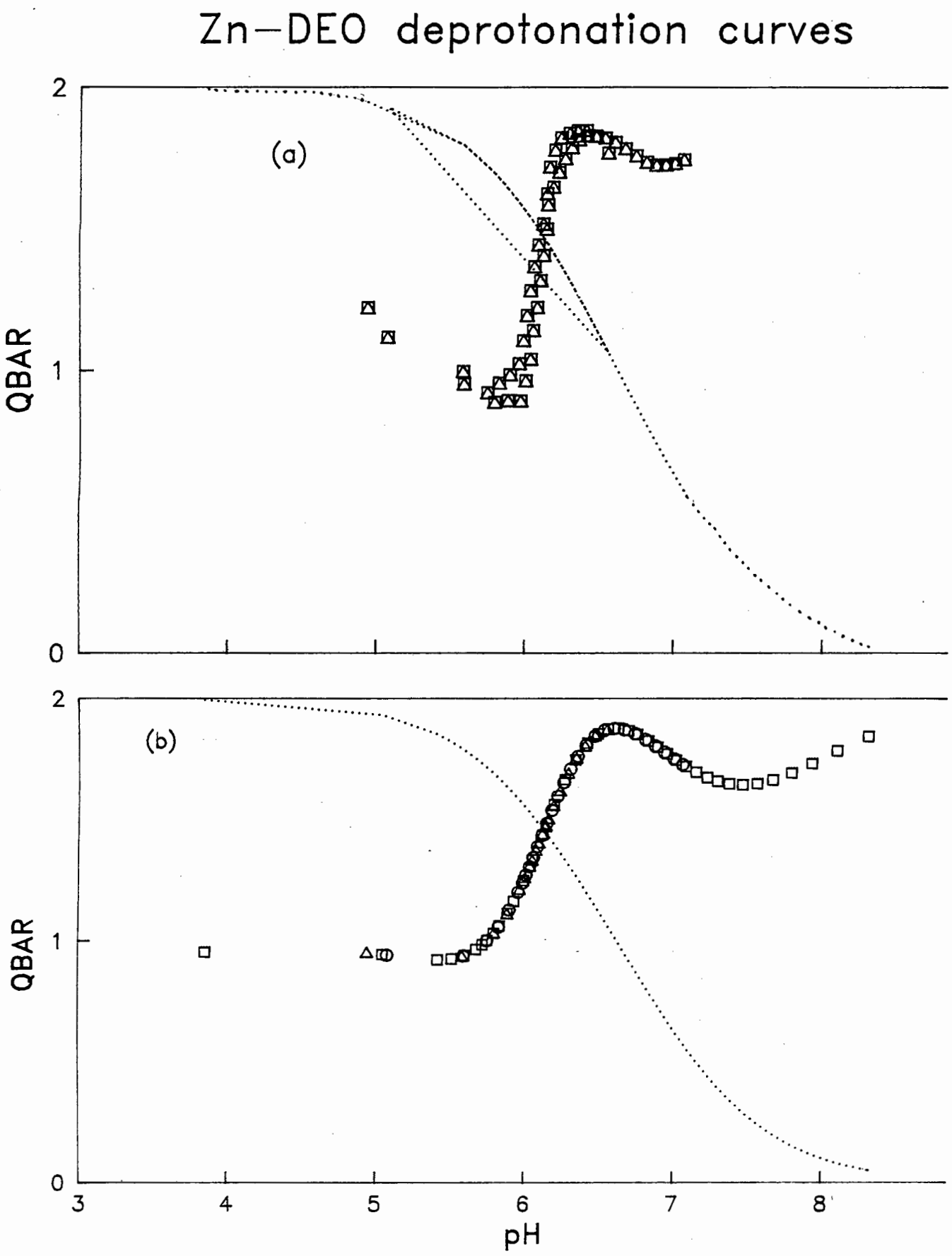

FIGURE 16 : The (a) experimental and (b) theoretical deprotonation curves of Q vs pH for the Zn-DEO system at 25°C 0.15M (Na) Cl. ... = n vs pH

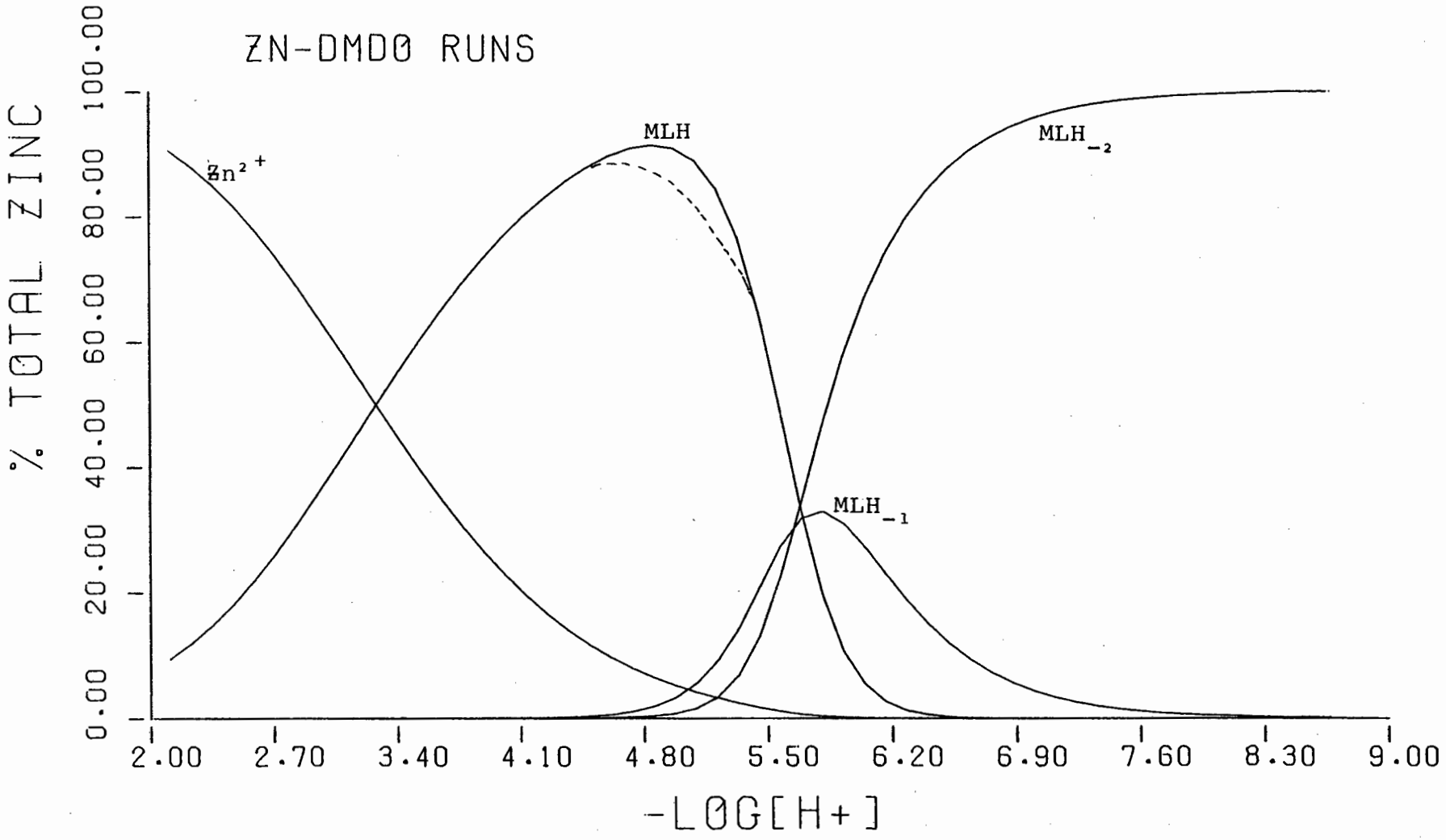

FIGURE 17 : The species distribution curves for the Zn-DMO system showing the percentage of zinc in each species in 1 : 1 ligand-to-metal solution at a concentration of 4mM.

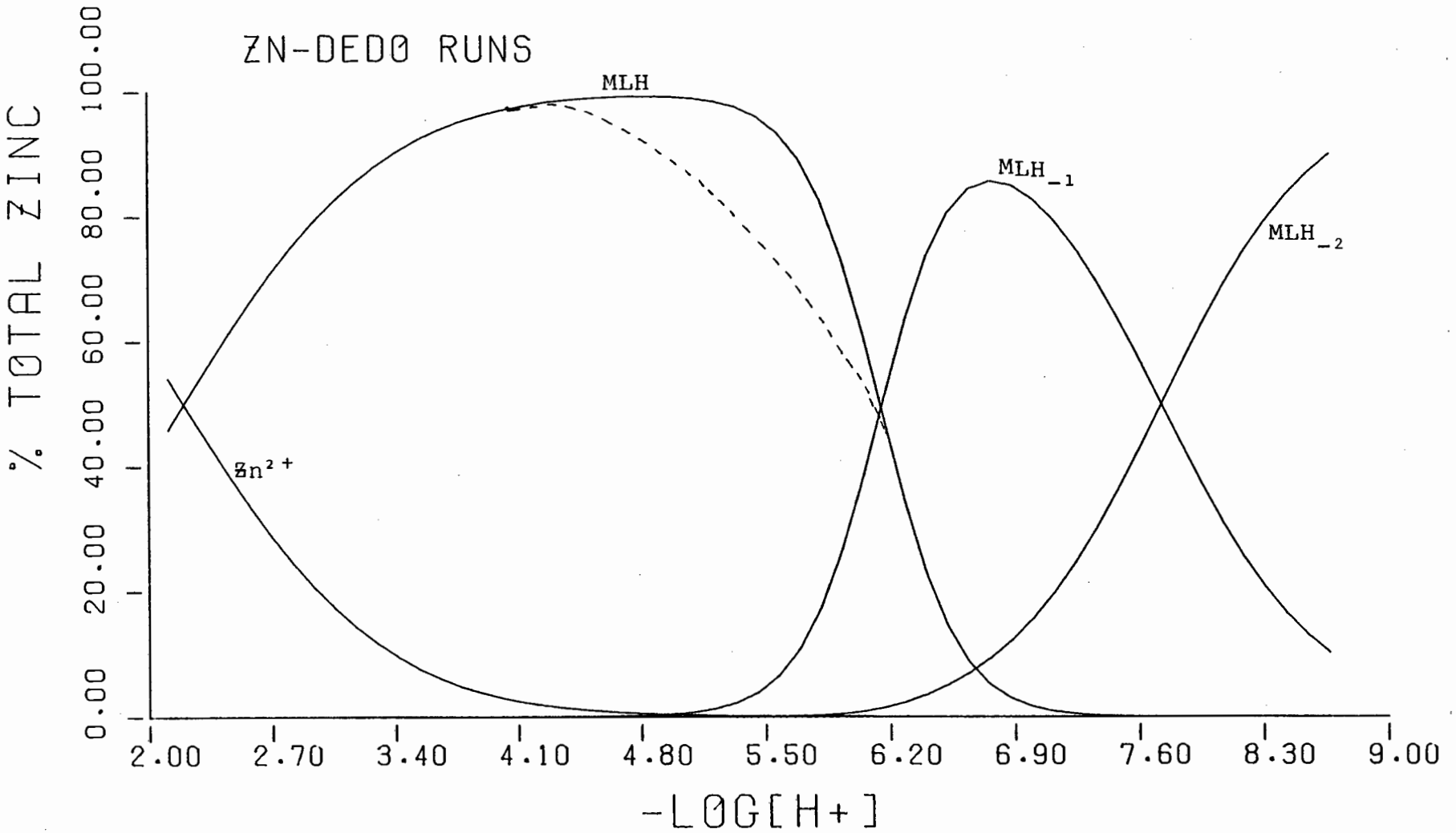

FIGURE 18 : The species distribution curves for the Zn-DEO system showing the percentage of zinc in each species in 1 : 1 ligand-to-metal solution at a concentration of 4mM.

3.5.4 Calcium

Figures 19 and 20 show the formation curves for the Ca-DMO and -DEO systems respectively. The symbols represent different metal to ligand concentrations. In both systems the curves are superimposable, showing no existence of polynuclear species. However, the two systems are different in the complexation ability of their ligands.

Consider the Ca-DEO system first. There is a stepwise formation sequence up to $\bar{Z}$ values of 1. In the low pA region deprotonation is seen to take place, evident in the backward fanning of the titration curves. For the equilibrium

$$MLH \rightleftharpoons ML + H^+$$

the pKa value for the deprotonation of the complex is 4.9, whereas the pKa_1 for DEO is 7.04. This decrease in the pKa upon coordination of the metal ion cannot be due to an inductive effect of the Ca^{2+} ion, for coordination is occurring at the end of the molecule and deprotonation is occurring at the other end. (See page 59)

This would mean that it is not the protonated amine that gets deprotonated but the amide nitrogen.

The observed model is an accepted one as the theoretical and observed curves, Figures 20(b) and (a) respectively, are similar. The theoretical curve was plotted using the formation constants in Table 5.

The statistics of the constants are very good, also showing agreement between the two subsystems.

Figure 22 shows the deprotonation curves of the Ca-DEO system. At the beginning of the titrations, the $\bar{Q}$ = 1 and $\bar{n}$ = 2 indicating that effectively one proton of the four that the ligand is capable of losing, has been lost due to complexation with calcium. As the titration progresses more protons are lost with $\bar{Q}$ = 3 and $\bar{n}$ = 1 implying that this is the MLH_{-1} region with one proton still attached to the ligand. Finally, $\bar{Q}$ = 2 and $\bar{n}$ = 0 when all four protons have been lost.

Figure 24 shows the species distribution at different pH values. They represent the percentage of the Ca^{2+} ion present in each species. In agreement with the $\bar{Q}$, it can be seen that at the beginning of the titration 40% of calcium has been used up in the formation of the MLH species. The

ML species, though present, is a minimal amount with less than 20% of the maximum of calcium forming this species.

For the Ca-DMO system, a totally different process is observed. Firstly, there is only the formation of the MLH and ML species. Secondly, the pKa for the deprotonation of the complex is 5.9 which is one log unit lower than pKa_1 of DMO. This could imply that the nitrogens involved in the complexation are the amine nitrogens and that there is no deprotonation of the amide protons. However, this is not possible in the light of the following discussion.

Consider the Irving-Williams series [103]. This series which is from Ba^{2+} to Cu^{2+} is a measure of increasing acidity of the metal which is due to the decreasing size of the metal ion. Incorporated in this is the factor of hardness and softness of the metal ions and ligands. This factor states that the greater the number of d electrons, the greater is the tendency to favour S > N > O ligand in complex formation. The alkali earth metals of which calcium is one, and other metal ions that have few or no d electrons prefer to bind in the order O > N > S. Calcium is a hard acid [99] and so is nitrogen because of its small size, but because of the presence of the polarisable substituents attached to it, the behaviour changes. The change is to the softness of the series. With the addition of an electron withdrawing substituent, the softness is

reduced [99]. However, both DMO and DEO have similar substituents on their nitrogens, and in fact DEO should be softer than DMO because of the larger alkyl group attached to the amine. To explain why this observation is not seen, inductive and steric effects must be introduced. Due to the "stacking" of the ethyl groups, the electron cloud is confined to a particular region in the amine, whereas the methyl groups which are free to "sweep" around the amine nitrogen make the area of the electron cloud wider thus this process and the inductive effect make the DMO a soft base. This phenomenon is comparable to ethylenediamine [104]. The soft electropositive hydrogens make the nitrogens soft [99]. (See Figure 25)

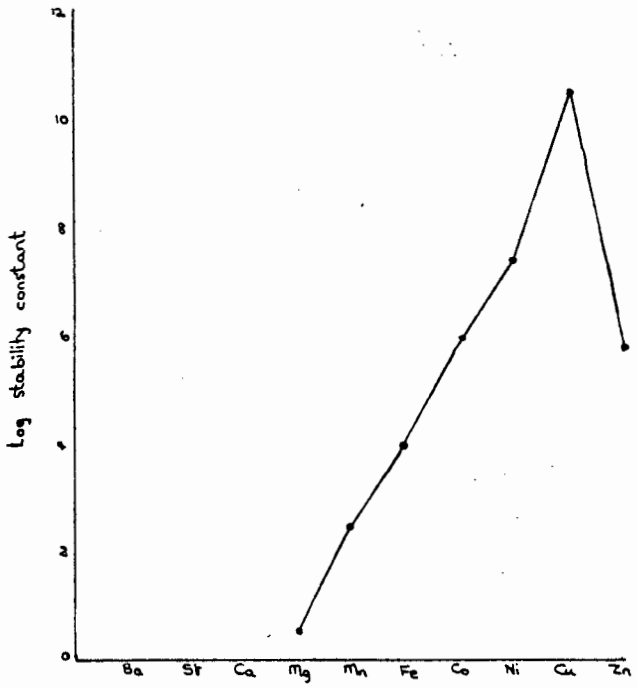

FIGURE 25 : The Irving-Williams effect showing the stability of ethylenediamine with the series Ba-Zn

This discussion, however, has been on the amine nitrogens only. The amide nitrogens, although they are having

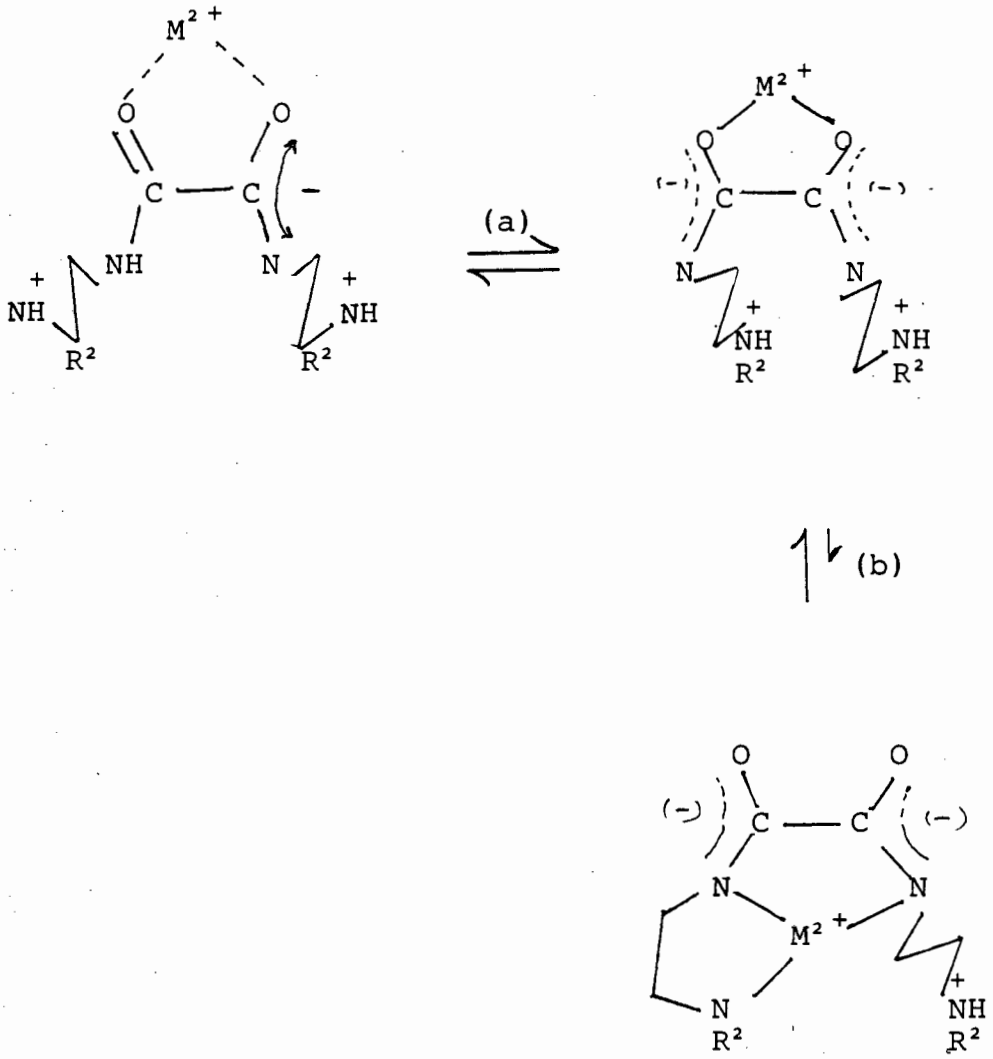

SCHEME 1 : Possible reaction mechanism for the hard acid Ca^{2+} with DMO.

The reaction (a) cannot be detected potentiometrically. ^{13}C NMR studies were tried but could not enlighten the situation.

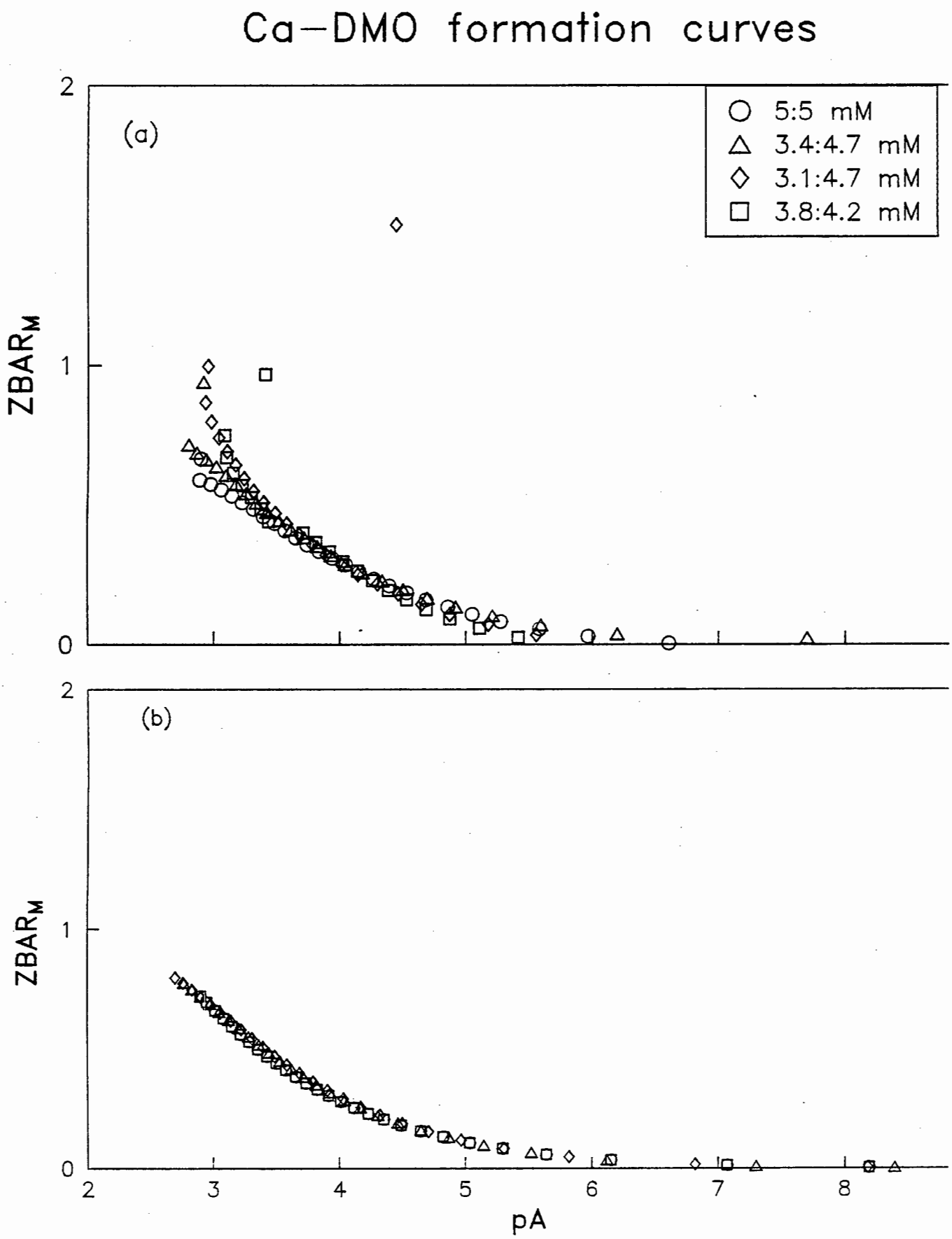

FIGURE 19 : The (a) experimental and (b) theoretical curves for the Ca-DMO system at 25°C and 0.15M (Na) Cl

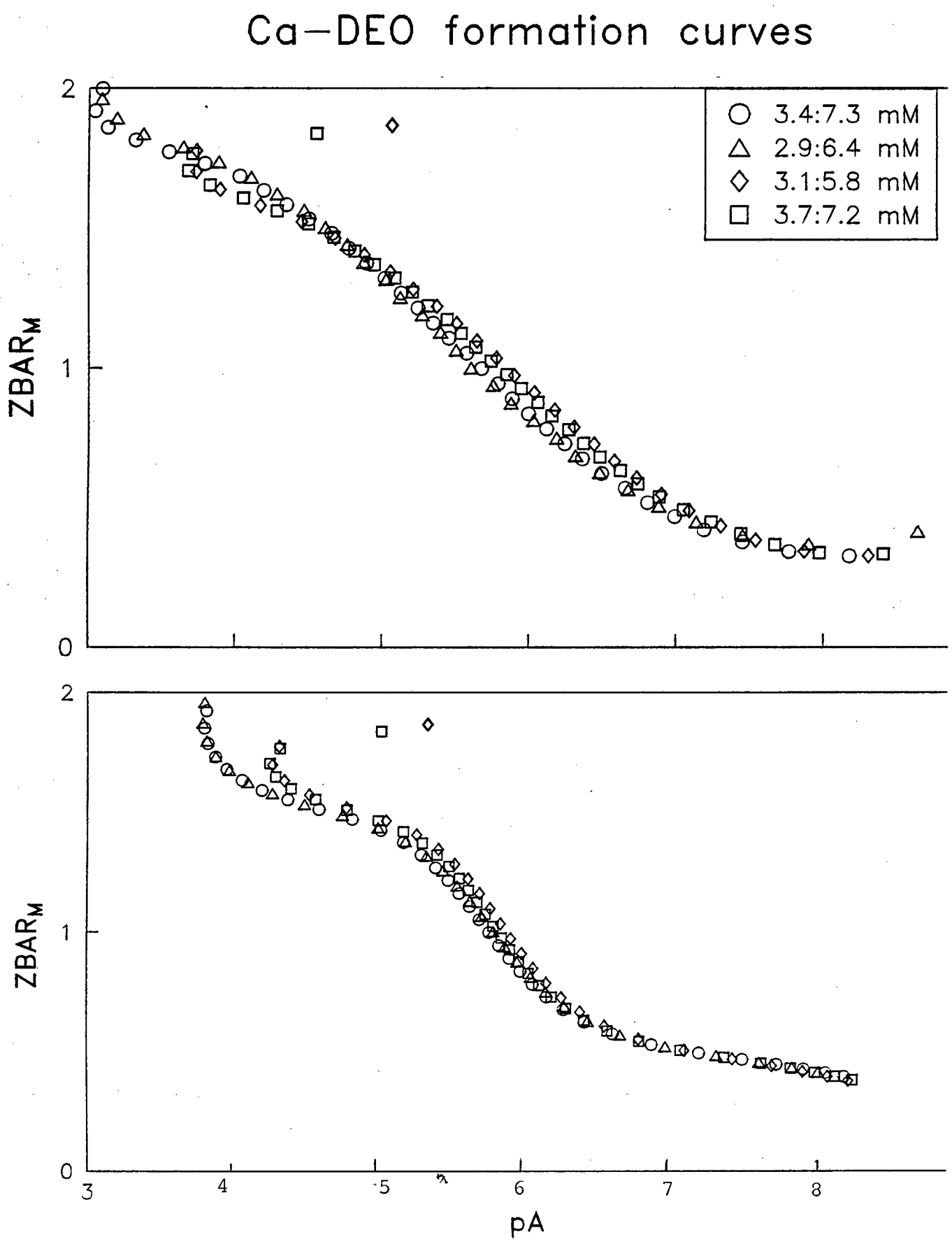

FIGURE 20 : The (a) experimental and (b) theoretical curves for the Ca-DEO system at 25°C and 0.15M (Na) Cl

TABLE 5

Logarithms of the overall formation constants, β_{pqr} for the Ca-DMO and -DEO systems, determined in this study at 25°C and 0.15 mol.dm^{-3} Na[Cl]

Pkw used = 13.59

ligand	pqr	β_{pqr}	U	R	pH range
DMO	110	3.64 ± 0.01	29.8	0.09	3 - 8.0
	111	9.49 ± 0.03			
DEO	110	8.427 ± 0.07			
	111	13.334 ± 0.02			
	11-1	4.289 ± 0.03			
	11-2	-2.876 ± 0.05			

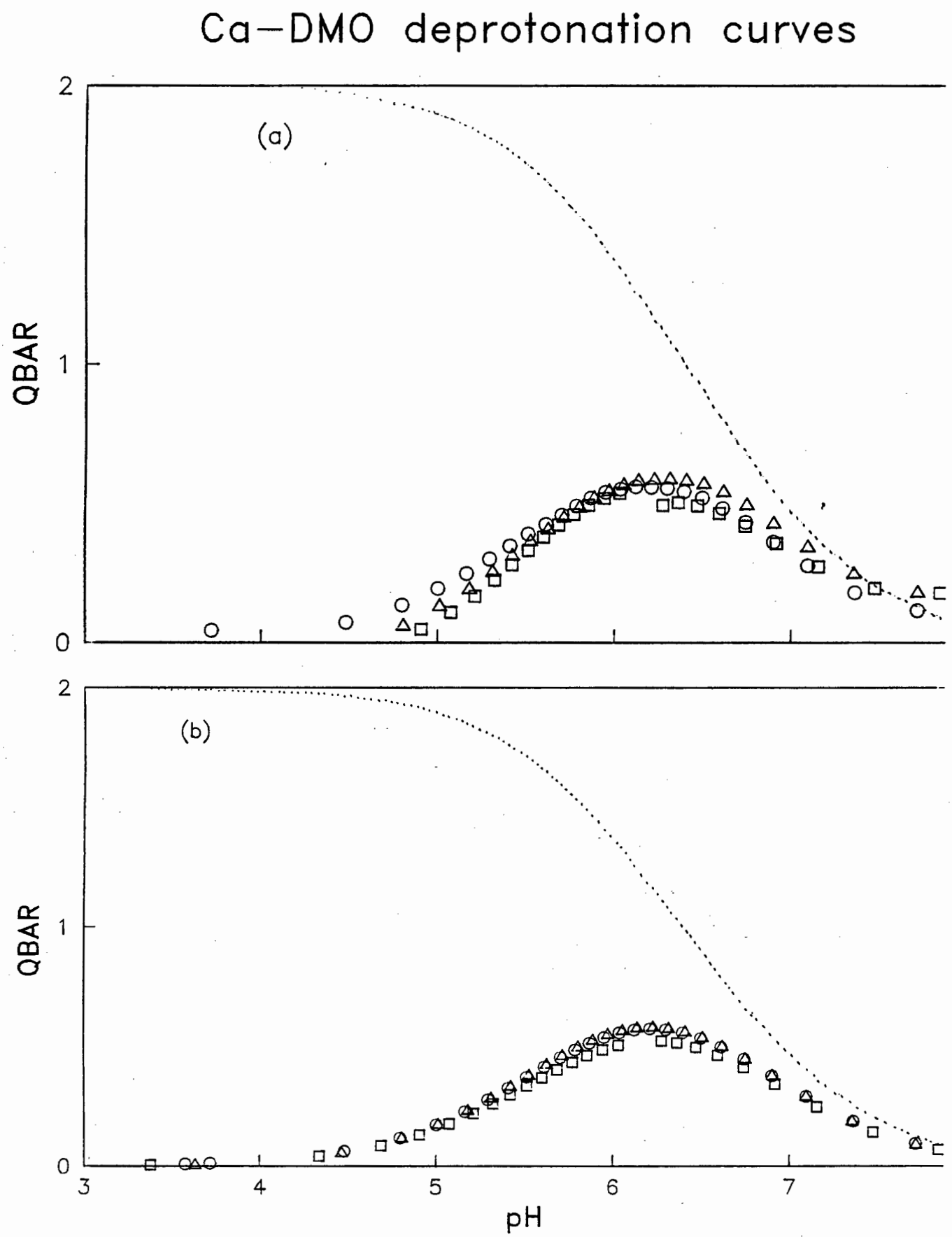

FIGURE 21 : The (a) experimental and (b) theoretical deprotonation curves of $\bar{Q}$ vs pH for the Ca-DMO system at 25°C and 0.15M (Na) Cl . ... = $\bar{n}$ vs pH

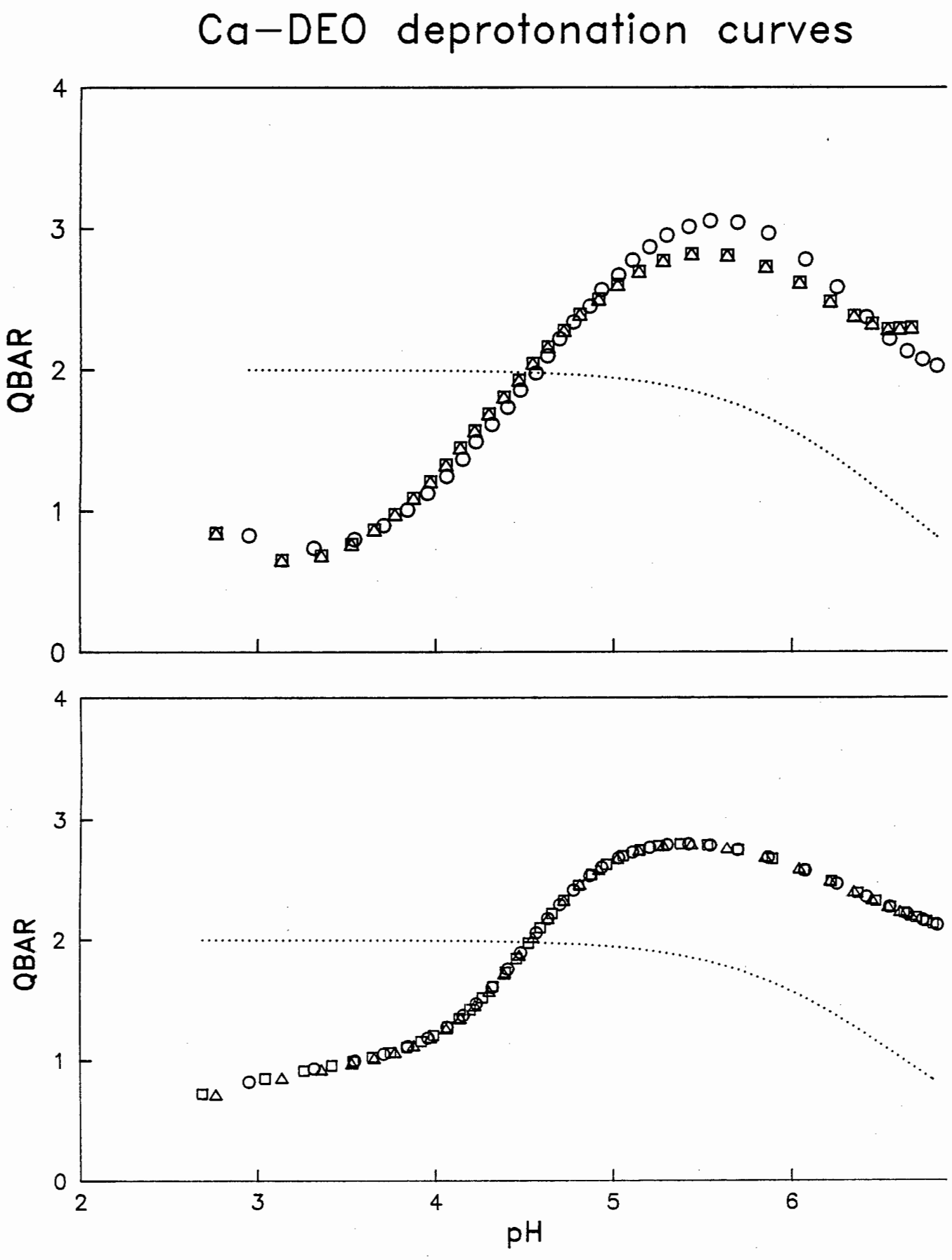

FIGURE 22 : The (a) experimental and (b) theoretical deprotonation curves of $\bar{Q}$ vs pH for the Ca-DEO system at 25°C and 0.15M (Na) Cl . ... = $\bar{n}$ vs pH

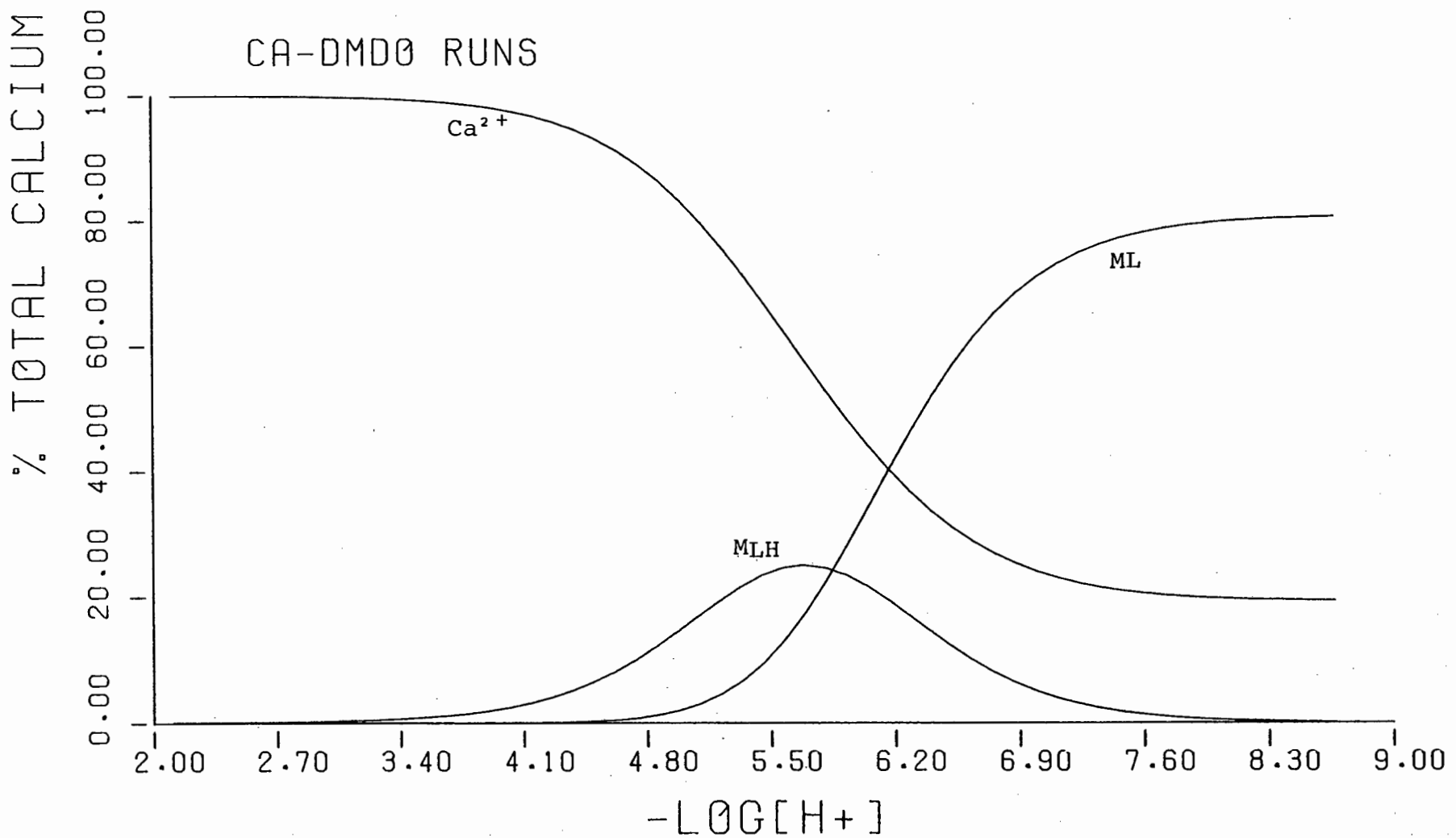

FIGURE 23 : The species distribution curves for the Ca-DMO system showing the percentage of calcium in each species in 1 : 1 ligand-to-metal solution at a concentration of 4 mM.

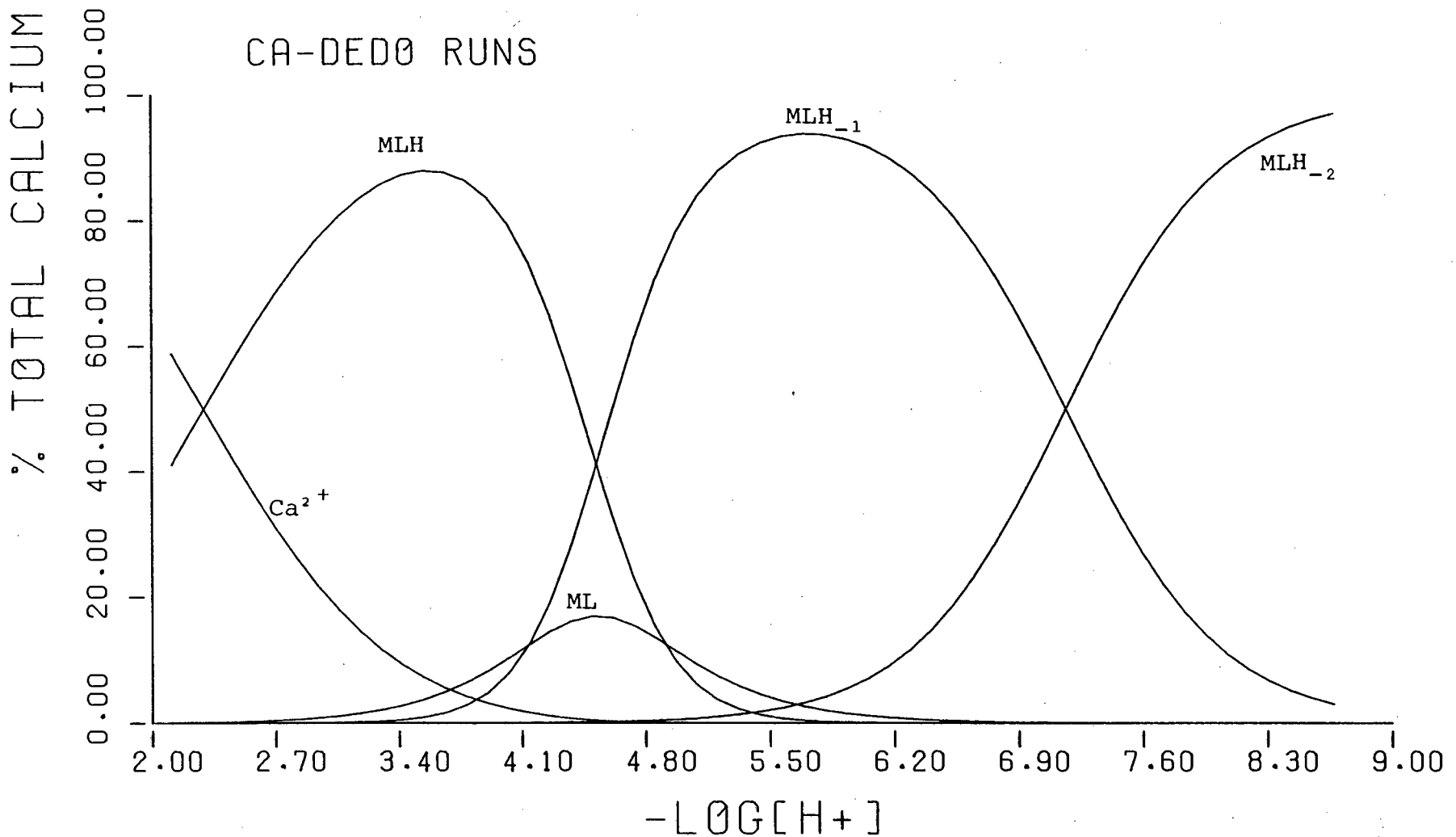

FIGURE 24 : The species distribution curves for the Ca-DEO system showing the percentage of calcium in each species in 1 : 1 ligand-to-metal solution at a concentration of 4mM.

substituents that are electropositive, experience the remote action of the electrowithdrawing oxygen thus making these nitrogens hard. In taking this discussion it could mean that of the four protons on the ligand, the amide ones are those lost during complexation (see scheme).

The theoretical curve (Figure 19(b)) has been plotted using the formation constants in Table 5. There is good agreement in both the curves and in the statistics of the constants with an objective function of 30 which is much lower than 100. Figure 21 shows the deprotonation curve. At the beginning of the titration $\bar{Q} = 0$ and $\bar{n} = 2$ indicating that there is no complexation. The $\bar{Q}$ does not rise to $\bar{Q} = 3$ which means that only a total of two protons out of the four has been lost at the end of the titration. Figure 23 shows the species distribution. This indicates the amount of calcium which is in complex form. It can be seen that even at pH 8, 20% of the calcium is still uncomplexed.

3.5.5 Magnesium

Figures 26 and 27 show the formation curves for the Mg-DMO and -DEO systems. The symbols represent different metal to ligand concentrations. In both systems the curves are superimposable showing no existence of polynuclear species. The shape of the curve shows a least tendency towards metal-ligand binding. There is, however, evidence of backward

fanning which is usually indicative of deprotonation of the complex, forming species like MLH_{-1}, or MLH_{-2}. Only the MLH_{-1} species could be detected in the low pA region. Although not evident in the shape of the curves there is weak stepwise formation of the species of the form

$$MLH \rightleftharpoons ML + H^+$$
$$ML \rightleftharpoons MLH_{-1} + H^+$$

These are obviously weak complexes as the curves do not show any considerable complexation. The theoretical curves 26(b) and 27(b), which were plotted using the formation constants in Table 6, show good agreement with the experimental curves.

Table 6 shows the overall formation constants obtained in this study. The statistics of the constants is low giving confidence that the chosen model is a true representation of the species in solution.

The constants of the Mg-DEO system are lower than those of the Mg-DMO system. This is in accordance with the pKa values of DEO being higher than those of DMO. Therefore, the lowered metal complex stability could be attributed to the inductive effect of the ethyl groups on the amine nitrogen.

For the DEO equilibrium

$$MLH \rightleftharpoons ML + H^+$$

it can be seen that the pKa is 6.8 which is about 0.2 log units less than pKa of the ligand. This value gives reason to believe that coordination is via the two amine nitrogens with the Mg^{2+} ion inducing the deprotonation of the second proton. Therefore the third deprotonation to give the MLH species is occurring on the amide nitrogen. A similar argument holds for the Mg-DMO system. The pKa for the deprotonation of the complex is 5.9 whereas the pKa_1 is 6.8, a difference of 0.9 log units. Although this value is higher than 0.2 log units for the Mg-DEO system, it is still acceptable in the above argument.

Comparing the stability of Mg and Ca, both these are alkali earth metals. It has been found that the formation constants for Mg are lower than those of Ca. The usual trend in the complex stability of the alkali earth metals is Mg > Ca > Sr > Ba. [105] This exception to the rule has also been observed in the Ca-EDTA and Mg-EDTA stability constants. [105] The reason given is that coordinating a small ion like Mg^{2+} with such a large ligand EDTA is difficult. The same reasoning could be applied here with DEO being too large a ligand to coordinate well with Mg. However, the DMO complexes for both Ca and Mg have similar

formation constants with Mg being stronger and forming MLH_{-1}.

Figures 28 and 29 show the deprotonation curves. At the beginning of the titration $\bar{Q} = 0$ and $\bar{n} = 2$ implying that there is no complexation. In the case of DEO it is only above pH6 that $\bar{Q}$ begins to rise and complexation takes place. Before intersection of the $\bar{Q}$ and $\bar{n}$ curves, ML or MLH species are formed but after the two curves intersect, the presence of deprotonated species is indicated. For these systems, the deprotonation function is not as easy to interpret as the $\bar{Z}$ function. This is particularly so for the DMO system where $\bar{Q}$ is seen to rise and then fall. This decrease in $\bar{Q}$ is due not to a decrease in complexation but a decrease in the number of protons which can be displaced (i.e. $\bar{n}$).

Figures 30 and 31 show the species distribution. This indicates the amount of magnesium which is in complex form. For the Mg-DMO system the predominant species is ML, whereas for the Mg-DEO system none of the species is dominant. In the high pH region MLH_{-1} shows the possibility of being the dominant species.

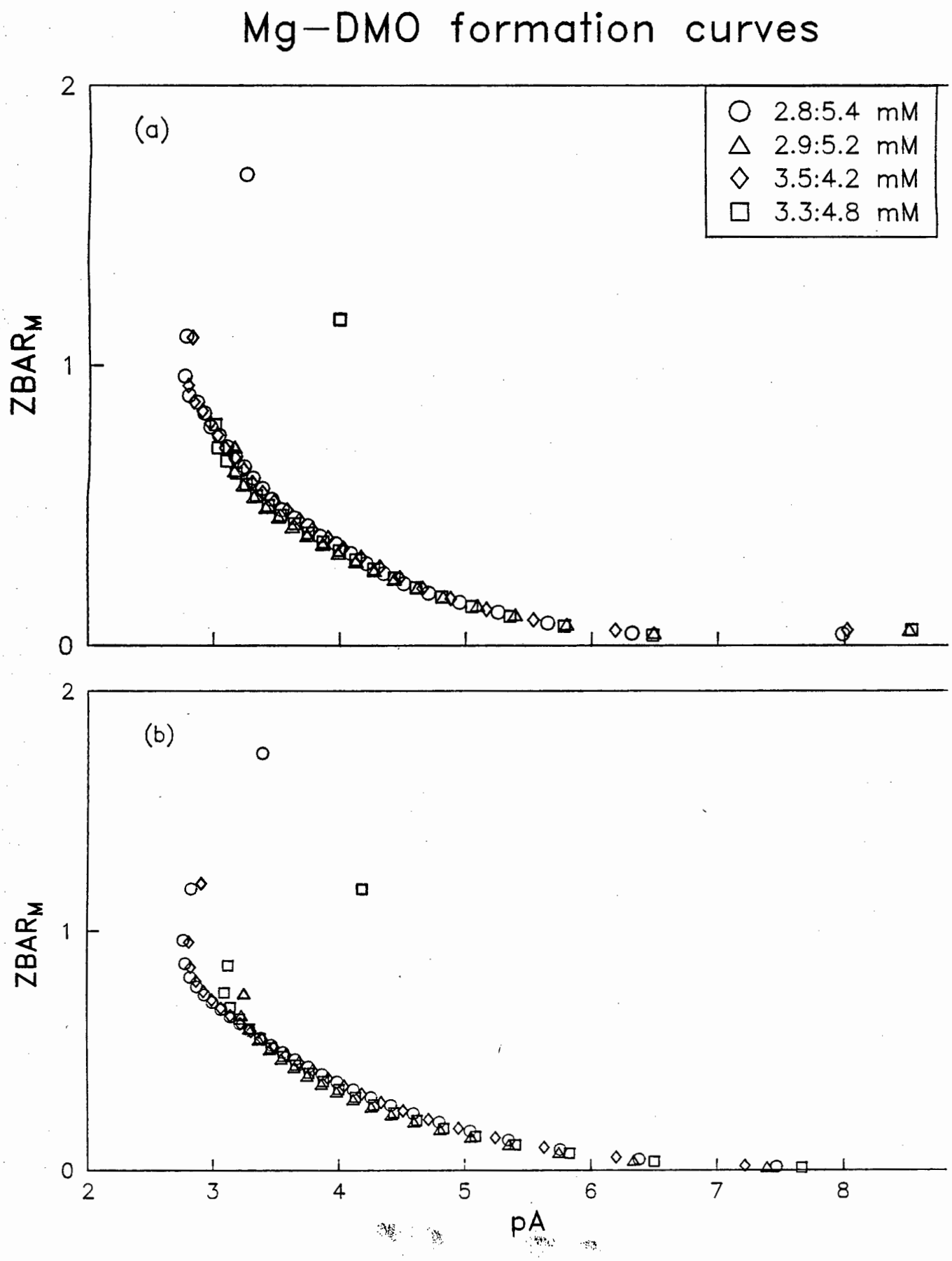

FIGURE 26 : The (a) experimental and (b) theoretical curves for the Mg-DMO system at 25°C and 0.15M (Na) Cl

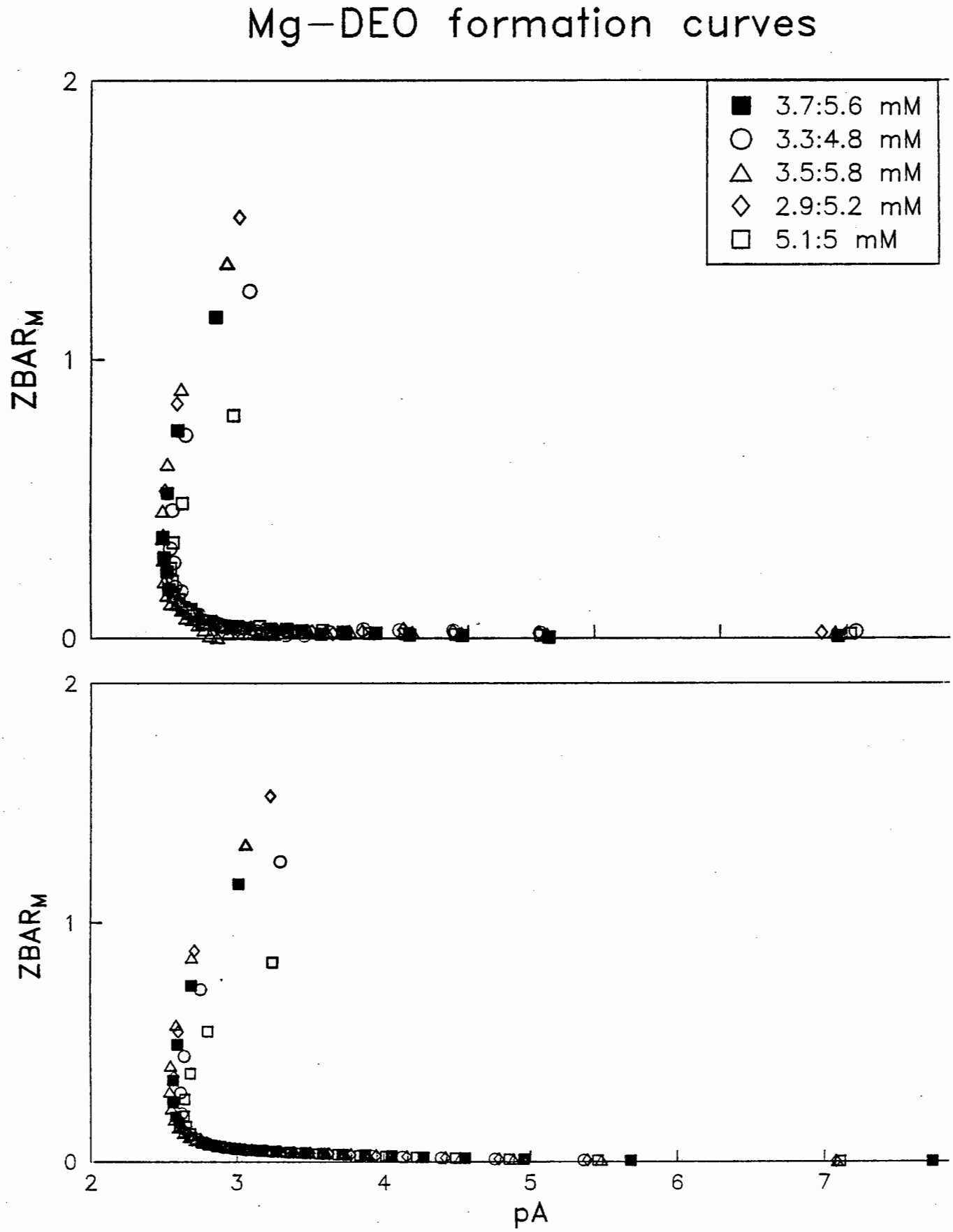

FIGURE 27 : The (a) experimental and (b) theoretical curves for the Mg-DEO system at 25°C and 0.15M (Na) Cl

TABLE 6

Logarithms of the overall formation constants, β_{pqr} for the Mg-DMO and -DEO systems, determined in this study at 25°C and 0.15 mol.dm^{-3} Na[Cl]

Pkw used = 13.59

ligand	pqr	β_{pqr}	U	R	pH range
DMO	110	3.82 ± 0.001	72,9	0.07	3 - 8.5
	111	9.74 ± 0.01			
	11-1	-4.65 ± 0.02			
DEO	110	1.74 ± 0.05	38.5	0.04	3 - 8.5
	111	8.56 ± 0.05			
	11-1	-5.95 ± 0.01			

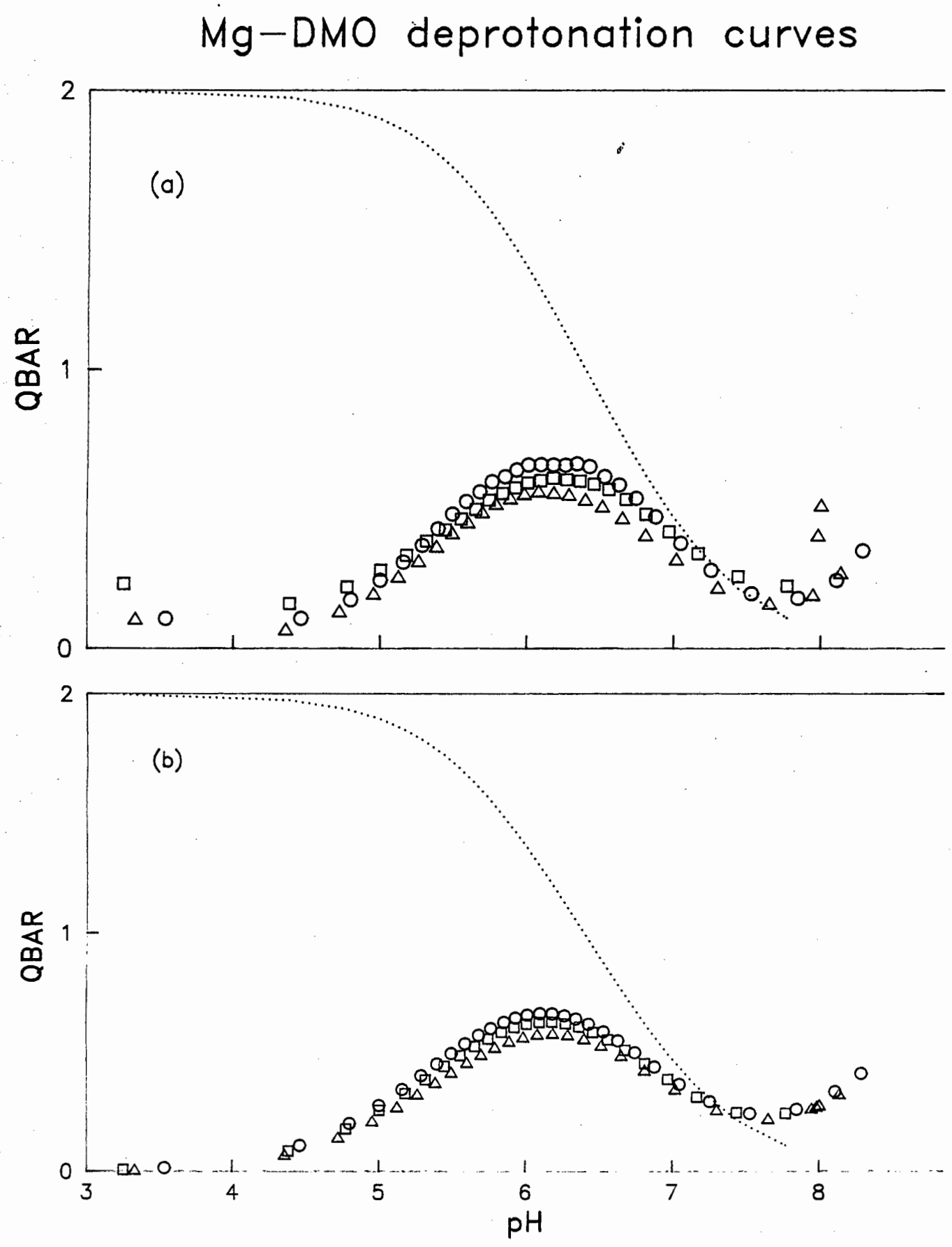

FIGURE 28 : The (a) experimental and (b) theoretical deprotonation curves for the Mg-DMO system at 25°C and 0.15M (Na) Cl ... = n vs pH

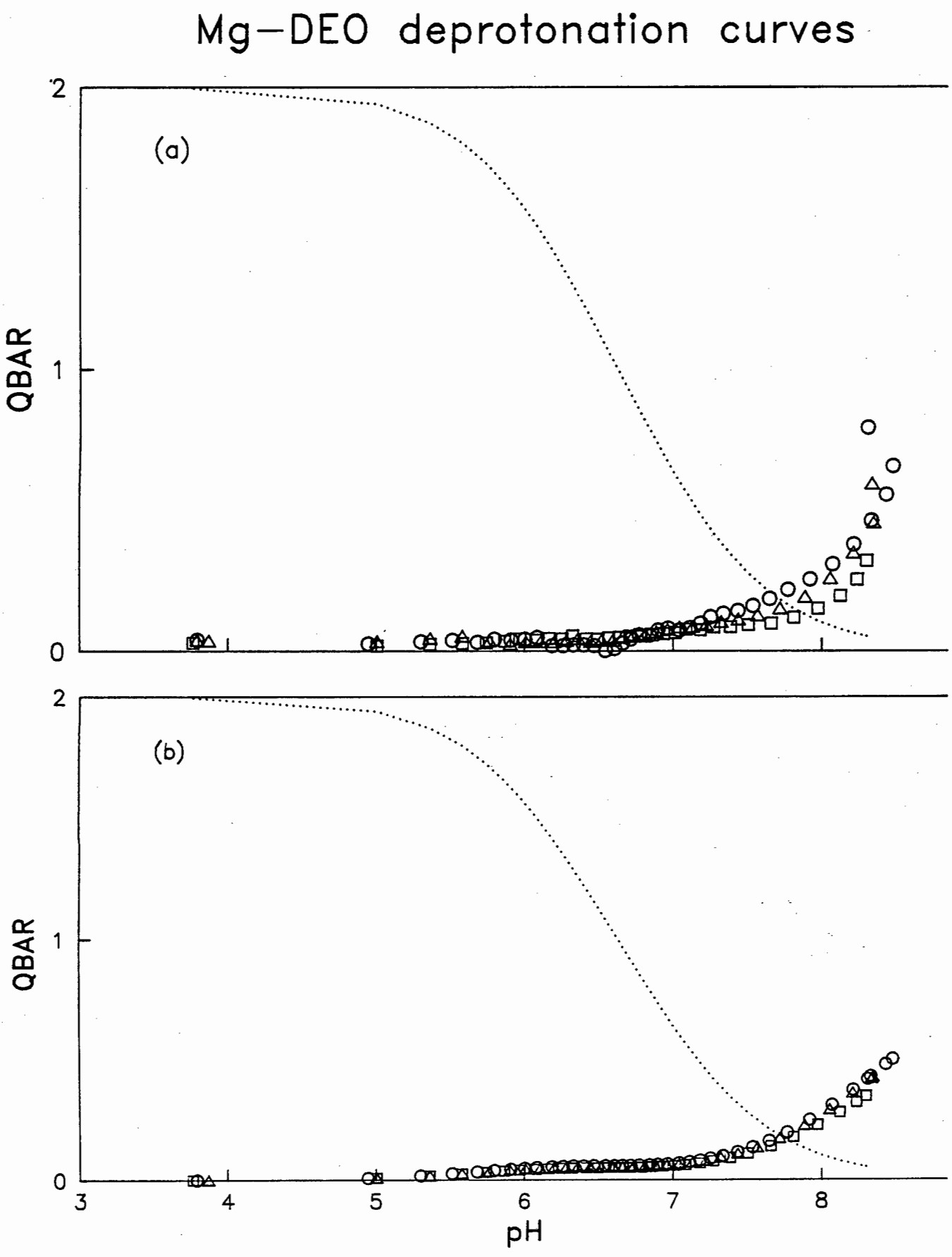

FIGURE 29 : The (a) experimental and (b) theoretical deprotonation curves for the Mg-DEO system at 25°C and 0.15M (Na) Cl ... = n vs pH

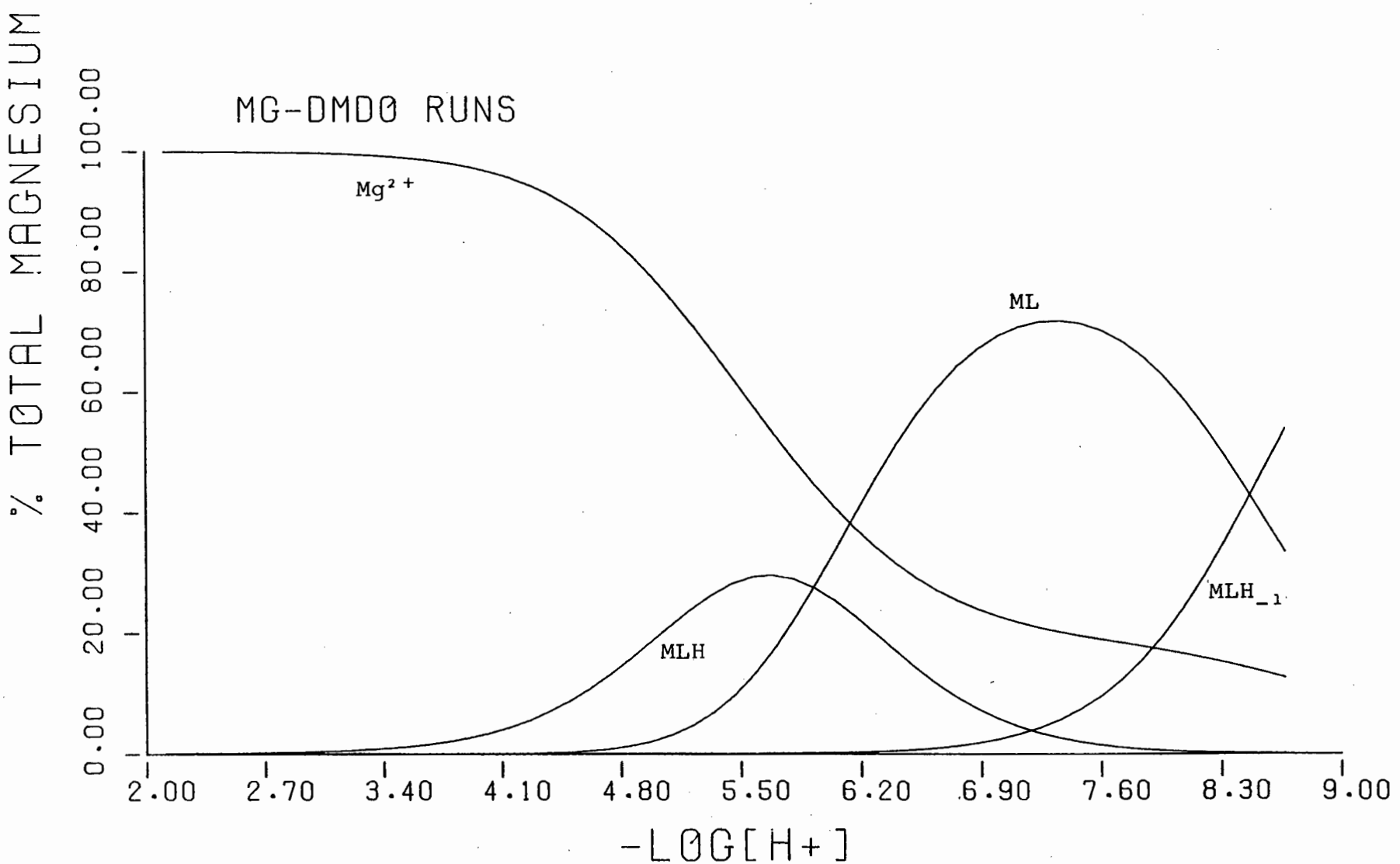

FIGURE 30 : Species distribution curves for the Mg-DMO system at a concentration of 4mM.

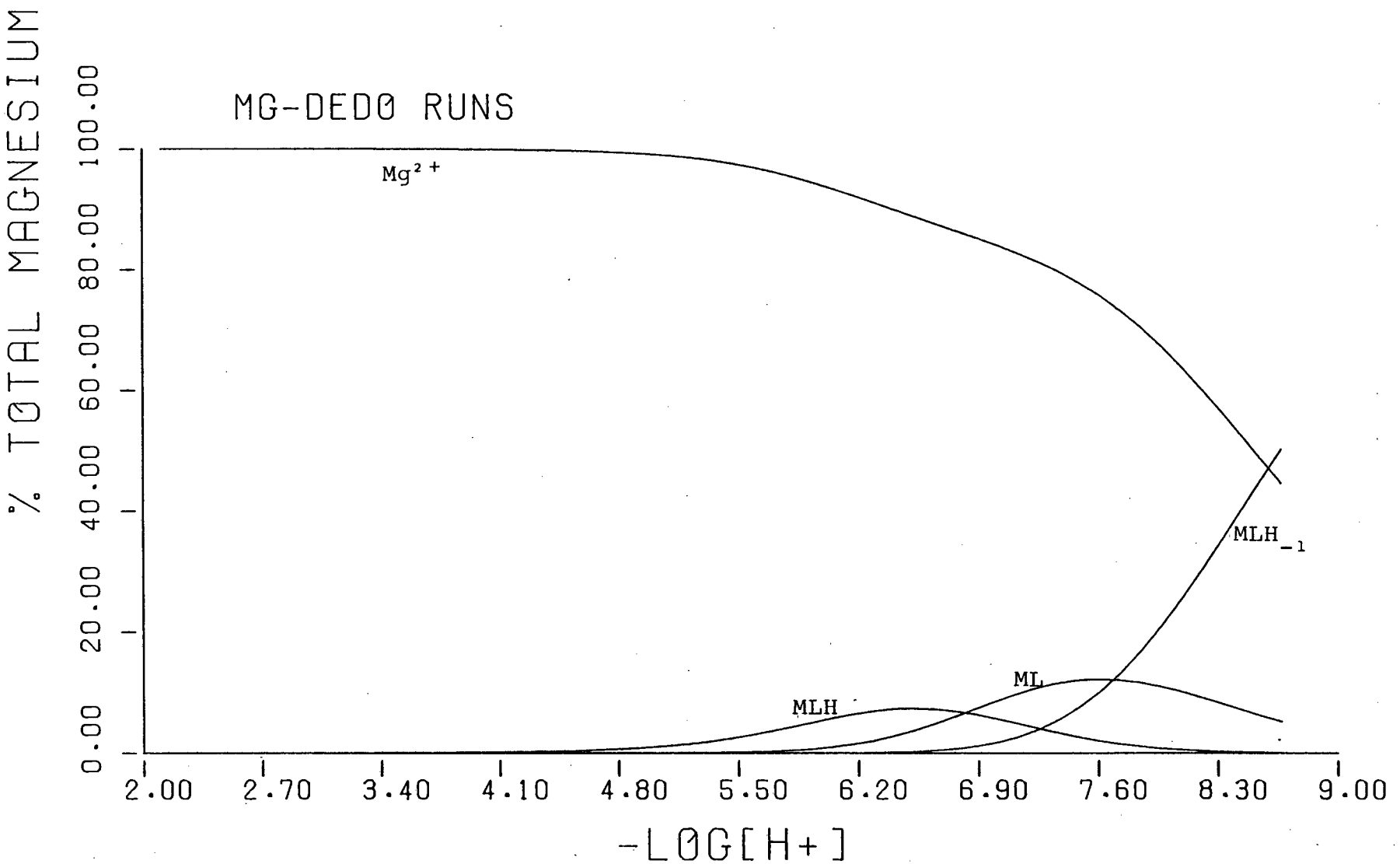

FIGURE 31 : Species distribution curves for the Mg-DEO system at a concentration of 4mM.

3.5.6 Manganese

Figures 32 and 33 show the formation curves for the Mn-DMO and -DEO systems. The symbols represent metal to ligand concentrations. Like the Mg-DMO and -DEO systems the shape of the curves shows least tendency toward complexation. In both systems the curves are superimposable showing no existence of polynuclear species. In the backward fanning of the curves the species that could be detected is the MLH_{-1} only. Figures 32(b) and 33(b) show the theoretical curves plotted using the constants in Table 7. There is good agreement between the two subsystems.

Table 7 shows the overall formation constants obtained in this study. The models chosen for the systems are the true reflection of the species in solution. This is indicated by the statistics of the formation constants. The constants are so close to those of the Mg-DMO and -DEO systems that similar arguments apply in these Mn-DMO and -DEO systems. However, in the Mn-DEO system the ML species could not be detected without causing high error in the statistics. Therefore the simple model was chosen.

For the DMO equilibrium

$$MLH \rightleftharpoons ML + H^{+}$$

The pKa value is 5.82 while pKa_1 of the ligand is 6.8. The difference between the two pKa's is 0.98 which is acceptable for the argument that coordination occurs at the amine first. The inductive effect of the Mn^{2+} ion enhances the loss of the second proton faster than in protonation. The constants for the species MLH and MLH_{-1} in both systems are equal. This means that there is most likely a property that contributes to the weakness of the complexes which is not the same as in the other metal ions studied.

Mn has properties that are similar to Fe. Mn is capable of a number of oxidation states and is also fairly electropositive. Usually the metal ion Mn^{2+} forms complexes which possess high spin $3d^5$MnII, hence there is no ligand field stabilisation energy. [106] Due to this property Mn^{2+} forms complexes with low stability constants, lower than Fe^{2+} through to Cu^{2+}.

Figures 34 and 35 show the deprotonation curves. As in the protonation curves, only one inflection is evident for the loss of two amine protons. When n = 1 there is one proton left on the ligand out of the four the ligand is capable of losing. The $\bar{Q}$ and $\bar{n}$ intersect at $\bar{Q}$ = 1. At this stage three protons have been lost from the ligand due to complexation. At the end of the titration the curves are vertical showing precipitation.

Figures 36 and 37 show the species distribution indicating the amount of manganese present in each species. In both systems the dominant species is the MLH_{-1}.

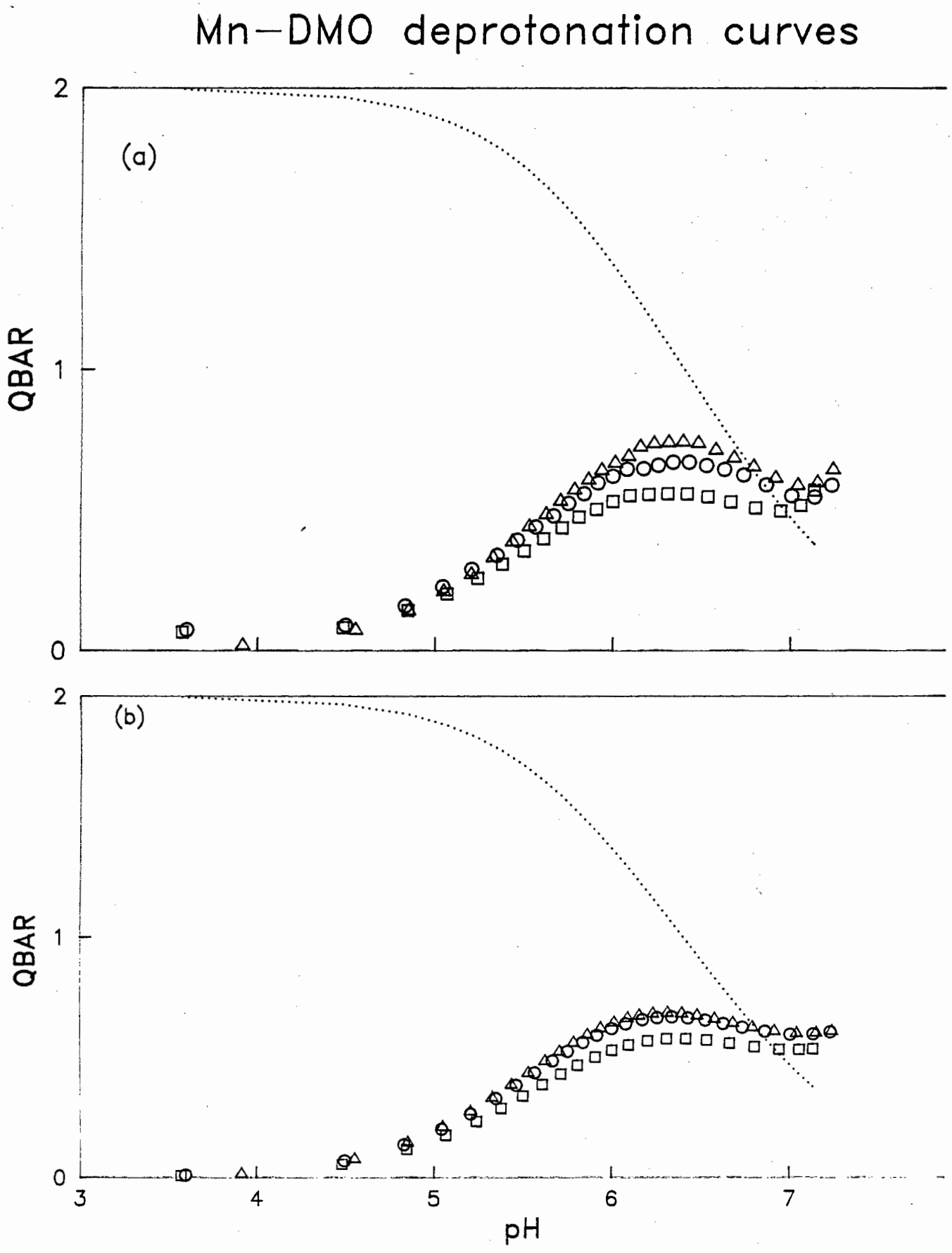

FIGURE 34 : The (a) experimental and (b) theoretical deprotonation curves for the Mn-DMO system at 25°C and 0.15M (Na) Cl

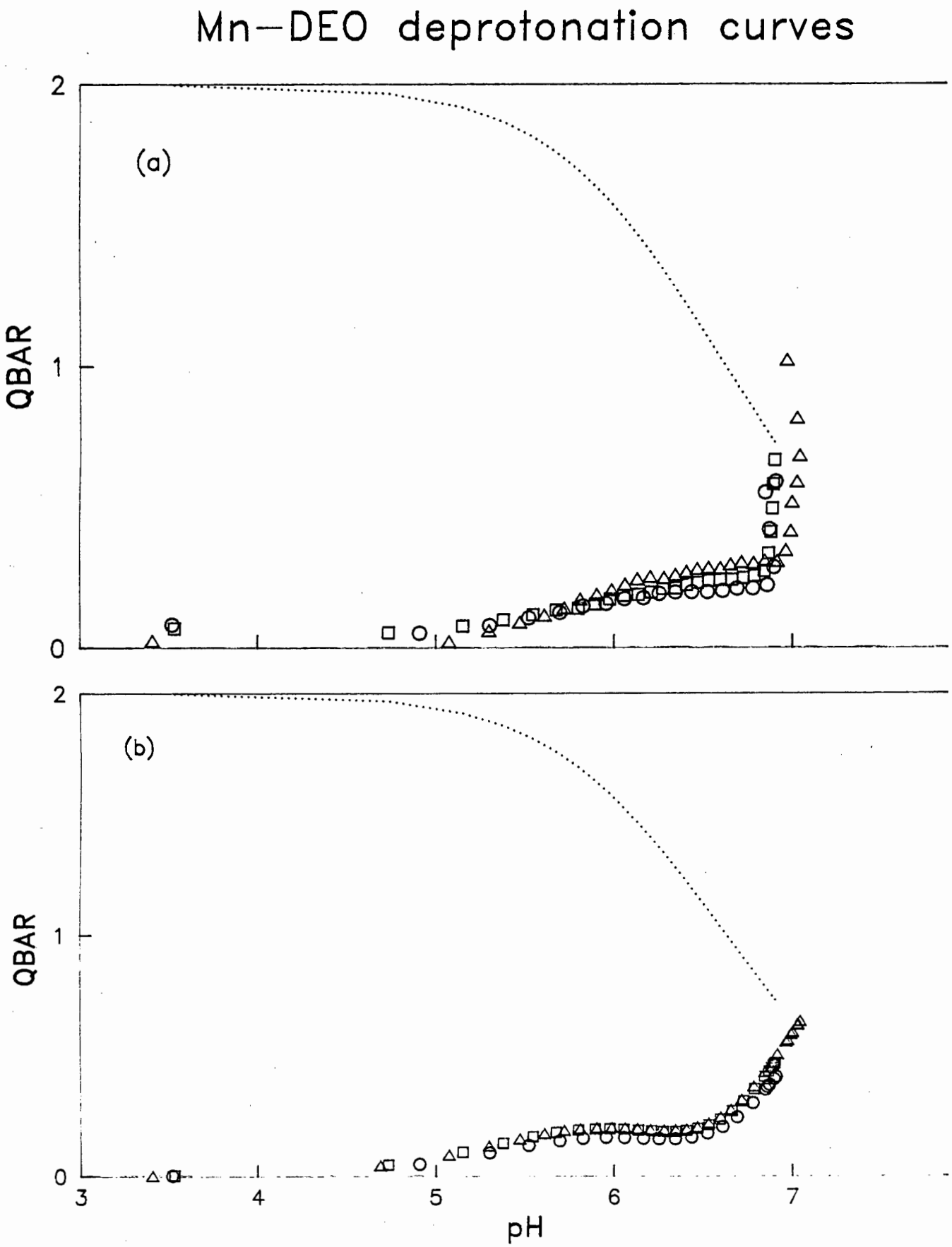

FIGURE 35 : The (a) experimental and (b) theoretical deprotonation curves for the Mn-DEO system at 25°C and 0.15M (Na) Cl

TABLE 7

Logarithms of the overall formation constants, β_{pqr} for the Mn-DMO and -DEO systems, determined in this study at 25°C and 0.15 mol.dm^{-3} Na[Cl]

Pkw used = 13.59

ligand	pqr	β_{pqr}	U	R	pH range
DMO	110	3.869 ± 0.005	71.59	0.03	3 - 7.5
	111	9.751 ± 0.01			
	11-1	-3.75 ± 0.01			
DEO	111	9.50 ± 0.03	60.1	0.05	3 - 7.5
	11-1	-4.17 ± 0.02			

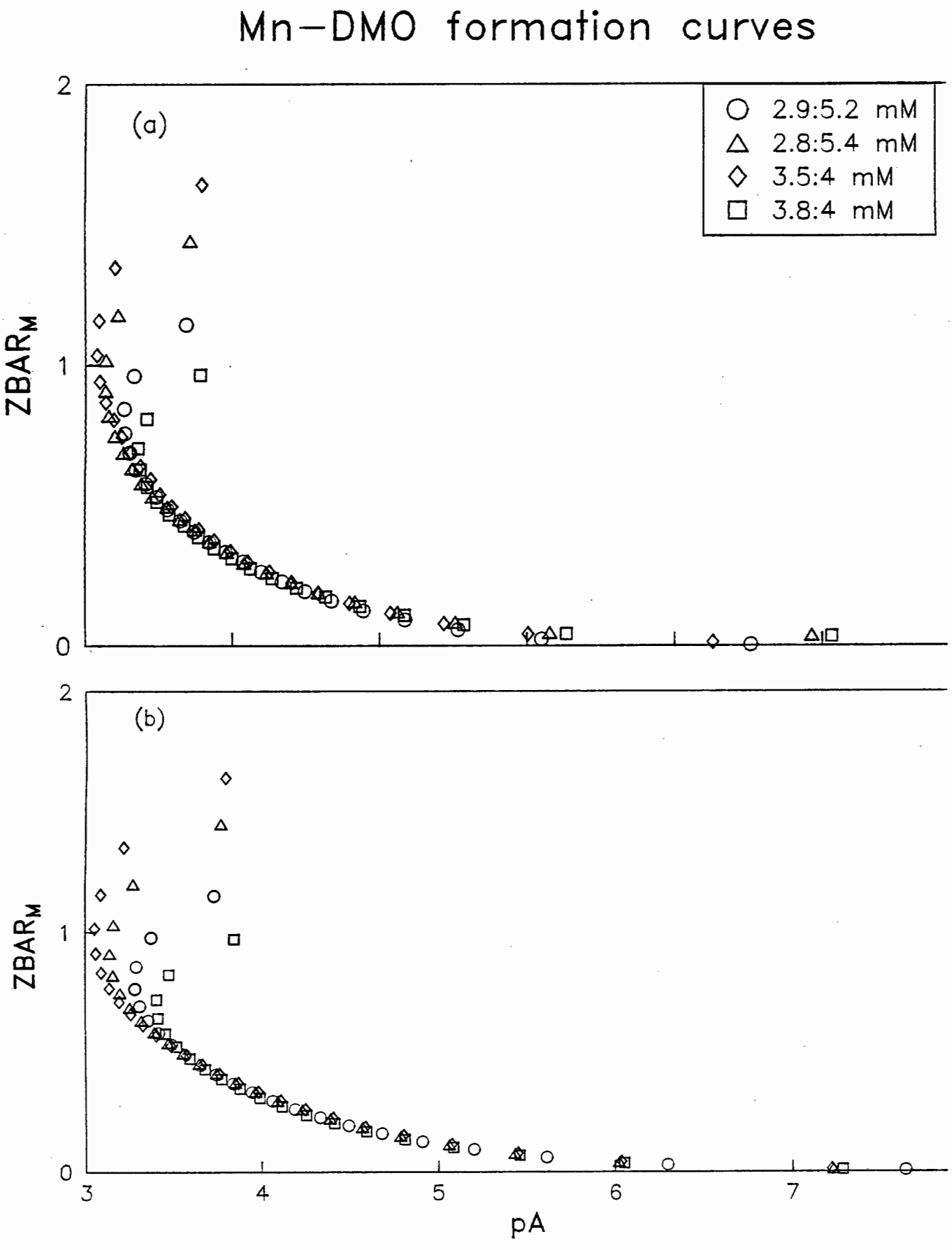

FIGURE 32 : The (a) experimental and (b) theoretical curves for the Mn-DMO system at 25°C and 0.15M (Na) Cl

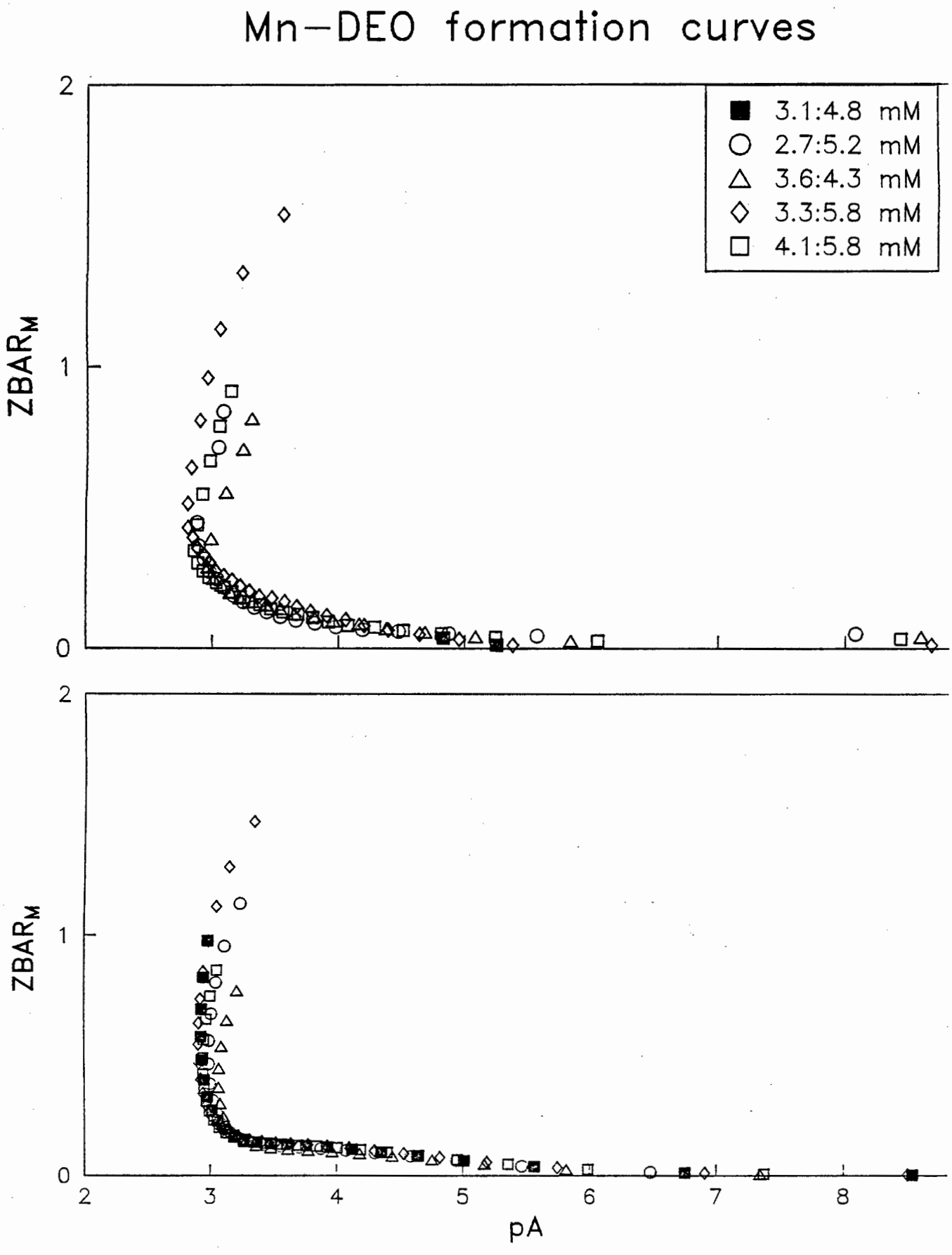

FIGURE 33 : The (a) experimental and (b) theoretical curves for the Mn-DEO system at 25°C and 0.15M (Na) Cl

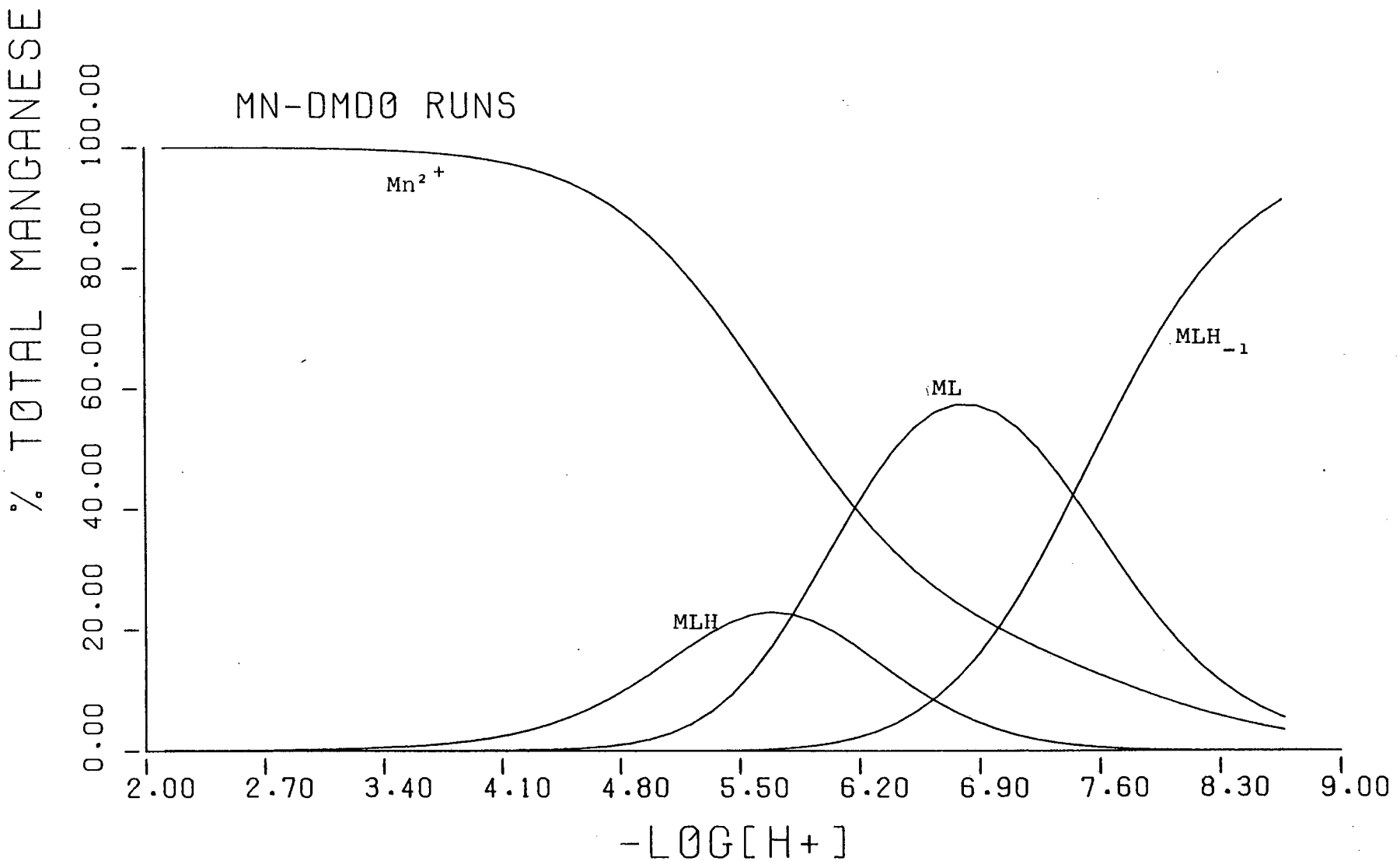

FIGURE 36 : Species distribution curves for the Mn-DMO system at a concentration of 4mM.

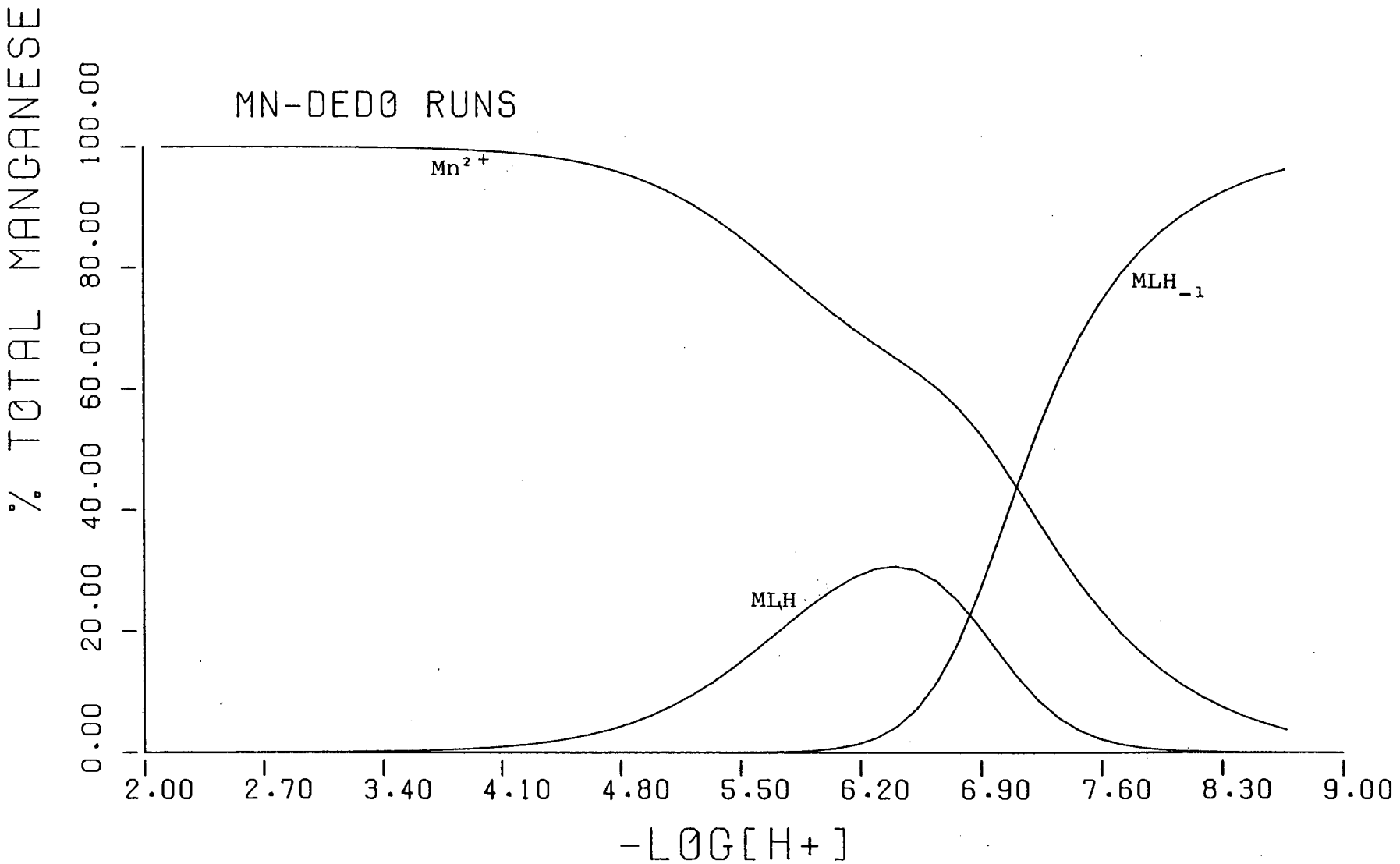

FIGURE 37 : Species distribution curves for the Mg-DEO system at a concentration of 4mM.

3.5.7 Nickel

Figures 38 and 39 show the formation curves for the Ni-DMO and -DEO systems respectively. The symbols represent different metal to ligand concentrations. In both systems the curves are superimposable showing no existence of polynuclear species. However, the shape of the curves shows weak complexation. In the middle of the titrations the curves show a tendency towards being perpendicular to the pA axes. This is the section where precipitation started, continuing towards neutral pH. At the end of the titrations the curves show a great deal of backward fanning which implies that the species dominant in these systems is the deprotonated complex, MLH_{-1} or MLH_{-2} . Figures 38(b) and 39(b) show the theoretical curves plotted using the constants in Table 8. There is good agreement between the two subsystems.

Table 8 shows the overall formation constants obtained in this study. The statistics of the constants is good giving confidence that the chosen model is a true representative of the species in solution.

The constants of the Ni-DEO system are lower than those of the Ni-DMO system. The lower constants could be attributed to the inductive effect of the ethyl groups on the amine nitrogen. This is in agreement with the pKa values of the

ligands, i.e. pKa values of DEO are higher than those of DMO. There is no detectable stepwise formation as in

$$MLH \qquad ML + H^{+}$$

$$ML \qquad MLH_{-1} + H^{+}$$

which means that the amine protons are lost almost simultaneously, possibly due to the inductive effect of the Ni^{2+} ion.

Figures 40 and 41 show the deprotonation curves. When $\bar{Q}$ = 0, $\bar{n}$ = 2 implying that no protons have been lost due to complexation. However, there is a sharp rise to $\bar{Q}$ = 1 indicating the loss of the two amine protons, while $\bar{n}$ = 1.7 implying that there are two protons still attached to the ligand. With increase in pH there is loss of three protons, $\bar{Q}$ = 3 and $\bar{n}$ = 1. At the end of the titration when $\bar{Q}$ = 2, $\bar{n}$ is not quite zero. This is because the titrations were terminated due to the presence of a precipitate.

Figures 42 and 43 show the species distribution which indicates the amount of nickel in each species. From these figures it can be seen that the dominant species is the MLH_{-2}.

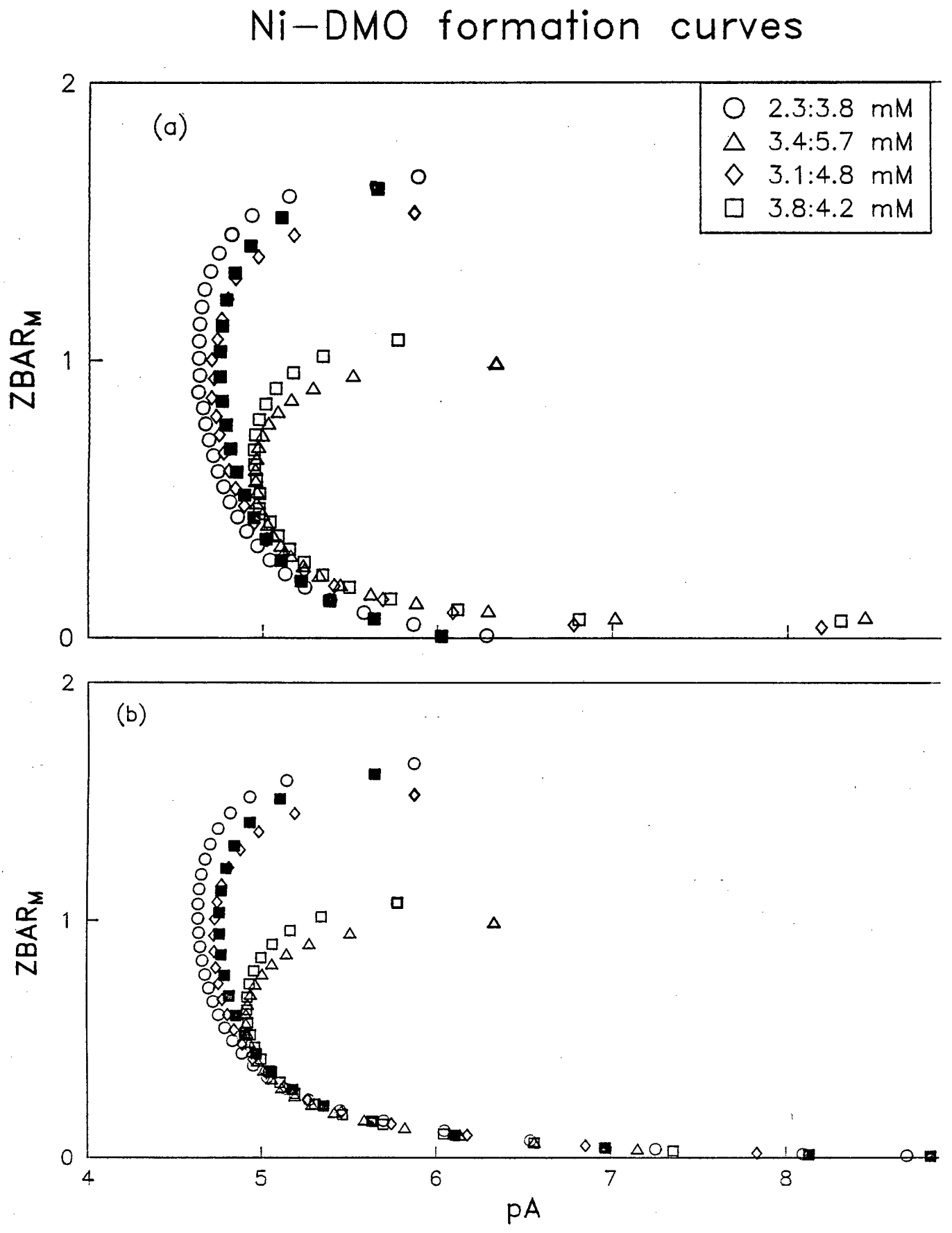

FIGURE 38 : The (a) experimental and (b) theoretical curves for the Ni-DMO system at 25°C and 0.15M (Na) Cl

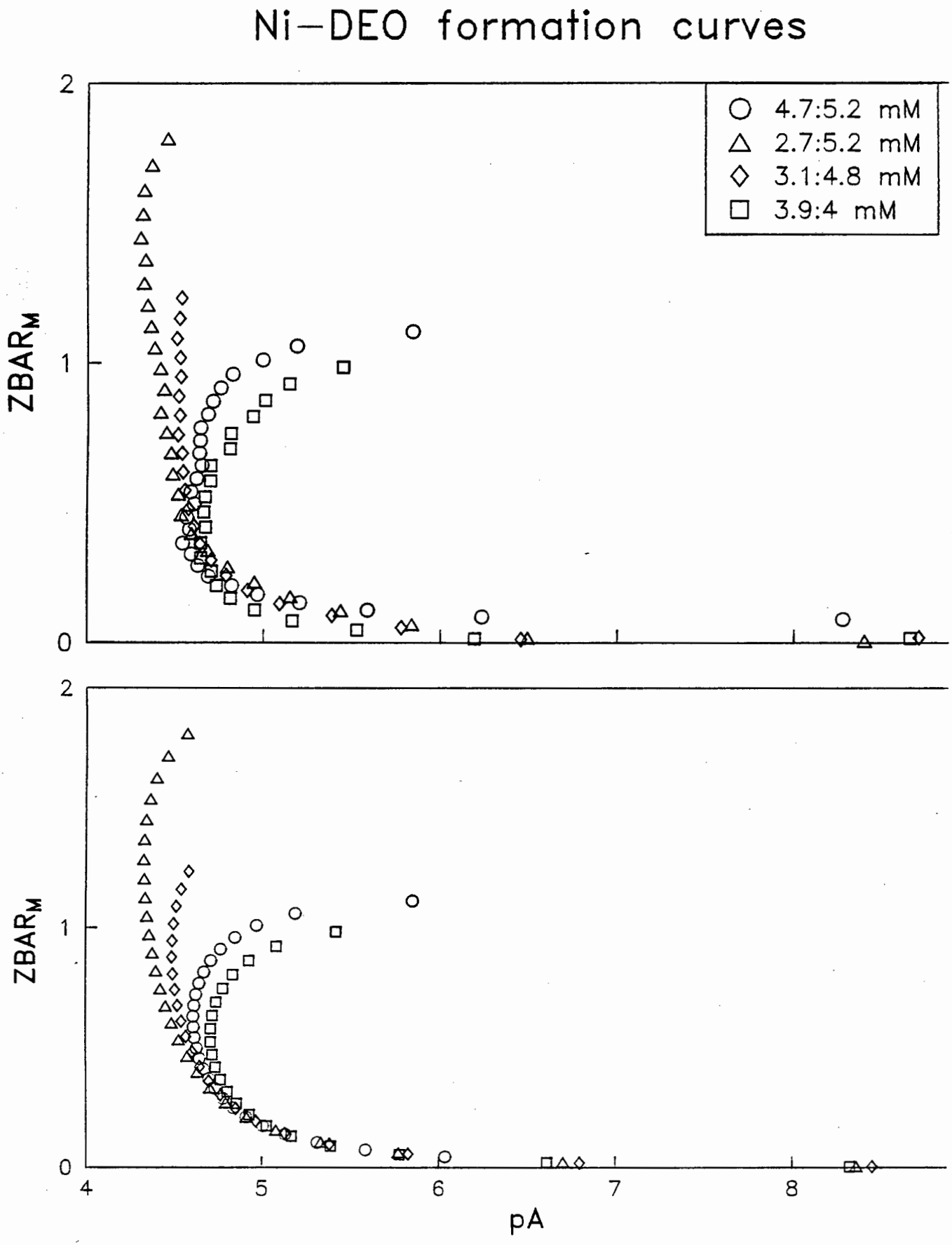

FIGURE 39 : The (a) experimental and (b) theoretical curves for the Ni-DEO system at 25°C and 0.15M (Na) Cl

TABLE 8

Logarithms of the overall formation constants, β_{pqr} for the Ni-DMO and -DEO systems, determined in this study at 25°C and 0.15 mol.dm^{-3} Na[Cl]

Pkw used = 13.59

ligand	pqr	β_{pqr}	U	R	pH range
DMO	111	10.66 ± 0.03	86	0.015	3 - 7.5
	11-1	-0.81 ± 0.01			
	11-2	-6.61 ± 0.01			
DEO	111	9.79 ± 0.03	44	0.13	3 - 7.5
	11-1	-1.52 ± 0.01			
	11-2	-7.70 ± 0.03			

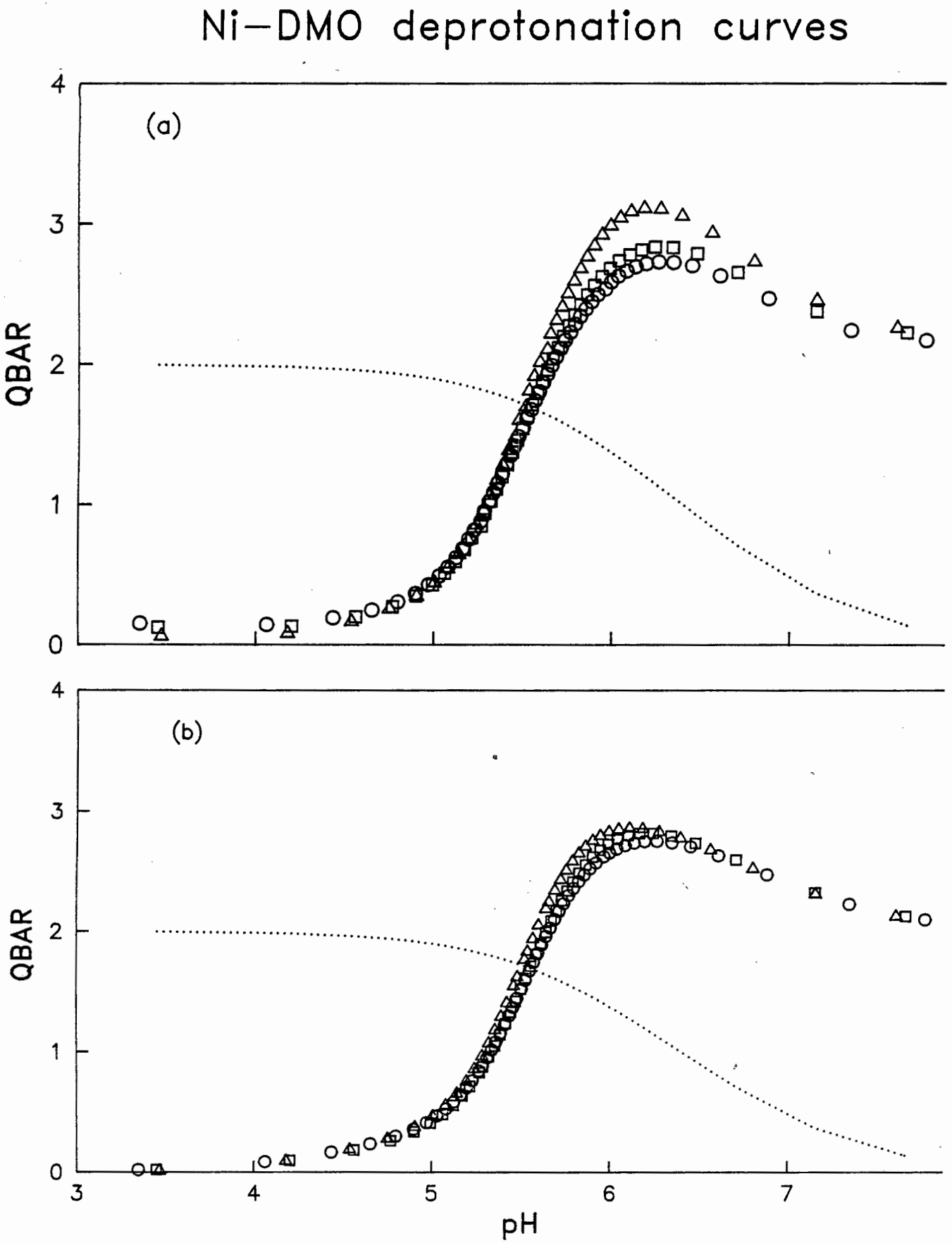

FIGURE 40 : The (a) experimental and (b) theoretical deprotonation curves of Q vs pH for the Ni-DMO system at 25°C and 0.15M (Na) Cl ... = n vs pH

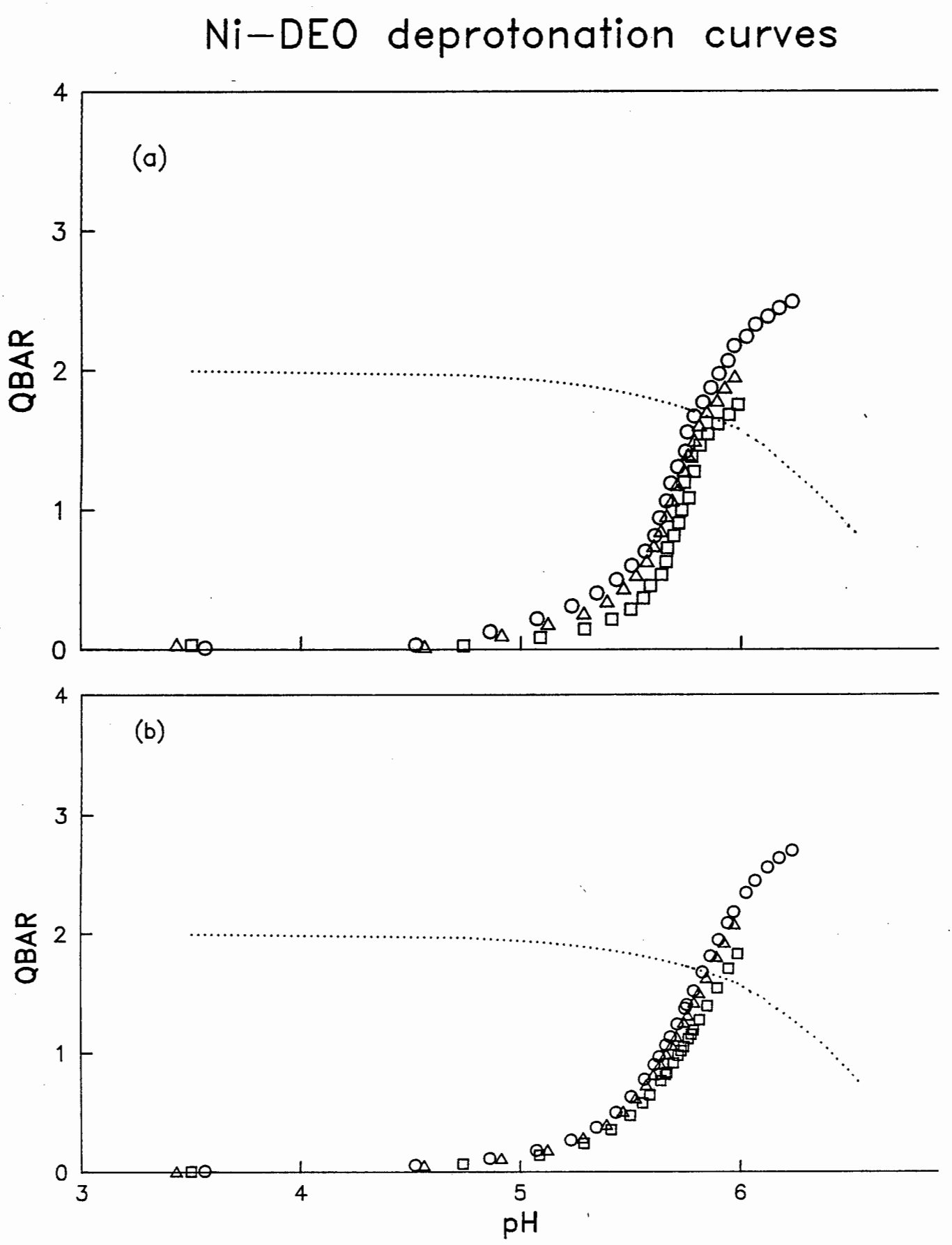

FIGURE 41 : The (a) experimental and (b) theoretical deprotonation curves of $\bar{Q}$ vs pH for the Ni-DEO system at 25°C and 0.15M (Na) Cl ... = $\bar{n}$ vs pH

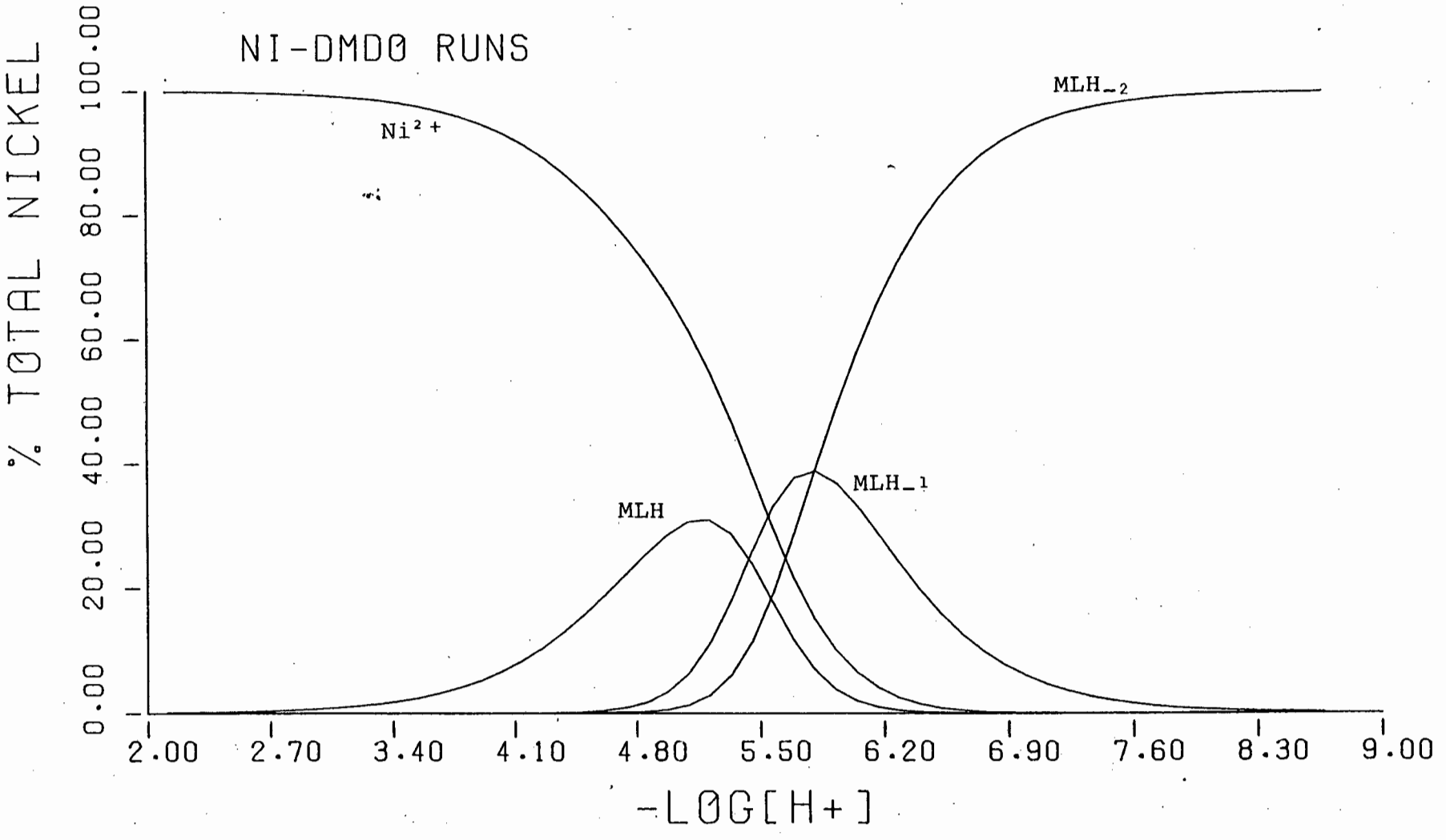

FIGURE 42 : Species distribution curbes for the Ni-DMO system showing the percentage of nickel in each species in 1 : 1 ligand-to-metal solution [4mM].

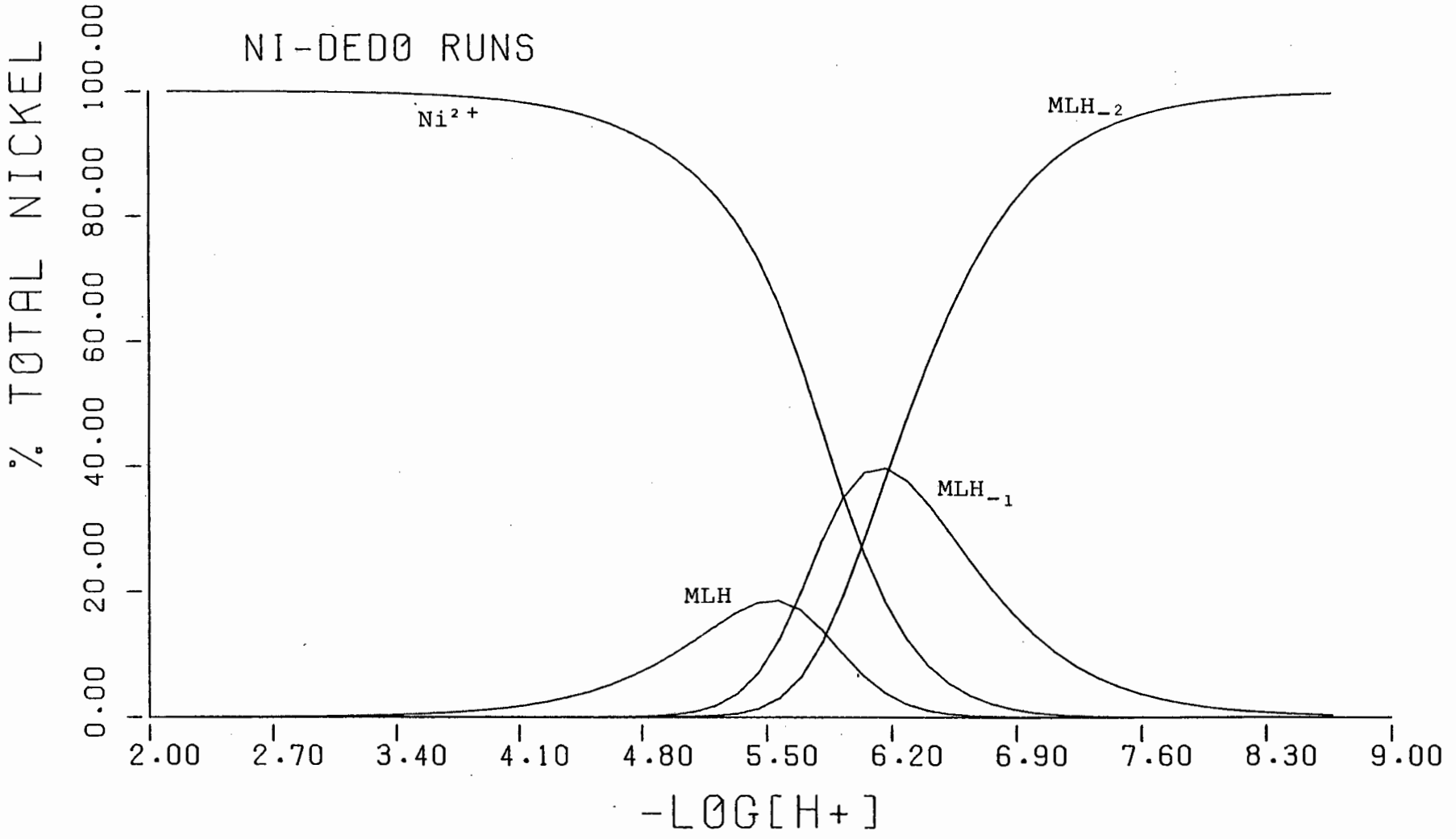

FIGURE 43 : Species distribution curves for the Ni-DEO system showing the percentage of nickel in each species in 1 : 1 ligand-to-metal solution [4mM].

3.5.8 Cobalt

Figure 44 shows the formation curves for the Co-DMO system. The Co-DEO system data could not be analysed satisfactorily using any of the abovementioned procedures. The reason being the presence of thick precipitate even at very low metal ion concentrations. This difficulty, however, is not only peculiar to this study. Morris and Martin [107] in their studies, found that the CoII ion promotes ionisation of amides only at or near pH 10. At this stage precipitation will have occurred. To overcome this they used 20 : 1 molar ratio of ligand to metal and these were studied spectrometrically.

The Co-DMO system in Figure 44 shows the characteristic bad and indefinable curves. However, results similar to the Ni-DMO system could be extracted. Figure 44(b) shows the theoretical curves obtained using the constants in Table 9. The agreement is not so good, however, the experimental curves do show some resemblance to the theoretical curves in their backward curving.

Table 9 shows the overall formation constants obtained in this study. The standard deviation is high which shows the difficulty of obtaining true values in the presence of a precipitate.

Despite the unfortunate result of a precipitate, interpretation of the system could be made. As in the Ni-DMO system, there is no detectable stepwise formation of species

$$MLH \rightleftharpoons ML + H^+$$

$$ML \rightleftharpoons MLH_{-1} + H^+$$

implying that the amine protons are lost simultaneously as the CoII ion is coordinated. This is because of the inductive effect of the CoII on the amine nitrogens.

Figure 45 shows the deprotonation curves. When $\bar{Q} = 0$ and $\bar{n} = 2$ at the beginning of the titration there are no protons lost because of complexation. However, there is a sharp rise to $\bar{Q} = 1$ indicating the loss of the two amine protons. At the end of the titrations $\bar{n} \sim 0$ and $\bar{Q} \sim 2$ implying that all four protons on the ligand have been lost due to complexation. Titrations had to be stopped because of the precipitate in the solution.

Figure 46 shows the species distribution at different pH values. The curves represent the percentage of Co^{2+} ion present in each species.

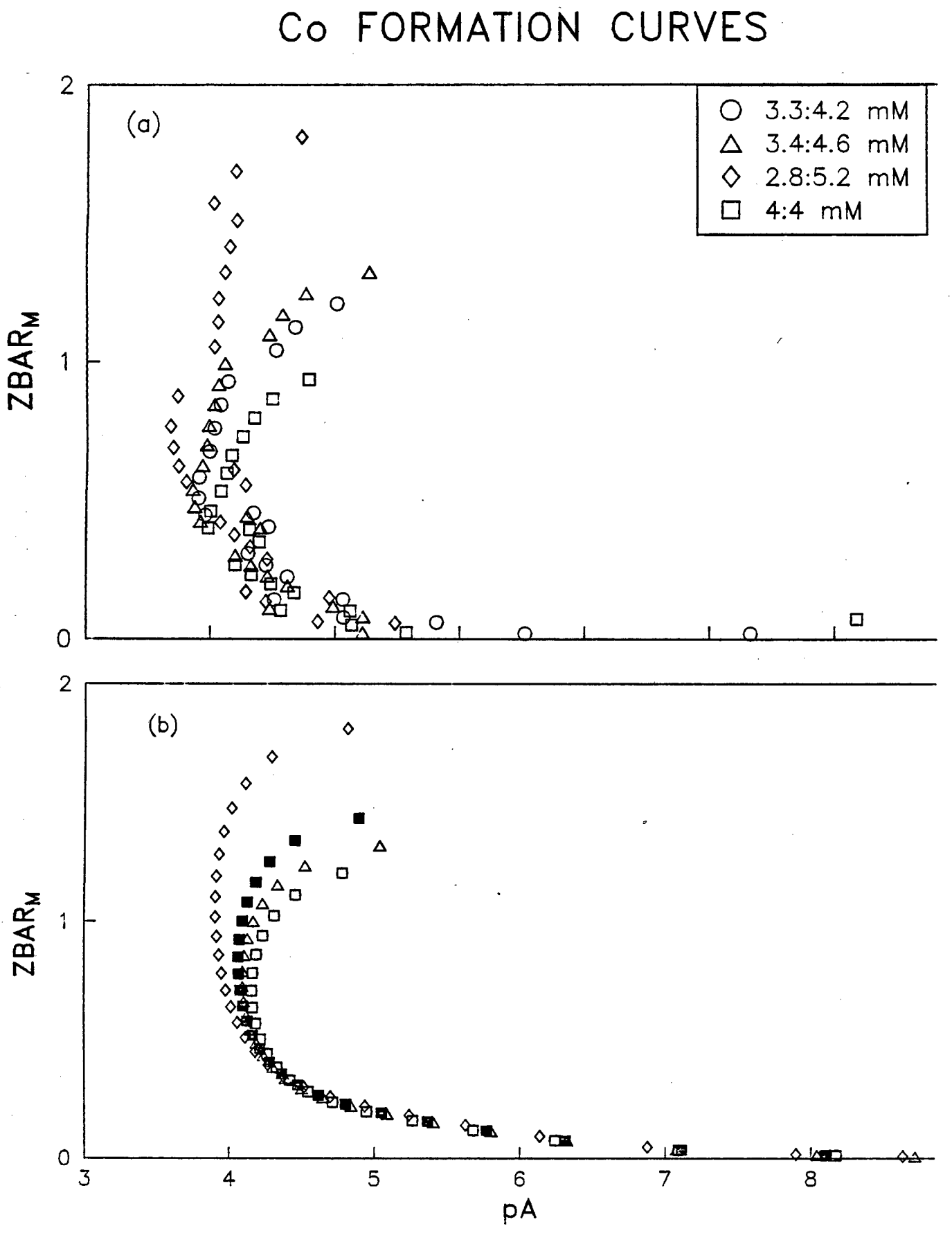

FIGURE 44 : The (a) experimental and (b) theoretical curves for the Co-DMO system at 25°C and 0.15M (Na) Cl

TABLE 9

Logarithms of the overall formation constants, β_{pqr} for the Co-DMO and -DEO systems, determined in this study at 25°C and 0.15 mol.dm^{3+} Na[Cl]

Pkw used = 13.59

ligand	pqr	β_{pqr}	U	R	pH range
DMO	111	10.03 ± 0.07	91.3	0.23	3 - 7.0
	11-1	-1.76 ± 0.05			
	11-2	-8.3 ± 0.08			

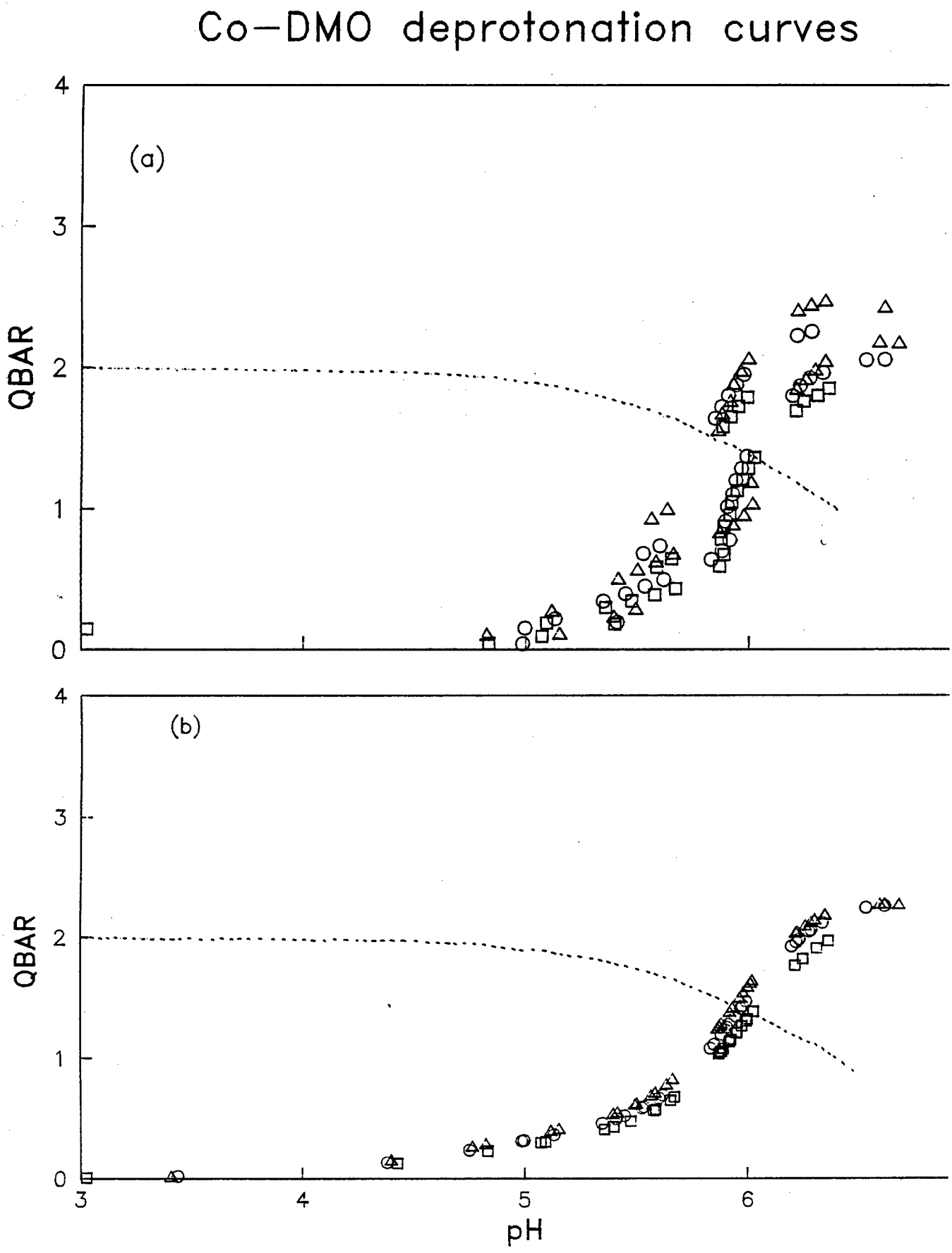

FIGURE 45 : The (a) experimental and (b) theoretical deprotonation curves for the Co-DMO system at 25°C and 0.15M (Na) Cl ... = $\bar{n}$ vs pH

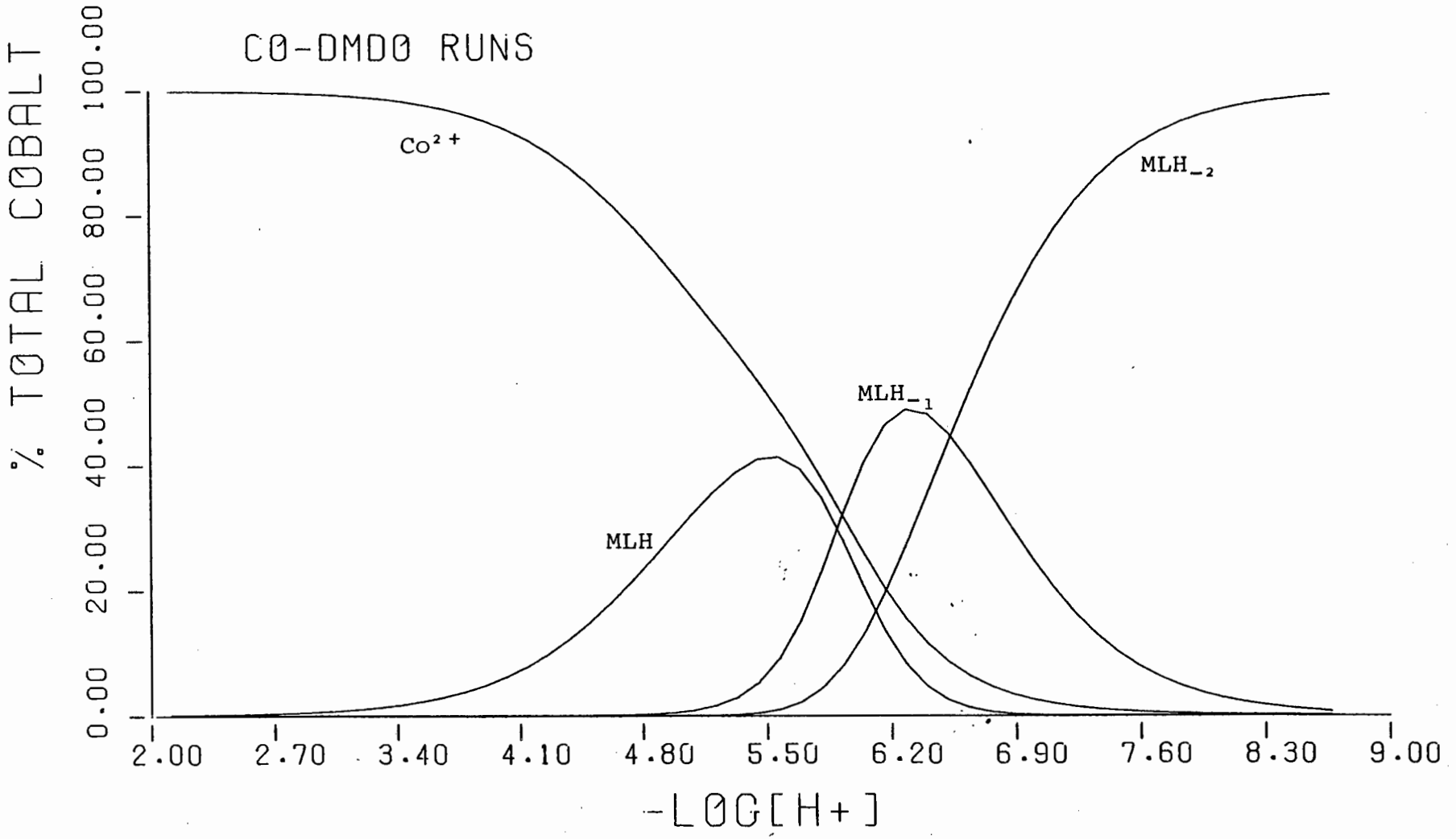

FIGURE 46 : Species distribution curves for the Co-DMO system showing the percentage of cobalt in each species in 1 : 1 ligand-to-metal solution [4mM].

3.6 Discussion

Most of the metal systems studied were plagued by the formation of precipitates. This resulted in the titration range being limited to the neutral pH.

What was envisaged from the studies is that the ligands should be highly selective for copper. Modification of the core structure, trien, was aimed at achieving this. Trien is known in Cu chelating studies.

Bosnich et al. [82] state the following criteria for decision in favour of a particular sterochemistry.

a) Conformational demands of the ligand

b) Hydrogen-hydrogen repulsions within the complex or steric repulsions between ring substituents

c) Specific internal interactions, such as hydrogen bond

d) Cumulative ring-strain

e) Entropy effects

f) The size of the central metal ion

g) The size of the donor atom

h) The electronic demands of the central metal ion

i) Solvation effects and crystal packing forces

The ligands DMO and DEO have two different types of nitrogens with which to bind a metal ion, the amine and the amide nitrogens. These have different affinity for the metal ion. Generally it is known that the base strength in nitrogen donor ligands depends on the availability of the nitrogen lone pair of electrons. An electronwithdrawing substituent, like an oxygen atom on the nitrogen, decreased the basicity while an electron donating substituent, like an alkyl group, increased the basicity. However, increasing the number of alkyl groups on the nitrogen does not always result in increased basicity. The tertiary substituted alkylamines are less basic than their primary substituted counterparts. This anomaly has been explained by the solvation effect which increases the apparent strength of the amine by hydrogen-bonding. Both DMO and DEO are subject to the abovementioned factors.

Besides the properties of the metal ion, the only difference in the stability of the two complexes was the result of the alkyl group's inductive effect on the nitrogens. The metal DEO systems have lower formation constants than those of the

DMO systems. This difference can be attributed to the higher pKa values of the DEO over those of DMO as a result of the inductive effect of ethyl groups on the amine nitrogens.

On comparing DMO and DEO the above factors have been eliminated except conformational strain and steric repulsions between ring substituents. The ethylene groups attached to the amine of the DEO are bulky and steric hinderances should be greater. A solution to this problem could be packing of the ethylene groups which could possibly create a hydrophobic end of the structure.

The remarkable stability of the Cu system could be explained by taking into consideration the ability of the ligands to encapsulate this small metal ion. However, Ni which has the same ionic radius size as Cu did not show any increased stereoselectivity. This can be explained by the Irving-Williams series

$$Mn^{2+} < Fe^{2+} < Co^{2+} < Ni^{2+} < Cu^{2+} > Zn^{2+}$$

which shows that Cu is more likely, over all the other metal ions in this series, to be coordinated. The low stability of the other larger metal ions could be due to their arrangement outside the chelating cage due to the resistance towards unwinding of the ligand. Another aspect could be even if they are also encapsulated by the ligands, the

resultant structure is of low stability as regards the metal ions property. For instance Co^{2+} prefers tetrahedral complex structure, and Ni^{2+} is the same for bulky ligands as these are, i.e. bulkier than ethylenediamine. For Co^{2+} ion chelation by strong ligand fields octahedral complexes are formed. The high spin complex (d^5) for Mn^{2+} has no ligand field stabilisation energy which contributes to its thermodynamic stability. In such cases the ligands DMO and DEO could show various facultative dispositions [108] which are not very stable as compared to the Cu-DMO and -DEO systems.

Stability of complexes containing chelate rings increases as the number of rings increases [87]. However, stability decreases as the ring size increases from five to seven membered. This latter statement brings in the cumulative ring strain effect. In previous studies of similar diamino-diamide ligands [80 and references therein] fused ring systems of five-five-five (5,5,5) have been found to be strained. The relief was brought about by altering the ring structure and forming 5,6,5 sequence. The 5,5,5 structure ring strain cannot however be experienced in trien complexes. The explanation is that the ethylene group (the middle one) can cause ring puckering which relieves the strain. In DMO and DEO this is not possible. The presence of the carbonyl groups in the middle ethylene group forces the structure to have a planar configuration.

The stability of the complex in the present 5,5,5 system could possibly result from the first and third ring's ethylene groups adopting a gauche [104] conformation.

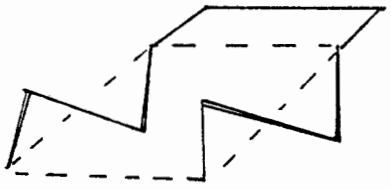

Bearing in mind that empirical formula of a compound does not give any information about its stereochemistry, the MLH structure, however, can be proposed.

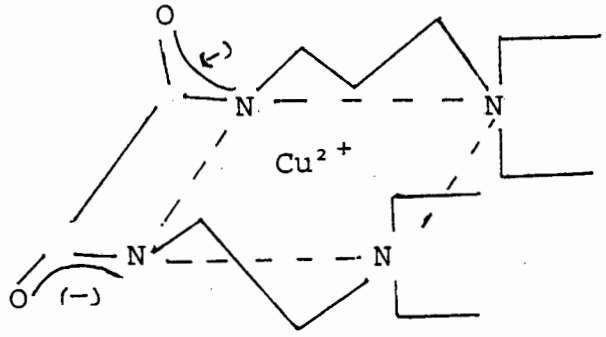

In this hypothesised structure in solution allowance has been made for the bulky ethylene groups. Cu ion is six coordinated in a square planar ring with the two longer and weak bonds, above and below the ring plane, coordinated to water molecules.

Comparing a series of ligands which are similar in the elemental composition of their chelate rings, N, N'-bis (2-aminoethyl) oxalamide (BAO), DMO and DEO the following deductions are made: Stereoselectivity seems to increase with increasing size of the side-chain on the amine nitrogens i.e. $H << CH_3 < CH_2-CH_3$, resulting in the formation of the neutral species.

TABLE 10

Logarithms of the overall protonation and formation constants of the Cu, -BAO, -DMO and -DEO systems

ligand	β_{LH}	β_{LH_2}	β_{ML}	$\beta_{MLH_{-1}}$	$\beta_{MLH_{-2}}$	ref
BAO*	9.31	17.74	9.41			109
DMO	6.85	12.8	9.2	3.44	-2.94	this study
DEO	7.04	13.26	8.74	3.71	-2.98	this study

* conditions: 22°C in 0.1M KNO_3

The formation constants are presented in Table 10. For the ML species similar constants are obtained with these three ligands. The selectivity can be observed in the sequence (BAO) to (DMO) and to (DEO), for the MLH_{-2} species. In the BAO studies, the authors experienced a great deal of precipitation at about pH 7. They concluded that no stable compounds were formed with Cu^{2+}. Only ML which was formed at approximately pH6 was evident.

It seems, however, that very little change would be observed if an extra CH_2 group was added to the ethyl group at the amine, thus making it longer. This is postulated from the graphical presentations in Figure 47.

The stability seems to reach a plateau at ligand = DEO. The side-chain length effect is also observed in dipeptides. [110] On going from Ala-Ala* to Leu/Leu** the difference in the complex stability ranges from 0.15 to 0.4 log units. The DMO and DEO systems are very similar to those of the dipeptides except that carboxylic group are involved in complex formation in the peptide systems.

The metal ions Co^{2+}, Ni^{2+} and Cu^{2+} which share a number of properties have presented interesting results. These ions also share the property that they can either be hard or soft, and form complexes with N-containing ligands.

For the first transition series, the stability constants are roughly in the order of ionic potential (i.e. charge to ionic radius) and size of the metal ions. The sequence of the divalent transition metal ions known to promote amide deprotonation in glycylglycine (a dipeptide) in increasing order of effectiveness is CoII < NiII < CuII. [107]

---

* Alanin = Alanine
** Leu = Leucine

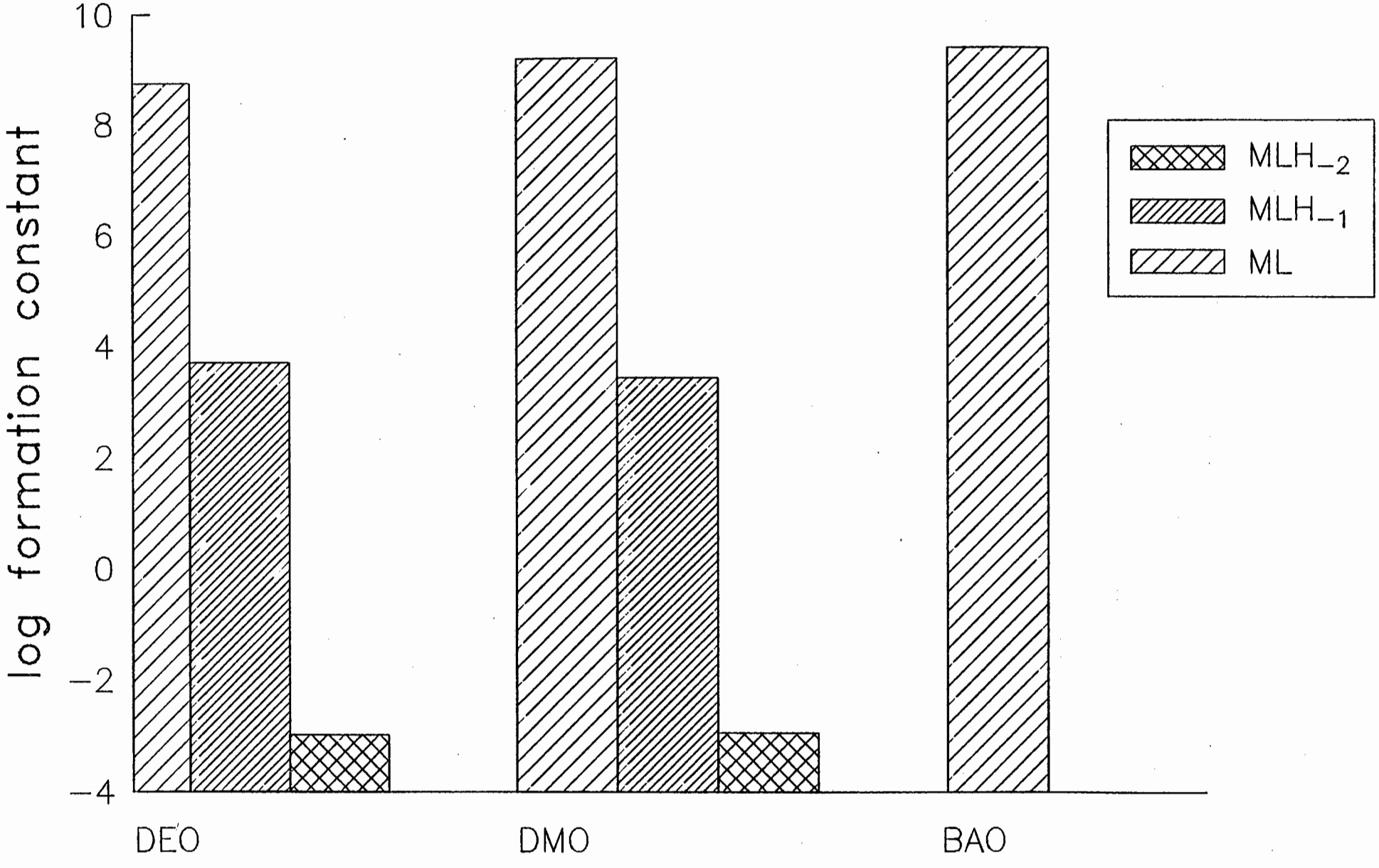

FIGURE 47 : Bar chart showing the effect of increasing the amine side chain by CH_2

Quantitatively, the most successful metal ion in promoting the deprotonation was CuII. At pH < 7 the amines as well as the amides were deprotonated.

CHAPTER 4

SPECTROSCOPIC STUDY OF THE Cu-DEO COMPLEX

4.1 Introduction

Spectral properties are due to differences between the ground state and the excited state of molecules. Electronic spectra are much easier to measure directly, however, the use of such data is not always a trivial matter. Generally light at the visible and ultraviolet region of the spectrum is absorbed by a complex for a variety of reasons. These are [1] the ligand spectra. Ligands like solvents used in complex preparations have their characteristic absorption bands which are usually in the ultraviolet region. Counter-ion spectra, knowledge of the spectrum of the counter-ion that is associated with the complex, must be known in order to interpret the spectrum. Charge transfer spectra are the result of transitions between orbitals that are mainly those of the metal ion and those of the ligand. Ligand-field spectra are from the split d-orbitals of the metal, having been split in a ligand field and these are known as the d-d spectra.

For a given metal ion, ligands can be arranged in order of increasing Δ(10Dq, the ligand field splitting parameter). This order which is more or less independent of the nature of the metal ion is called the spectrochemical series. [87]

$$Cl < S^{2-} << OH^{-} << H_2O < py = NH_3 < en < bipy < phen < CN^{-}$$

This series implies that if the position of maxima in the spectrum of m^{n+} with one ligand is known, approximate predictions about the position of the bands for complexes of this metal ion with other ligand can be made. Variations to the general rule may occur.

The CuII ion has a d^9 electronic structure. It has the largest spin orbit coupling coefficient. However, complexes of CuII are characterised by a single broad poorly resolved absorption band. Frequently Cu complexes are found to have highly distorted structures - Jahn-Teller distortion - which results in stereochemistries of uncertain description. [113] This is the reason why the above generalised results cannot be used in determining copper-coordination geometries.

With the introduction of proteins into the system the situation becomes more complex. In conventional chemistry, stereochemical regularity is the norm, however, natural ligands provide an irregular distorted environment for metal ions. The Beer-Lambert's law holds for solutions in which there are no interactions between the various chromophores. However, if there are interactions between chromophores as is often the case with proteins, the absorption band can either:

- shift to shorter wavelength (blue shift)
- shift to longer wavelength (red shift)

- split into two bands
- show increase in intensity (hyperchromism) or
- show decrease in intensity (hypochromism)

Chromophores of interest in biochemistry are often heteronuclear groupings of atoms. This creates unequal charge distribution over the atoms, giving rise to a permanent dipole movement μ [114] which represents the charge separation. Absorption of light by a chromophore results in a change of dipole moment which gives rise to the electric transition dipole μ. This is the difference between the permanent dipole moment of the ground state and the dipole moment of the excited state.[114].

$$\left| u_i^2 \right| = D_i = 1.63 \times 10^{-38} \cdot \frac{\varepsilon_i \ \Delta_i}{\lambda_i} \qquad \ldots \quad (i)$$

D_i = dipole strength

ε_i = molar extinction coefficient

λ_i = absorption maximum wavelength in nm

Δ_i = half band width in nm

In a solution with chromophores absorbing light at the same frequency, this gives rise to the dipole interaction potential V_{12} for chromophore 1 and 2. Taking $\bar{\lambda}_2$ as the wavelength of the absorption maximum of monomers

and λ_+ or λ_- as the wavelengths of the shifted absorption maxima

$$V_{12} = (\lambda_{\pm}^{-1} - \lambda_i^{-1})ch \qquad \ldots \text{(ii)}$$

c = velocity of light in a vacuum

h = Planck's constant

Monomers which are dispersed in solution represent a random state for the chromophore. Aggregation to form specific dimers, trimers etc. results in a more ordered state, therefore giving

$$D_i^R - D_i^O < 0 \qquad \text{for hyperchromism} \qquad \text{(iii)}$$

and $$D_i^R - D_i^O > 0 \qquad \text{for hypochromism} \qquad \text{(iv)}$$

R = random

O = ordered

For the purpose of analysing the splitting or shifting of bands, the sign of V_{ij} depends on the relative orientation of the transition dipole movement. In this case it is the ith transition dipole moment in chromophore 1 interacting

with the jth transition dipole moment in chromophore 2. Under the Franck-Condon principle there is no change in geometry during an electronic transition and hence:

$$V_{ij} < O(\vec{u}_i \vec{u}_j) \qquad \text{for hyperchromism}$$

i.e. there is a head-to-tail alignment or coplanar arrangement and

$$V_{ij} > O(\vec{u}_i \uparrow\uparrow \vec{u}_j) \qquad \text{for hypochromism}$$

i.e. there is a stacking of chromophores. This is due to the strong electric transitions that are in the plane of an unsaturated or aromatic chromophore.

The molecules to be studied are the Cu-DEO and Cu-BSA-DEO. The former will be to substantiate the structure postulated in potentiometry while the latter tertiary complex would be studied to establish the effect that DEO would have on the Cu-BSA complex under physiological conditions.

4.2 Experimental

A complex of 1 : 1 ratio DEO to Cu was prepared using deionised distilled water at a concentration of 1.85 x 10^{-3} mol.dm^{-3}. NaOH was used to vary the pH. All the solutions were run at an ionic strength of 0.15 mol.dm^{-3} Na[Cl] in the pH range 6.5-10.7. Spectra were recorded on a Beckman UV 5260 spectrophotometer at 25°C.

For the Cu-BSA studies, crystalline BSA was obtained from Miles Laboratory, U.S.A., lot no 385, fraction V and purity 98%. To remove any trace of copper that could be contaminating BSA, it was passed through a column of Chelex 100 using acetate buffer pH 5.0 to equilibrate the column. The BSA was dissolved in double distilled water and passed through the column. The eluate was then dialysed and lyophilised and the CuII content before and after purification was determined by atomic absorption using a graphite furnace.

A 1 : 1 Cu-BSA complex of concentration 2 x 10^{-4} mol.dm^{-3} was prepared. As with the Cu-DEO system, the ionic strength was 0.15 mol.dm^{-3} Na[Cl] at constant pH 7.4. A 2 x 10^{-3} mol.dm^{-3} solution of DEO at pH 7.4 was prepared and added to the Cu-BSA solution in initial 10ul increments to final 30ul increments. Spectra were recorded on a Varian Superscan 3 spectrophotometer at 37°C.

The low concentration of BSA, the pH 7.4 and the temperature of 37°C were used so as to be as close to physiological conditions as possible. The increments of DEO were initially 10ul up to 30ul until the final concentration of DEO was about 2×10^{-4} $mol.dm.^{-3}$.

4.3 Results and Interpretations

The spectra of variable pH study of the Cu-DEO system are shown in Figure 1. Spectra 2, 3 and 4 form isosbetic points between the two peaks. This indicates that in this pH range 7.0-9.4 there at least two species in equilibrium. The spectrum at pH 6.5, however, does not go through the isosbetic point indicating the presence of two absorbing species in solution. These spectral changes can be explained in terms of the species formed in solution at the different pHs.

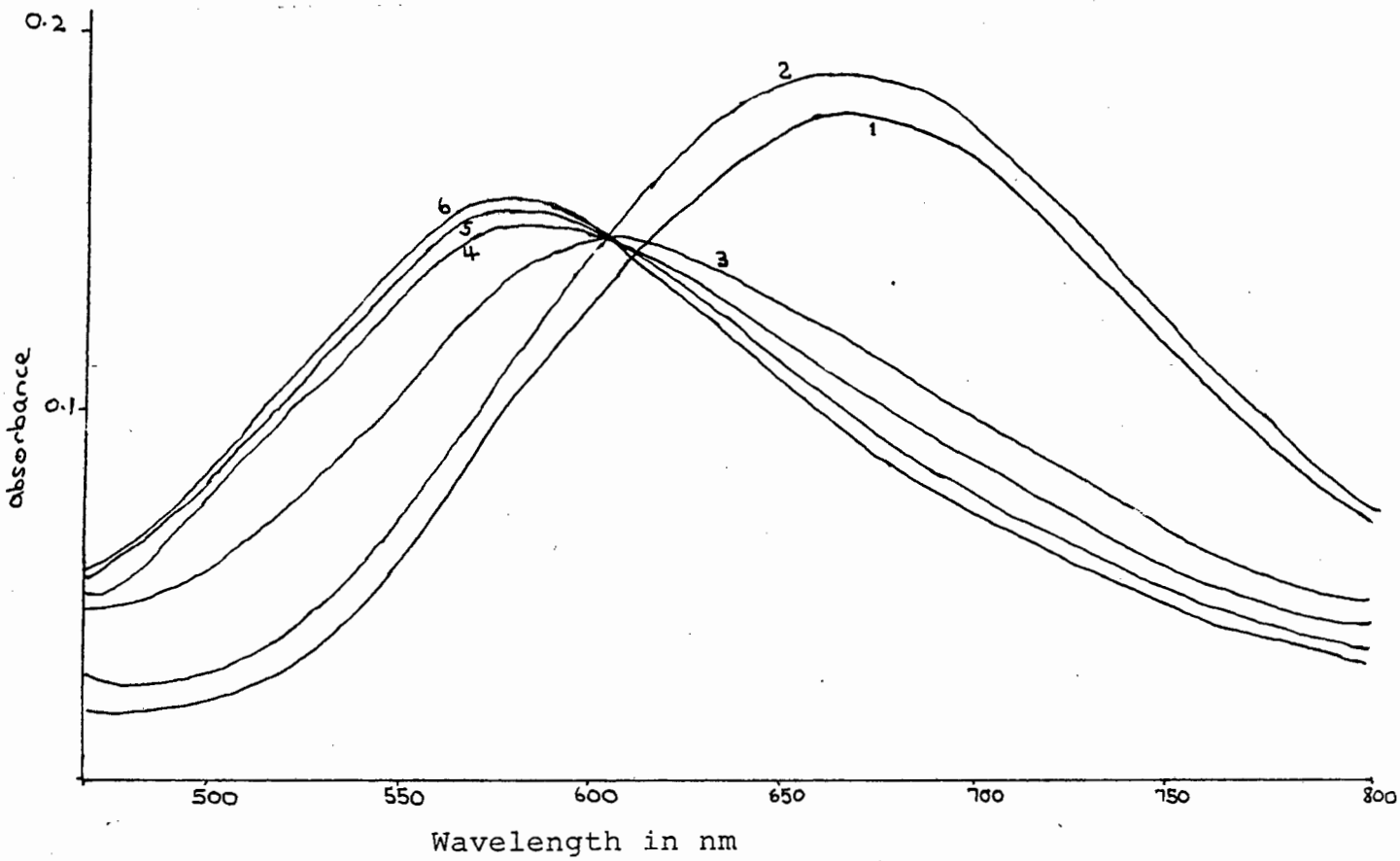

FIGURE 1 : Variable pH spectra for the Cu-DEO system at metal-ligand of 1 : 1, 1.85 x 10^{-3} M

Curve	1	pH 6.5
	2	7.0
	3	8.0
	4	9.4
	5	10.0
	6	10.5

Figure 2 shows the species distribution of this system. At pH 10, 100% of the copper exists in the MLH_{-2} species while at pH 7 the copper is distributed between two species ($\simeq$ 50% in MLH_{-2} and another 50 in MLH_{-1}). Below pH 6.8 the ML species became apparent shifting the spectrum to higher wavelength. Combining the results of the species distribution and the electronic spectra at different pHs, it is possible to calculate the spectra of the individual species. Beer-Lambert's Law gives the three species equilibrium

$$A = l\left(\varepsilon_{ML}\,[ML] + \varepsilon_{MLH_{-1}}\,[MLH_{-1}] + \varepsilon_{MLH_{-2}}\,[MLH_{-2}]\right)$$

which can be solved for ε . The results of this analysis are given in graphic form in Figure 3. This figure represents the electronic spectra of each species if it existed in the solution on its own. These spectra can be used to comment on the structure of the different complexes.

The electronic spectra of MLH_{-2} have extinction coefficients of $< 100\,\ell mol^{-1}$ which is characteristic of spin allowed, Laporte forbidden transition. [115] The intensity of these transitions is slightly higher than normal because the Laporte selection rule is strictly only true for complexes of cubic symmetry while in this case the copper complexes have a lower symmetry being geometrically and Jahn-Teller distorted. Typical values of the extinction

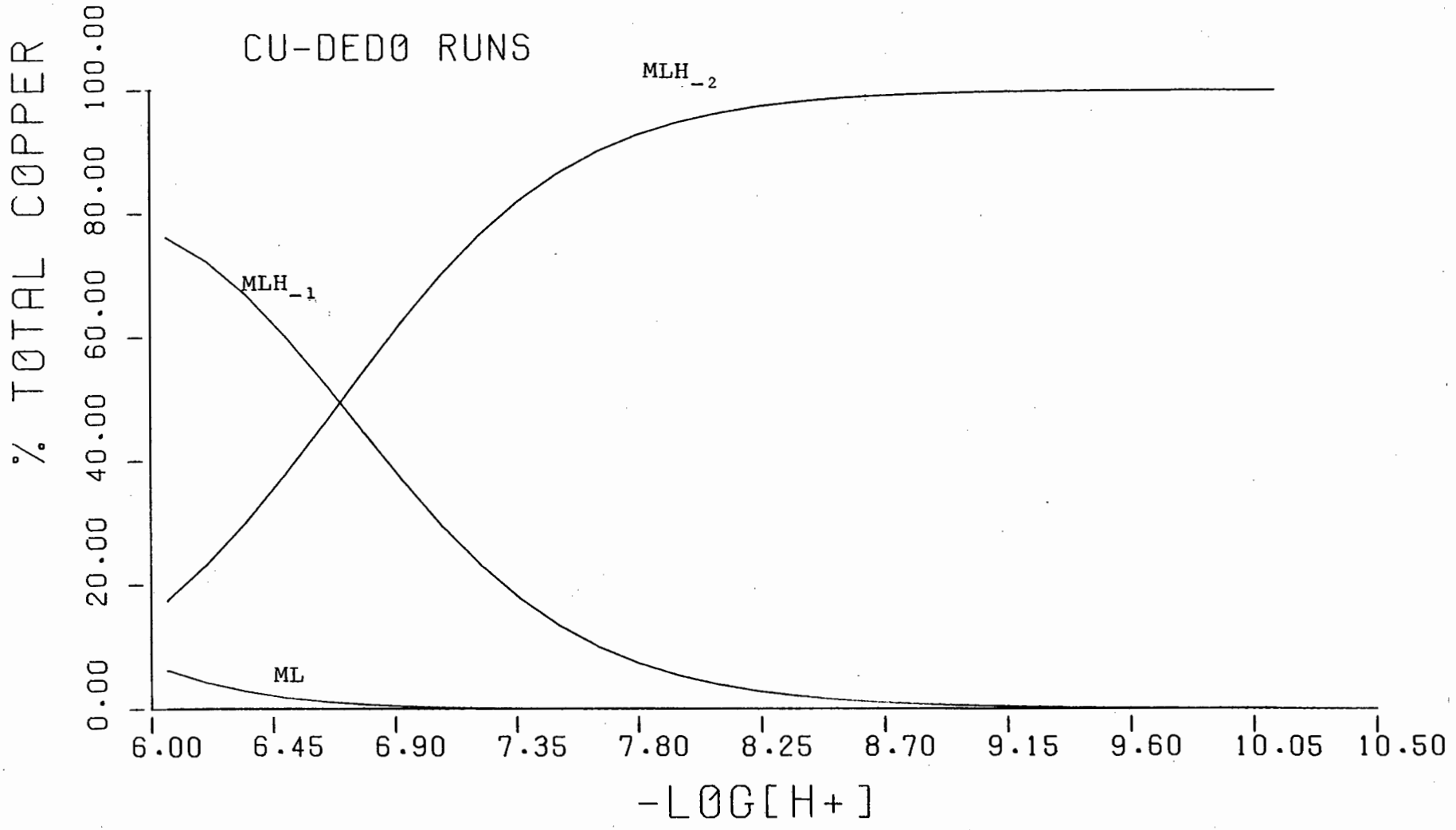

FIGURE 2 : Species distribution of the Cu-DEO system at metal-ligand of 1 : 1, 1.85 x 10^{-3}M

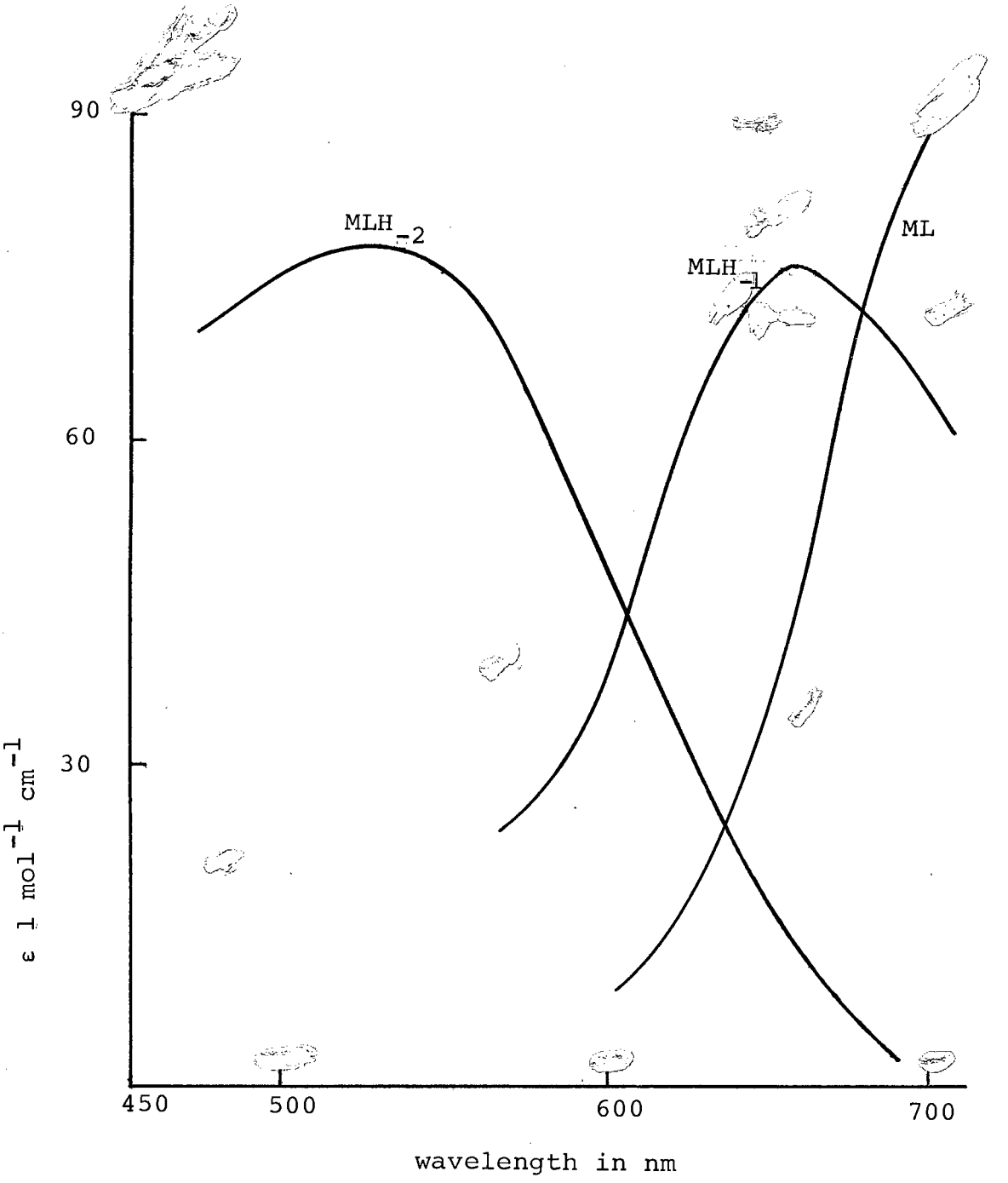

FIGURE 3. Molar absorbances of the various Cu-DEO complexes in the visible region.

coefficient of octahedral spin allowed electronic transition are 1-10 while square planar complexes have extinction coefficients in the range $10 - 10^{2}$. The complexes in this study are between the latter extremes. Comment can also be made on the relative structure of these two complexes. In going from MLH_{-1} to MLH_{-2}, λ_{max} shifts to shorter wavelength. The same effect is shown in Figure 4 in which NH_3 is added to CuII. NH_3 is on the right of H_2O in the spectrochemical series which means that as successive H_2O molecules are replaced by NH_3, Δ, the crystal field splitting parameter, increases shifting the spectrum to the left. At the same time the symmetry of the complex is lowered resulting in an increased absorbance. Based on these observations, it can be concluded that in going from MLH_{-1} to MLH_{-2}, firstly there is a change in the coordination of the copper and since λ_{max} moves to lower wavelength this change is most likely due to coordination of another nitrogen atom.

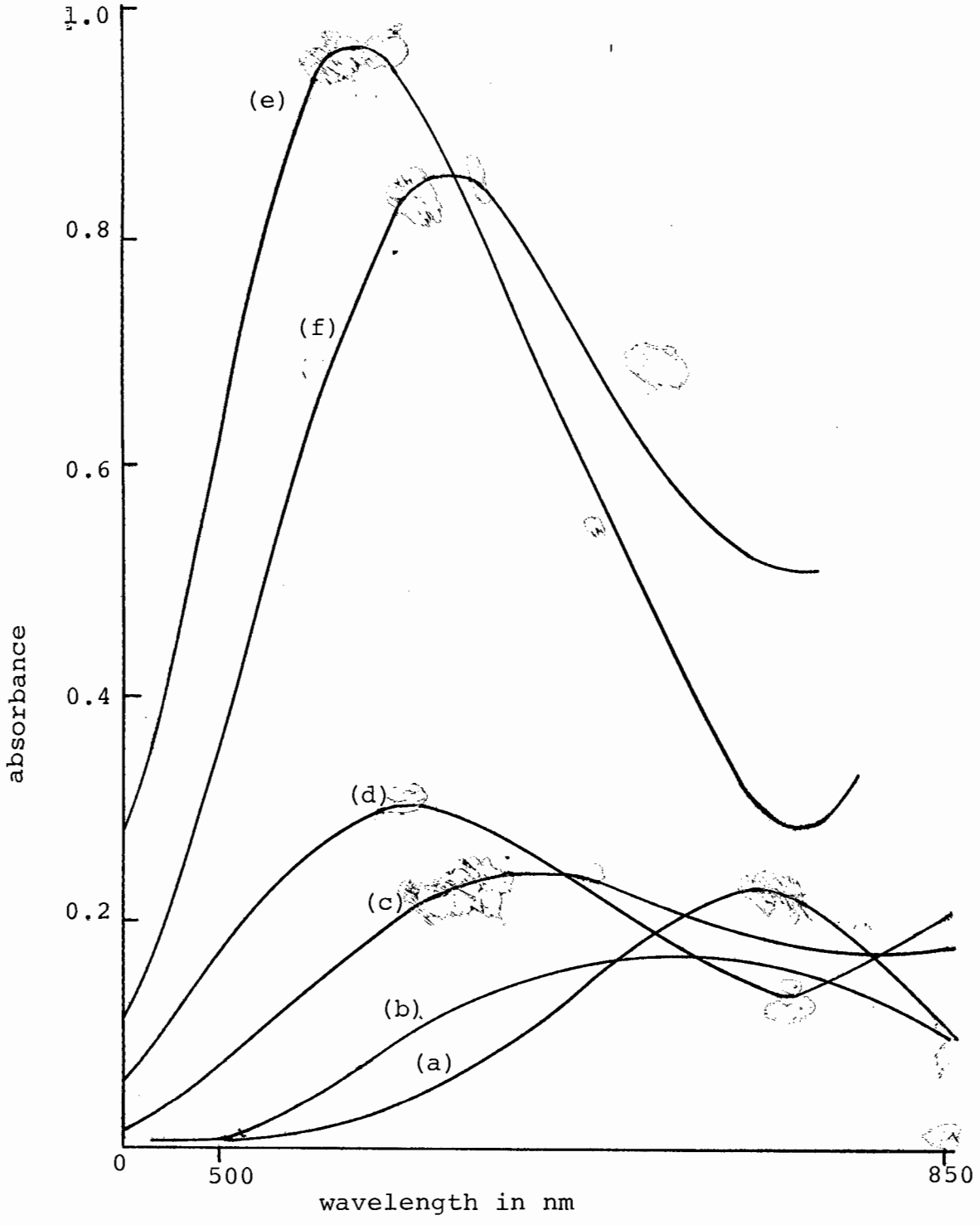

FIGURE 4. Spectra of $Cu(NH_3)_n(H_2O)_{6-n}$ showing the Jahn-Teller effect on increasing the number of NH_3 molecules, (a) $0NH_3$ (b) $1NH_3$ (c) $2NH_3$ (d) $3NH_3$ (e) $4NH_3$ (f) $5NH_3$ in molar equivalents.

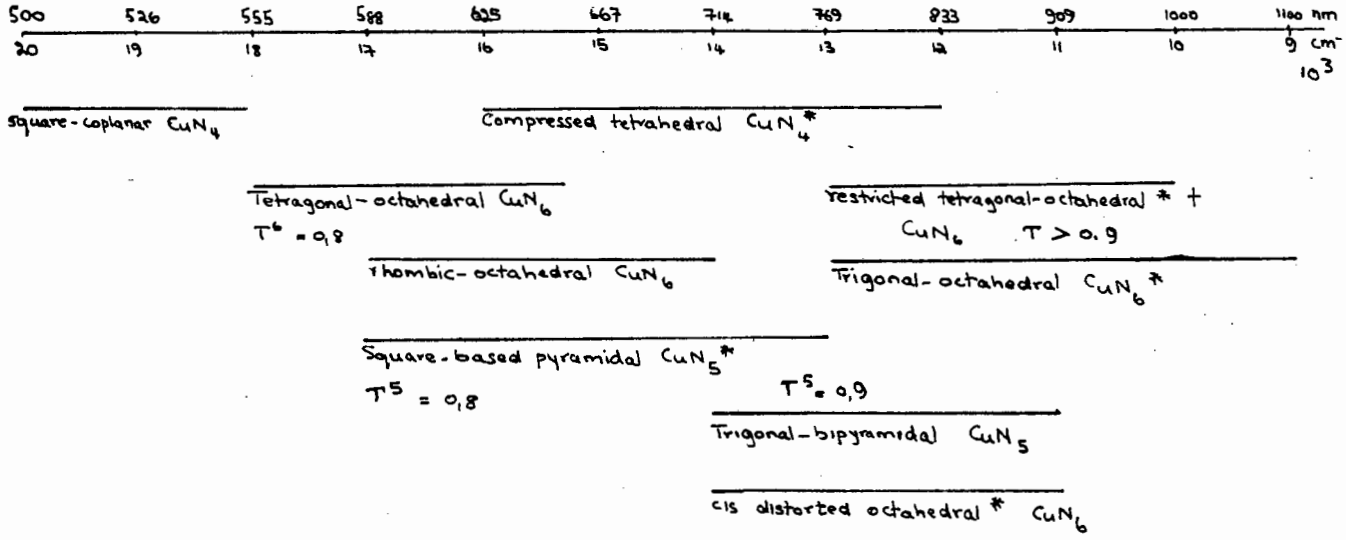

* Chromophores indicated involve a clearly resolved shoulder to low frequency

\+ In most cases the restriction arises through out-of-plane co-ordination by chelate ligand

FIGURE 5 : Summary of energy ranges for closely related $Cu-N_x$ chromophores with different sterochemistries

Figure 5 shows typical wavelength ranges for copper complexes. From this it can be seen that the Cu-DEO complexes all fall in the tetragonally-distorted, octahedral range. A compressed tetrahedral structure is unlikely with this ligand in aqueous solution.

Tetragonal distortion of an octahedral structure can result in either elongation or compression of the axial bonds. This is given by the tetragonality factor τ [113].

$$T = \frac{\text{mean in-plane Cu-L distance}}{\text{mean out-of-plane Cu-L distance}} \quad \ldots \quad (ii)$$

From this equation the following can be deduced. If T is less than one, then the distortion is by elongatged z-axial bonds, however if T is greater than one, the distortion is by compression and if the value of T is one then the structure is a regular tetrahedron.

Silver and Getz [116] give the potential Wells as shown in Figure 6.

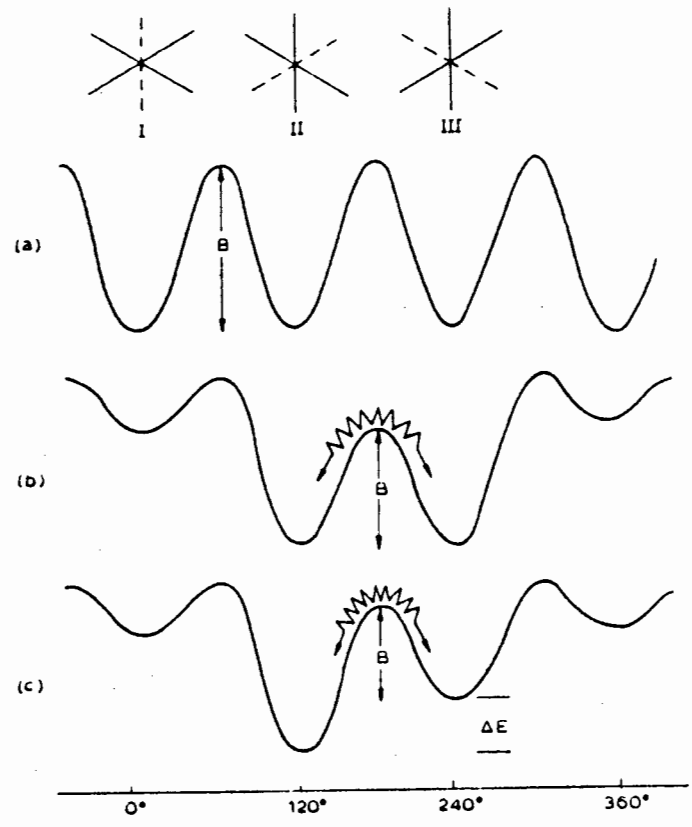

FIGURE 6 : The circular cross-section of the warped potential energy surface. (a) 3 wells of equal energy (b) 2 wells of equal low energy and (c) 1 low energy well

(a) In weak coupling, all three Wells have the same energy and equal population i.e. the barrier height B is the same.

(b) For $B < kT$ (temperature T), then this represents regular octahedral structure which suffers a dynamic Jahn-Teller effect. Strong Jahn-Teller coupling gives one Well of higher energy. In this state the module will be fluxional with interconversion of two elongated axes at each copper site. As far as the bond lengths are concerned the system would appear compressed octahedral. This, however, is a dynamic situation

labelled by Hathaway et al. [6] as the pseudo-compressed octahedral.

For $B > kT$, then there arises the static disordered situation with all three distortions occurring simultaneously. Their elongation axis being misaligned in the perpendicular directions. A Cu atom may be elongated along any of of the two orthogonal axes with the third axis unaffected. Crystallographically the average of these two mixed systems would be observed. This state is referred to as the pseudo-compressed tetragonal octahedral or compressed rhombic octahedral.

In the above instances, $B < kT$ and $B > kT$, crystallography cannot readily distinguish between them. This is because they yield averaged distortion, the former a time and the latter a statistical averaged distortion.

(c) In Figure 6(c) all the three Wells have different energy. If $B > kT$ a tetragonal stereochemistry which is statistically distorted and temperature independent is observed. The ^{T} values range from 0.8-0.85 implying that 2 axial (out of plane) bonds are longer. (See equation (ii))

For B < T a fluxional structure with a value of T that is temperature dependent is observed.

It has been found that most CuII complexes fall into the former (Figure 6(c)) condition i.e. B > kT. [113] The values of T in this case are < 1. In Figure 5 the region where the Cu-DEO complexes fall in, is that of T = 0.8-0.85 which implies that the complexes have a tetragonal stereochemistry with two elongated bonds.

The tetragonal stereochemistry can be further expanded by looking at the possible transitions involved. Generally, the greater the tetragonality, for example, the longer the axial bond in the d^9 CuII complexes, then the greater will be the energy of the d_{z^2}---$d_{x^2-y^2}$ transition. [113] The broad band which is usually visible in electronic spectra of CuII is an envelope of d_{xy}---$d_{x^2-y^2}$ and d_{xz} d_{yz}---$d_{x^2-y^2}$ transitions. As the axial bond lengthens, the latter two transitions shift to the blue region of the spectrum. [113] The blue shift ~~has~~ is interpreted to imply that as the axial bond weakens the CuII ion attracts the in-plane ligands more strongly. This results in the $d_{x^2-y^2}$ orbitals becoming more antibonding and the $d_{xz}d_{yz}$ orbitals becoming more stable. This means that in the Cu-DEO complex there are therefore 4 short, planar and strong Cu-N bonds and 2 long, axial and weak Cu-O bonds (of the H_2O molecules) due to Jahn-Teller effect.

The effect of increasing tetragonal elongation eventually removes the axial ligands from coordination sphere of the central atom which leaves a square planar structure. This implies that there is no sharp line dividing the tetragonal from the square structure.[87]

In conclusion, the structures proposed for the MLH_{-1} and MLH_{-2} complexes depicted in Chapter 3 are consistent with these results.

Figures 7 and 8 show the spectra obtained in the study. Looking at the spectra it can be seen that there is a broad band in the visible region (λ_{max} = 526nm) and another in the near UV region of the spectrum. Comparing the Cu-BSA complex with hemocyanin, a copper protein, the latter shows similar bands (Figure 9). These bands have been assigned to the copper moiety of the protein. [119] As can be seen from the spectra BSA and DEO do not absorb in the visible region.

varian

SuperScan

Part No. 71-100033-00

FIGURE 7

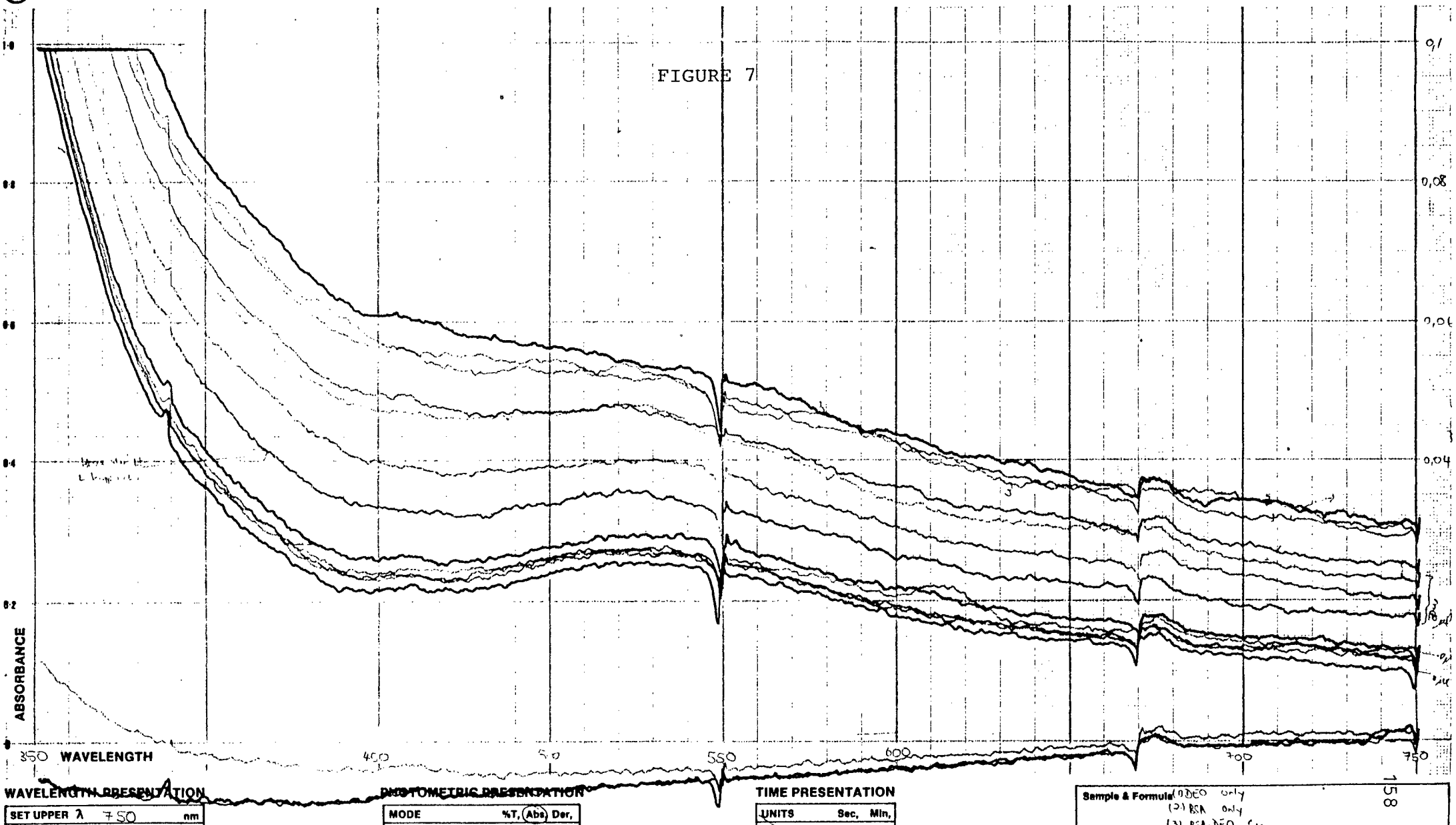

WAVELENGTH PRESENTATION

SET UPPER λ	750	nm
SCAN RANGE	40 nm	(1 nm/cm)
X AXIS	80 "	(2 ")
	200 "	(5 ")
	(400) "	(10 ")
	800 "	(20 ")
SCAN SPEED	10, 20, 50, 100, (200)	nm/min

PHOTOMETRIC PRESENTATION

MODE	%T, (Abs), Der,	
FULL SCALE	0·05	Abs
Y AXIS	(0·10)	"
	0·50	"
	1·0	"
	2·0	"
	4·0	"
	100%	T
REC. OFFSET		Abs.

TIME PRESENTATION

UNITS	Sec,	Min,
FULL SCALE	20	
X AXIS	40	
	100	
	200	
	400	

Sample & Formula	(1) DEO only (2) BSA only (3) BSA-DEO - Cu.		
Concentration	BSA-Cu 2mg·ml⁻¹M DEO 1mM-5mg·ml⁻¹	Date	19 | 11 | 87
Reference			Ref. No.
Path Length	10 mm	Operator	Kuku
Slit Width	1,5 mm		

varian

△

SuperScan

Part No. 71-100033-00

FIGURE 8

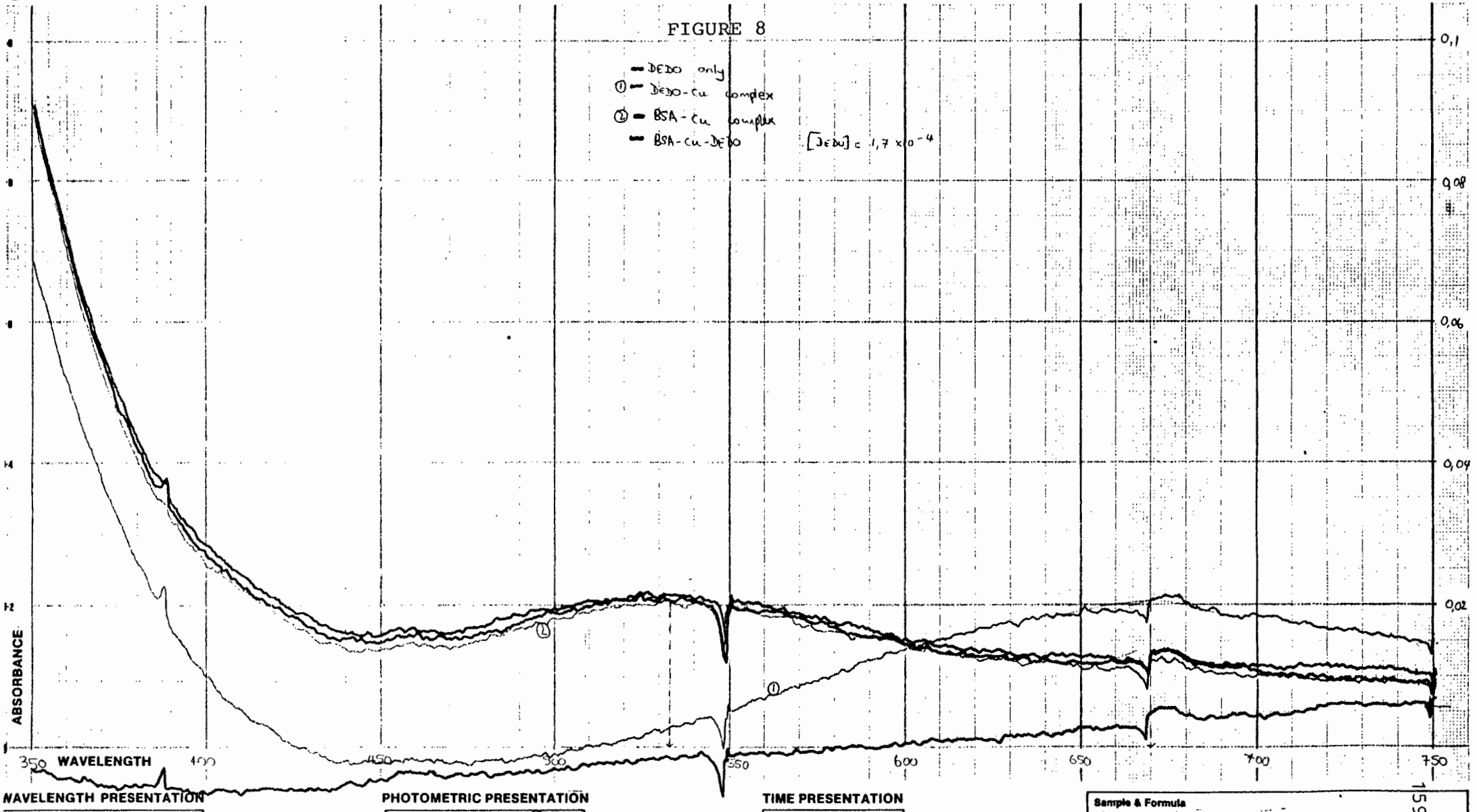

WAVELENGTH PRESENTATION

SET UPPER λ	750	nm
SCAN RANGE X AXIS	40 nm	(1 nm/cm)
	80 "	(2 ")
	200 "	(5 ")
	400 "	(10 ")
	800 "	(20 ")
SCAN SPEED	10. 20. 50. 100. (200) nm/min	

PHOTOMETRIC PRESENTATION

MODE	%T, (Abs) Der,	
FULL SCALE Y AXIS	0·05	Abs
	0·10	"
	0·50	"
	1·0	"
	2·0	"
	4·0	"
	100%	T
REC. OFFSET		Abs.

TIME PRESENTATION

UNITS	Sec, Min,
FULL SCALE	20
X AXIS	40
	100
	200
	400

Sample & Formula: BSA - Cu - DEDO		
Concentration 2 x 10⁻⁴	Date 18/11/87	Ref. No.
Reference H_2O		
Path Length 10 mm	Operator Lutu	
Slit Width 1·5 nm		

159

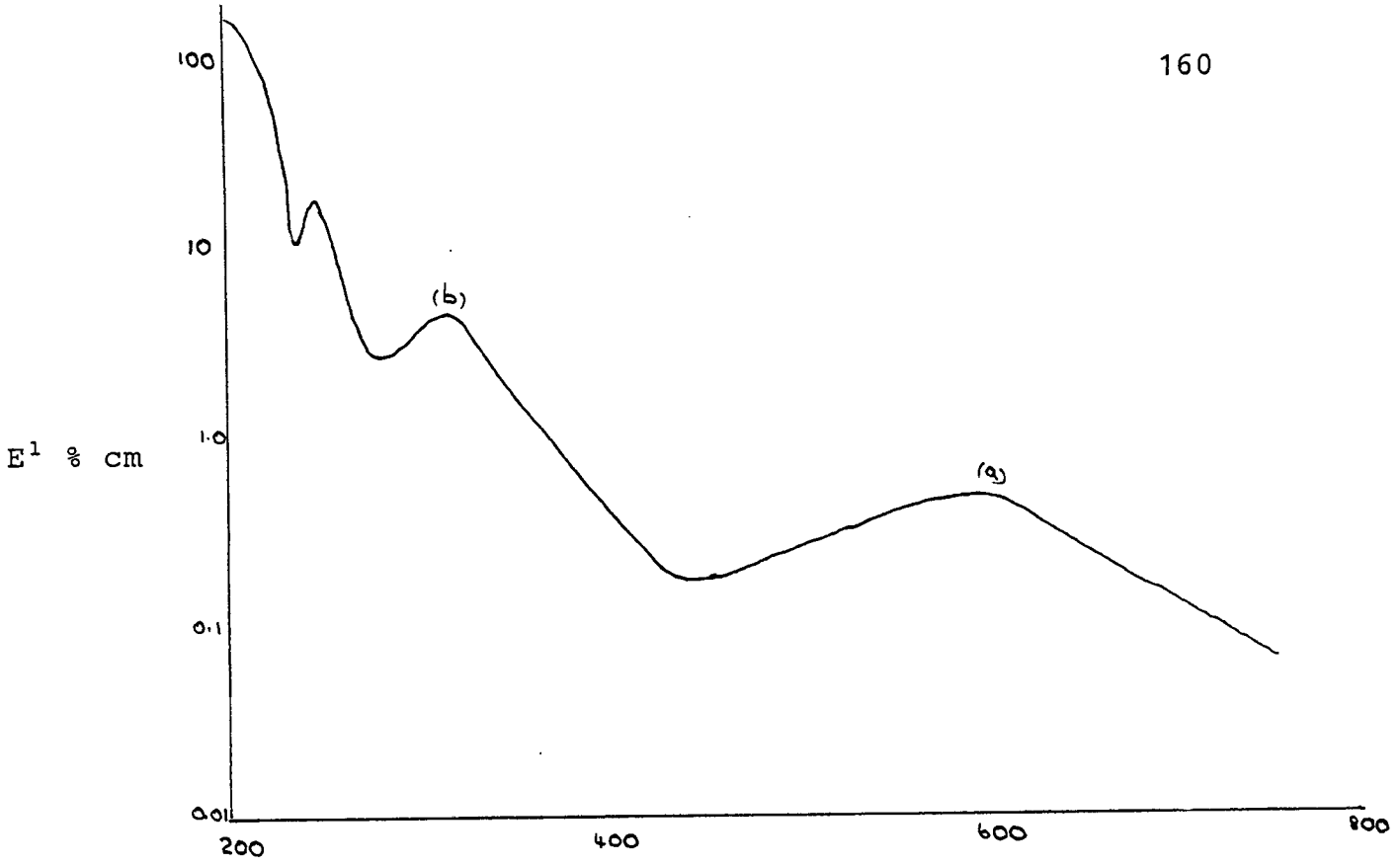

FIGURE 9 : The visible and near-UV spectrum of hemocyanin, bands (a) and (b) arise from the copper moiety

A number of factors have to be borne in mind in these spectra analyses. The structure of the albumin is single strand polypeptide. It is known that proteins show a great deal of hyperchromism in the UV region with denaturing. [114] In these spectra, however, this property can be ruled out since BSA does not absorb anywhere near the scanning region and it is unlikely that its denatured structure would do so.

Another aspect to look at is shown in the following table:

TABLE 1

λ_{max}	Cu-BSA	= 526nm	ε = 101.5 l mol^{-1} cm^{-1}	(a)
λ_{max}	CU-HSA[(b)]	= 525nm	ε = 101 l mol^{-1} cm^{-1}	(c)

(a) obtained in this study

(b) HSA = human serum albumin

(c) reference 61

The bovine, rat and human serum albumin have similar sequence of the amino acids in the (1-24)NH_2 terminal of the protein.[61] The absorbance wavelength of the CU-BSA and Cu-HSA complexes are very similar and so are the extinction coefficients. With the similarity in extinction coefficients and the binding site of the BSA to that of HSA, it is therefore apparent that the Cu-BSA complex prepared in this study is similar to the Cu-HSA in structure. This means that during the purification of BSA the copper binding peptides were not disturbed.

The Cu-BSA-DEO spectra show both a shift to longer wavelength and an increase in intensity as the DEO concentration increases. The red shift is highly evident in the near UV region. This could be due to the increase in DEO since the Cu-DEO complex has an intense band in the UV region. (See Figure 8)

The interpretation of this phenomenon is that with increase in DEO, the copper is removed from the BSA and so the Cu-DEO peak increases while the Cu-BSA peak decreases. The latter is evident by the 'flattening' of the λ_{max} of about 526nm, as a result of being swamped by the Cu-DEO peak.

Only qualitative results can be discussed here as the quantity of copper removed per increment of DEO cannot be determined under the conditions of this study. Also the exact mode of action of DEO is not clear. It could be any of the two possible ways, one that DEO is competing with BSA for copper and from the increase in absorbance, it can be implied that the copper ion is released from BSA straight on to the DEO. Another possible way could be that DEO attaches itself on to the protein, thus changing the structure of the protein which enhances the release of copper. The latter method is similar to that postulated for D-penicillamine. [44]

The conclusion arrived at in this study is that DEO is capable of removing copper from BSA <u>in vitro</u>. The challenge from endogenous amino acids <u>in vivo</u> is modelled using the computer blood plasma model ECCLES. [26] The mode of action will, however, still not be clear.

CHAPTER 5

SUPEROXIDE DISMUTASE ACTIVITY TEST

5.1 Introduction

Superoxide and other free radicals contribute significantly to sustaining chronic inflammation by promoting connective tissue degradation. The autoimmune response of RA is also initiated and maintained by these radicals. A typical polymorphonuclear leukocyte population in RA synovial fluid is reported as 10^7 cells cm^{-3} [121] and on the other hand superoxide radicals are released extracellularly by activated polymorphonuclear leukocytes at a rate of up to 10nmol 10^{-6} $cell^{-1}min^{-1}$. [122] Thus there is a large potential source of free radicals within the synovial cavity.

Consider the reactions involved in the cells of a healthy subject. During the transportation of electrons to molecular O_2 via the mitochondrial respiratory chain, as well as in various hydroxylation and oxygenation reactions, toxic, partial reduction of products of oxygen may be formed. These toxic substances O_2^- and H_2O_2 are presumed to be transient intermediates on the active site of the enzyme involved [123] and are capable of irreversible damage to various biomolecules. There is, however, some uncertainty in the electron transport chain of the mitochondria. It is not quite clear how electron flow in the chain is coordinated to yield four electrons. One suggestion is that the cytochromes may be functioning in pairs. This could be important since reduction by a single electron yields

O_2^- radical, whereas reduction by two electrons yields H_2O_2 [124].

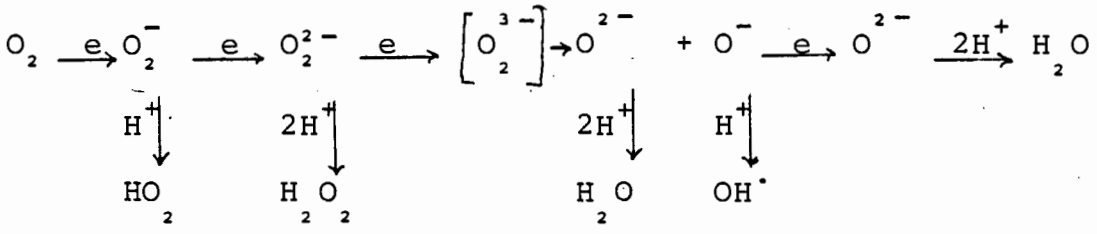

However, evidence indicates that the enzyme involved in the intermediates' formation is an Fe-sulfur protein [125]. This protein is involved at several points in the NADH to oxygen chain. The protein serves to bind the intermediates thus forming Fe-superoxides, Fe-peroxide and Fe-oxide which are transferred to the enzyme substrate to complete reaction to H_2O and the free enzyme. There is inevitably some leakage of the intermediates from the various reactions. The flux is, however, low. [124]

Normal cells contain superoxide dismutase which converts O_2^- thus:

$$2O_2^- + 2H^+ \longrightarrow H_2O_2 + O_2$$

The resultant toxic H_2O_2 is decomposed by the heme enzyme catalase, a flavoprotein oxidase found in the peroxisomes.

$$H_2O_2 \longrightarrow H_2O + \tfrac{1}{2}O_2$$

Therefore dismutase and catalase are interdependent in their protective action. Ascorbic acid, glutathione and vitamin E support these enzymes in serving as scavengers of the free radicals.

Superoxide dismutase is found in two forms, one in the extramitochondrial cytosol and the other form in the mitochondria. [125] The mitochondrial form contains Mn^{2+} and has a structure similar to superoxide dismutase of bacteria. The cytosol form has a different structure which contains Zn^{2+} and Cu^{2+}. The dismutase is present in high concentration and is extraordinarily active. This suggests that as soon as superoxide radicals are produced during oxygen reduction in the tissues they are quickly removed.

Extracellular fluids are poor in superoxide dismutase, however the human serum has antioxidants which protect the cell. They function by limiting the reactivity of metal catalysed production of radicals and their peroxide intermediates. [126, 127]

During phagocytosis, that is the process of engulfment of external solid microorganism by the cell membrane, the phagocytic leukocytes engulf these alien objects in the plasma membrane envelope. The leukocytes deliberately produce both O_2^- and H_2O_2 to destroy these microorganisms. These leukocytes are therefore fused with lysosomes and can

be released as puss. Under conditions where the leukocytes are not overloaded, these highly reactive entities are retained in the phagocytic vacuole. Damage therefore will only occur at the target cell. Under acute conditions, however, these toxic products are released into the extracellular fluid. This is the reason for the increased flux of O_2^- and H_2O_2 in the plasma. [124]

Lipid peroxidation, i.e. an oxidative deterioration of the unsaturated fatty acid molecules, is mediated by the free radicals. [9] Hydrogen atom abstraction in this reaction is the cause of a chain reaction which leads to the damage to lipid molecules e.g. membrane structure. The damaged lipid membrane forms peroxides.

Iron and copper are known to stimualte peroxidation by forming new radicals with the product peroxide. [9, 127] Copper has been found to be more effective in this reaction than iron.

$$2LOOH \xrightarrow[\text{complexes}]{\text{copper}} LO^{\cdot} + LO_2^{\cdot} + H_2O$$

This increases in free radicals, O_2^- and the H_2O_2 overpowers normal antioxidant defense. The same problem occurs in cells with antioxidant protection which cannot cope even with normal radical production. Under

these conditions digestion of the cartilage and inflammation occurs. Products of lipid peroxidation have been detected in the synovial fluid of RA patients. [9]

The proteins lactoferrin and transferrin are the important antioxidants when iron is the catalyst. For copper stimulated damage, albumin and ceruloplasmin are the antioxidants. Lower levels of serum albumin in RA patients might also contribute substantially to lower copper antioxidant protection. [9]

Copper complexes have been proven to be active as antiarthritic agents. [47, 57] This is the general form which includes both arthritic conditions viz. anti-inflammatory and antiulcer activities. SAARDs have been found to act differently from the above agents in that they have superoxide dismutase activity in the synovial fluid. They thus act as antioxidants. For D-penicillamine it has been shown [186] that its copper complex catalyses the dismutation of the O_2^- radical. This could be one way in which these drugs act on the RA patient's synovial fluid thus rendering them clinically active.

An in vitro test which has been developed by Roberts and Robinson [86] has been used in this study to estimate the dismutase activity of the ligands in this research. The test is based on the production of O_2^- radicals by purine

degradation, as in Figure 1. The reaction used in the test is:

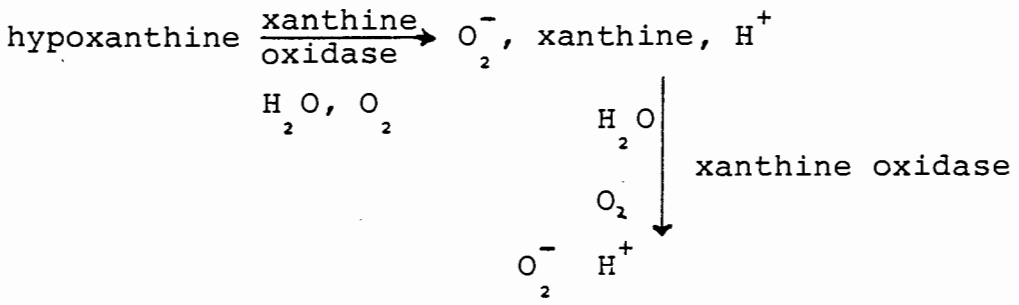

where the production of O_2^- is monitored using NBT (nitrobleutetrazolium). The ability of a test complex to inhibit O_2^- production is measured in the presence and absence of EDTA where the EDTA is introduced to simulate the competition that the drug is likely to experience with regard to other copper chelating ligands in vivo. Based on these results the ligand can be classified as:

1) Active - if the complex has dismutase-like activity <u>and</u> is stable in the presence of EDTA, $I_{50} << 20\mu M$ copper

2) Active and unstable - if the complex has dismutase-like activity but is not stable in the presence of EDTA, i.e. it loses copper to EDTA until the latter is saturated, $I_{50} \simeq 20\mu M$ copper

3) Inactive - The complex does not have dismutase activity.

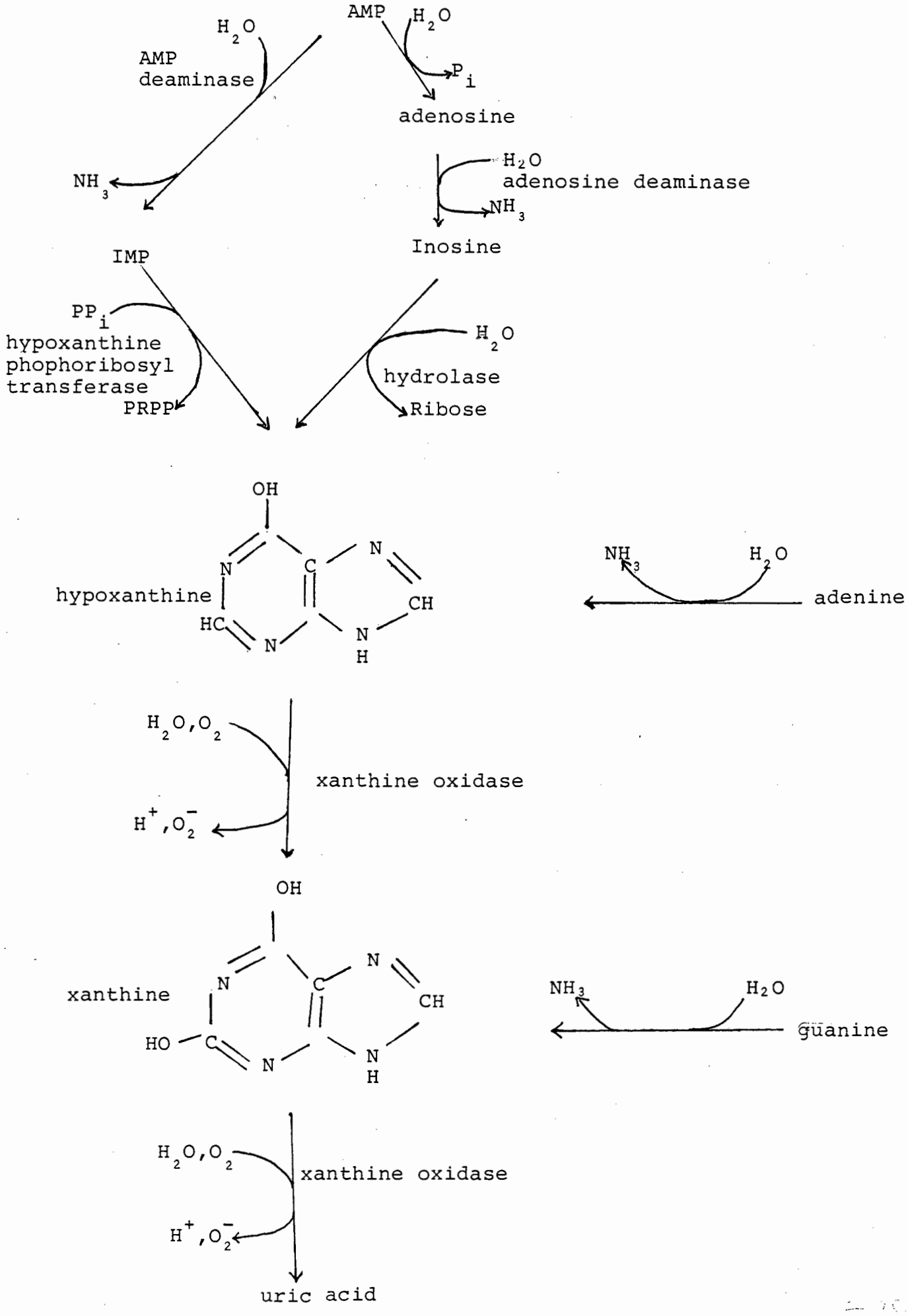

FIGURE 1 : Purine degradation pathway showing the production of superoxide

5.2 Experimental

5.2.1 Reagents

Hypoxanthine, xanthine oxidase (E.C. 1.2.3.2.) grade I, nitrobleutetrazolium grade III, Hepes buffer and the monosodium salt pH 7.5 were purchased from Sigma Chemical Company and used without further purification. EDTA and gelatin were purchased from BDH Chemical Limited, $CuCl_2-2H_2O$ from Saarchem Limited, while DEO and DMO were synthesised in this laboratory.

5.2.2 Method

A modified version of the method of Roberts and Robinson was used.

Solutions of copper and DEO were prepared independently at 10^{-2} M in 100mM Hepes buffer (HE buffer) pH 7.5. The copper and DEO solutions were then mixed in a molar ratio of 1 : 2 and diluted with HE buffer to a copper concentration of 10^{-4} M. Increasing amounts of a 10^{-3} M EDTA solution, in the HE buffer, were then mixed with identical aliquots of the Cu-DEO solution and incubated for 1 hour at 20°C. Duplicate aliquots of these solutions calculated to give a final EDTA concentration of 20μM were taken and tested for superoxide dismutase-like activity by the inhibition of the NBT by O_2^- .

The assay solution for superoxide dismutase-like activity contained 20μM hypoxanthine, 500μM NBT, 1mg/ml gelatin, Cu-DEO-EDTA solution and HE buffer in a total volume of 3ml. The reaction was initiated by the addition of 30μl xanthine oxidase (0.1 units/ml) and was allowed to go to completion in the dark overnight at 20°C. The reduced NBT was measured photometrically at 500nm on a Varian Superscan 3 spectrophotometer thermostated at 20°C.

In parallel with the above assay, control solutions were assayed. Inhibition of NBT reduction was calculated from the equation:

$$\% \text{ inhibition} = 1 - \frac{A_{EL} - A_O}{A_E - A_B} \times 100$$

where A_{EL} = test solution with xanthine oxidase absorption

A_O = test solution without xanthine oxidase

A_E = test solution without Cu-DEO

A_B = test solution without Cu-DEO or xanthine oxidase

5.3 Results and discussion

Figure 2 shows the dose-response curves obtained in this study. The curve without EDTA shows how active the ligand is on its own. The ligand shows percentage inhibition of 57 even at 1μM copper. In the presence of EDTA (20μM), however, the value for I_{50} is 6μM indicating its partial stability in competition with EDTA. Under the two conditions the complex has the same dismutase activity down to a copper concentration of 7.6μM. Below this concentration the activity decreases sharply, presumably due to loss of copper from the complex to EDTA.

For comparison, Table 1 gives a list of clinical antirheumatic drugs and the SOD-like activity of their copper complexes. Most of these ligands have been used clinically in the treatment of RA.

TABLE 1

Ligand	I_{50} μM (a)
DEO	6 (b)
D-penicillamine	8
Thiola	6
Captopril	11.5
Aspirin	20
Indomethacin	19
Carprofen	19
Diisopropylsalicylate	19.5
Trien	>> 20
L-cysteine methyl ester	> 20
Thiomalic acid	18.5
Azathioprine	>> 20
Chloroquine	19.5
Salphasalazine	20

(b) obtained in this study (a) ref. [86]

From the table the SAARDs have similar activities, for example D-penicillamine, thiola and captopril, while NSAIDs, for example, aspirin and indomethacin are active but unstable, see clarification in Section 5.1. Based on these observations DEO has activity similar to that of D-penicillamine and is therefore not only a good copper

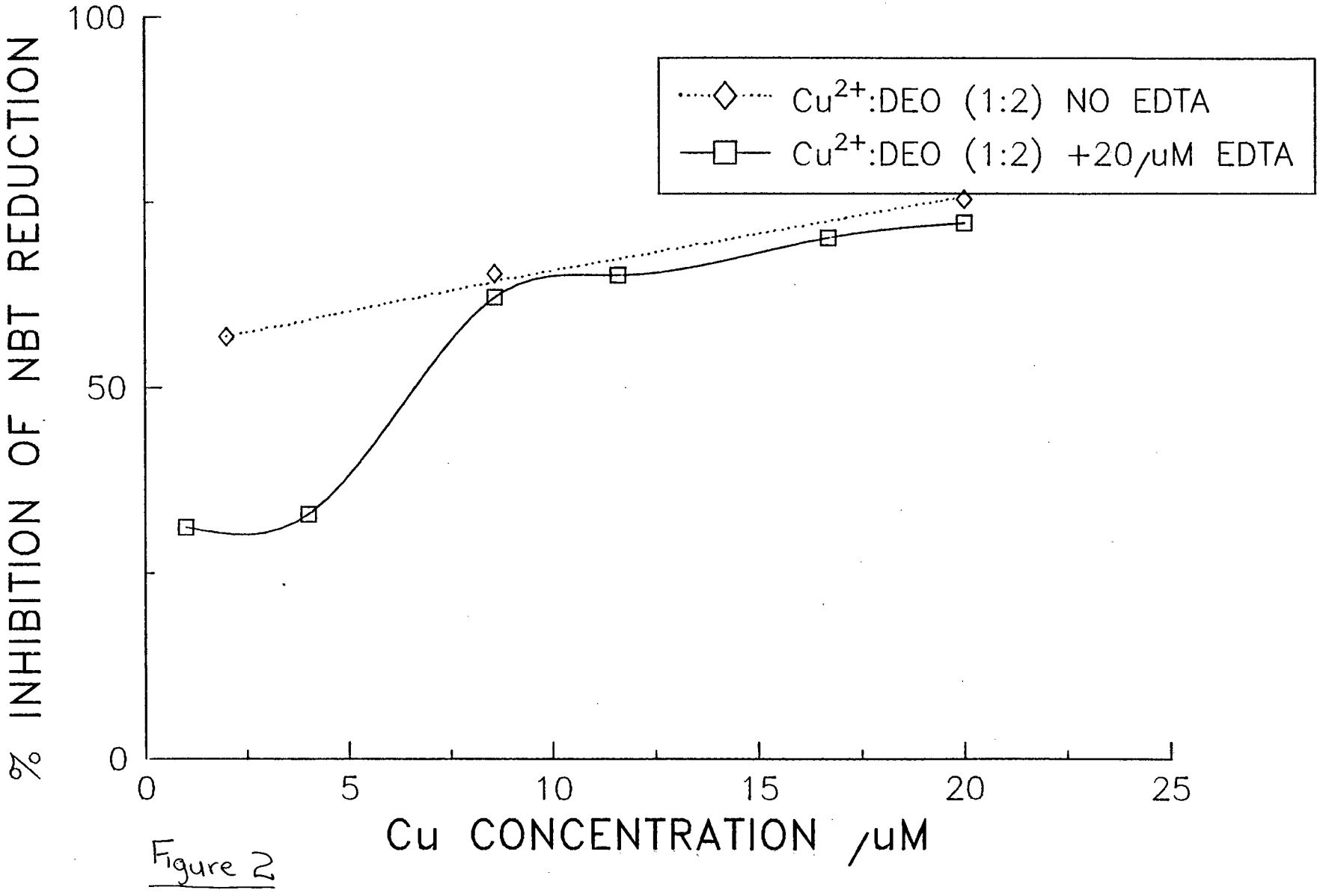
% INHIBITION OF NBT REDUCTION
100
50
0
0
5
10
15
20
25
Cu CONCENTRATION /uM
Cu2+:DEO (1:2) NO EDTA
Cu2+:DEO (1:2) +20/uM EDTA

Figure 2

chelating ligand but also the results show that it has the ability to dismutase superoxide radicals.

Table 2 shows the structure dismutase activity relationships for a series of polyamines. From the table it can be seen that ethylenediamine and its derivatives have a fairly high dismutase activity. The variation in activity can be explained by the difference in stability of their copper complexes. With increase in chain length, the stability of the copper complexes decreases and so the ligand is not able to compete with EDTA.

The addition of an electronegative group to the structure e.g. adding COOH to 1,2 diaminopropane forming 2.3 diaminopropionic acid has improved the stability of the complex and also the dismutase activity of the ligand increases. DEO has the advantage that at physiological pH 7.4 it forms neutral species resulting from the deprotonation of the amide nitrogens.

From the table DEO and trien show vast differences in their dismutase activity. Categorising these ligands it can be seen that trien is EDTA-like in activity while DEO is active to the test. Trien is a very good copper chelator and is used in the treatment of Wilson's Disease [79,80]. It is also the core structure of DEO. The amide groups on DEO have given the neutral copper complex a high stability and

TABLE 2

Compound	Structure	n	R	Test activity[a] I_{50} µM
ethylene diamine	$HN_2-(CH_2)_n-\underset{R}{CH}-NH_2$	1	H	6
1,3 diaminopropane		2	H	14
1,4 diaminopropane		3	H	17-20
1,5 diaminopropane		4	H	17-20
1,6 diaminopropane		5	H	17-20
1,2 diaminopropane		1	CH_3	6
2,3 diaminopropionic acid		1	COOH	5.5
2,4 diaminopropionic acid		2	COOH	11
DEO	$NR_2-(CH_2)_n-N-\overset{O}{\overset{\|\|}{C}}-C-\overset{O}{\overset{\|\|}{C}}-N-(CH_2)_n-NR_2$	2	CH_2-CH_3	6[b]
trien	$NR_2-(CH_2)_n-N\ \underset{H_2}{C}-C-\underset{H_2}{C}N(CH_2)_n-NR_2$	2	H	20

(a) reference 86

(b) in this study

the dismutase activity is comparable with other tested ligands.

From this test evidence is growing that a neutral copper complex which may favour copper transport and mobilisation in vivo is one with the core structure:

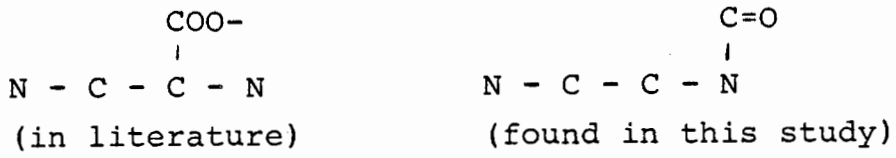

(in literature) (found in this study)

This was also suggested by other workers [12] who did not use this method to predict the structure but used computer simulated results. It is suggested that this structure can possibly form a tertiary complex Cu.L.His with Histidine. [86] Histidine has been found to be the vital amino acid in the albumin copper binding moeity [61], its I_{50} = 4,5uM copper. [86]

This core structure has also been found to catalyse superoxide dismutation - see Table 2. Such low molecular weight complexes have been tested using computer models [85] and were found not to be good copper mobilisers in vivo. DEO has the advantage that it only forms a 1 : 1 neutral copper complex and does not rely on ternary complex formation for stability.

The structure activity relationships table can therefore be useful in identifying more suitable candidates for trials as potential antirheumatic agents.

In conclusion, although DEO has not been subjected to clinical tests, from the above results it is a promising ligand for RA treatment.

CHAPTER 6
GENERAL DISCUSSION

6. General Discussion

The ligands DEO and DMO are diaminodiamide ligands, however, the heavy alkyl groups on the amine nitrogen has made the amino character more pronounced than the amide one. This is evident in the fragmentation patterns of their mass spectra. The basicity of the two amine nitrogens in each ligand is virtually the same. This is manifest in their protonation studies where the formation curves show only one inflection (page 56) (Figure 3.6). The difference in the LH_1 and LH_2 constants is about 0.8 log units. This trend is observed in similar structured ligands, e.g. 3,7-diazanonane-1,9-diamine (I), 1,9diamino-3,7-diazanonane-4,6 dione (II) and BAO (III) all of general structure.

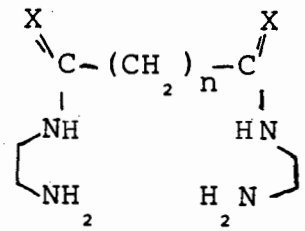

			log K_1	log K_2 [68]
I	X = H	n = 1	10.25	9.5
II	X = O	n = 1	9.08	8.82
III	X = O	n = 0	9.23	8.48

For metal complexation, DMO and DEO can be compared to linear and macrocyclic dioxotetraamines and also the polypeptides. They are similar to polypeptides in that they have four donor atoms and also form square planar complexes.

Structural differences do, however, exist, like the fact that for DMO and DEO the deprotonated amide groups are in one chelate ring. Another difference is in the terminal amine donors.

Table 1 shows the equilibrium constants of the different Cu-ligand systems. Going from L_1 to L_3 the stability constants of the ML species decreases. This is interpreted as being due to the inductive effects of the alkyl substituents on the amine nitrogen, hence reducing the metal complex stability. For the neutral complex MLH_{-2}, DEO and DMO (L_3 and L_2) have similar constants to L_5 and the tripeptide L_9 although the actual values are slightly lower. Generally they are about 0.8 log units lower. In both cases, L_5 and L_9, the ring cluster is 5.5.6 while DMO and DEO have 5.5.5 type. In an individual ring system the five-membered ring is the most stable, with the six-membered ring experiencing strain. However, in a system with linked rings as in the case of DMO and DEO, cumulative ring strain is experienced. The introduction of a six membered ring in the link relieves the strain therefore increasing the stability of the complex. In the series in Table 1, the most stable complex is that formed between Cu and the ligand L_6. In this macrocycle there are two five-membered rings and two six-membered rings. However, L_7 has a similar arrangement of the rings but is lower in stability. Looking at the structure it can be noted that the two six-membered

TABLE 1

Comparison of dioxo-tetramine and tripeptide equilibrium constants

ligand	$\log K_{LH_1}$	$\log K_{LH_2}$	$\log K_{ML}$	$\log K_{MLH_{-1}}$	$\log K_{MLH_{-2}}$
L_1 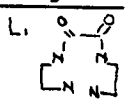	9.23	8.48	9.41[a]		
L_2 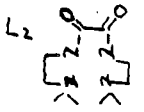	6.848(1)	5.952(1)	9.23(3)	3.44(4)	-2.94(3)[b]
L_3 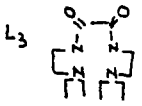	7.037(2)	6.218(1)	8.74(2)	3.71(2)	-2.98(1)[b]
L_4 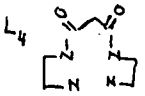	9.08(5)	8.82(5)[c]	7.93[a]		-5.1(5)
L_5 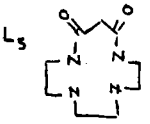	9.05(5)	3.82(5)			-2.2(2)[c]
L_6 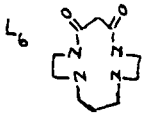	9.57(5)	5.97(5)			1.0(1)[c]
L_7 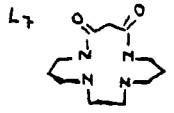	9.4(5)	6.52(5)			-4.5(4)[c]
L_8 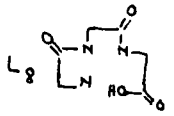	7.9	3.27			-6.5[d]
L_9 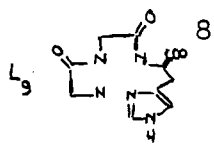	8.2	6.87[e]			-2.1[f]

The numbers in parenthesis show the standard deviation on the last digit.

(a) reference 109 (b) in this study (c) 68
(d) 131 (e) 132 (f) 130

rings are opposite each other but not including the amide ring. The L_6 on the other hand, has its six-membered rings also opposite each other but including the amide ring. This implies that the two side rings do not play a significant role in the complexation but the ring opposite the amide, noted as well for L_9. For the DMO and DEO this observation could mean that to improve the formation constant value, modification on the structure need only be concentrated on the side opposite the amide. The side rings overcome the strain by adopting the gauche conformation, whereas the amide ring is rather rigid and cannot be subjected to this type of conformation.

The cavities of the dioxotetraamines are small enough for the Cu II ion to bind to the amine, thus simultaneously deprotonating the amide. However, larger cavities show little effect of this, e.g. L_4, L_7 and L_8 which are capable of stretching, widening the cavity size. On the other hand, the ring opposite the amine cannot widen the cavity to any extent without inducing strain because the amide ring is rigid. It is this cavity size that was banked upon for the selectivity of Cu II over other metal ions.

The Cu II ion is smaller than the majority of metal ions in the biological system. Achieving high copper selectivity would imply that the metal ion homeostatis is not disturbed in the blood plasma.

The order of the ability to deprotonate the amide in DEO is represented in graphical form in Figure 1. For the transition metal ions Mn through to Zn (although not classified as a transition metal ion) the peak is observed at the Cu II ion. However, for DEO, the Ca II and Cu II ions have similar formation constants, with DEO slightly lower. This could pose a problem in the mobilisation of the metal ions in the blood plasma. However, DMO has no significant coordination with the other metal ions, except Cu, that could pose a serious problem. Therefore with DMO it seems that the envisaged selectivity has been achieved. The reason for the strong coordination would be the small cavity together with the weaker basicity than DEO. Therefore the Cu II ion is able to deprotonate the amide below pH 7 by fitting into the cavity.

The formation constants of Ca, Cu, Mg and Zn with DEO and DMO were incorporated into the computer blood plasma model ECCLES [26] programme. The free metal ion concentrations used in the simulation are shown in Table 2.

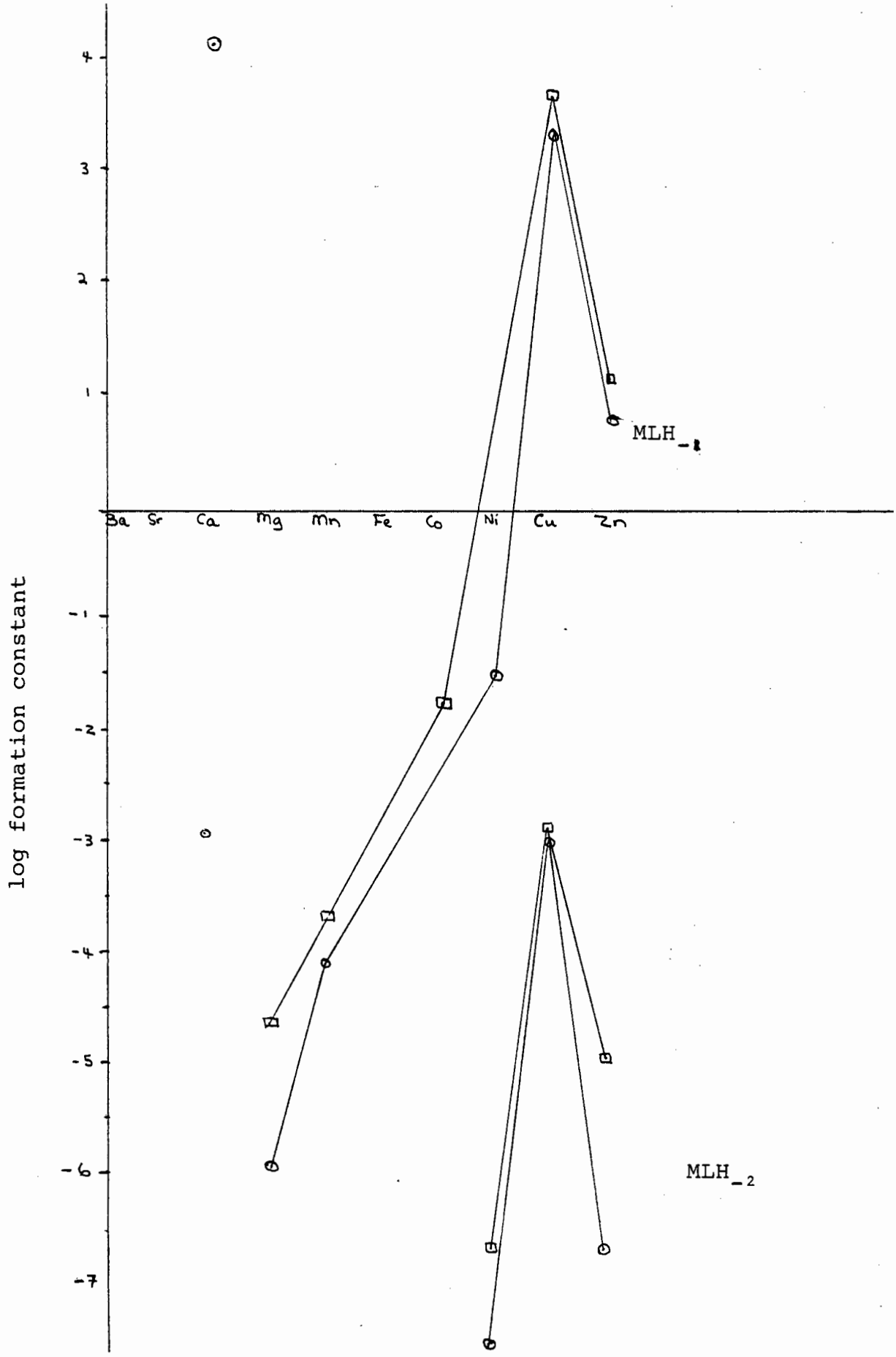

FIGURE 1 : DEO and DMO complexes with metal ions showing the Irving-Williams series behaviour

□ = DMO ○ = DEO

TABLE 2

Free concentrations of metal ions in blood plasma model used in the simulations

Metal ions	Concentration ($mol.dm^{-3}$)
Ca^{2+}	1.46×10^{-3}
Mg^{2+}	6.73×10^{-4}
Zn^{2+}	1.9×10^{-7}
Cu^{2+}	4.09×10^{-13}

The ability of the ligands to be able to compete for metal ions with plasma proteins can be estimated using the parameter Plasma Mobilising Index (PMI). This parameter is defined as:

$$PMI = \frac{\text{total concentration of the low-molecular-weight metal-ion fraction in presence of drug}}{\text{total concentration of the low-molecular-weight metal-ion fraction in normal plasma}}$$

Figure 2 shows the PMI curves for DMO and DEO. From the curves it can be seen that the metal ions most likely to be excreted are the Ca II, in the case of DEO and Zn II in the case of DMO. Excretion of metal ions is possible with the

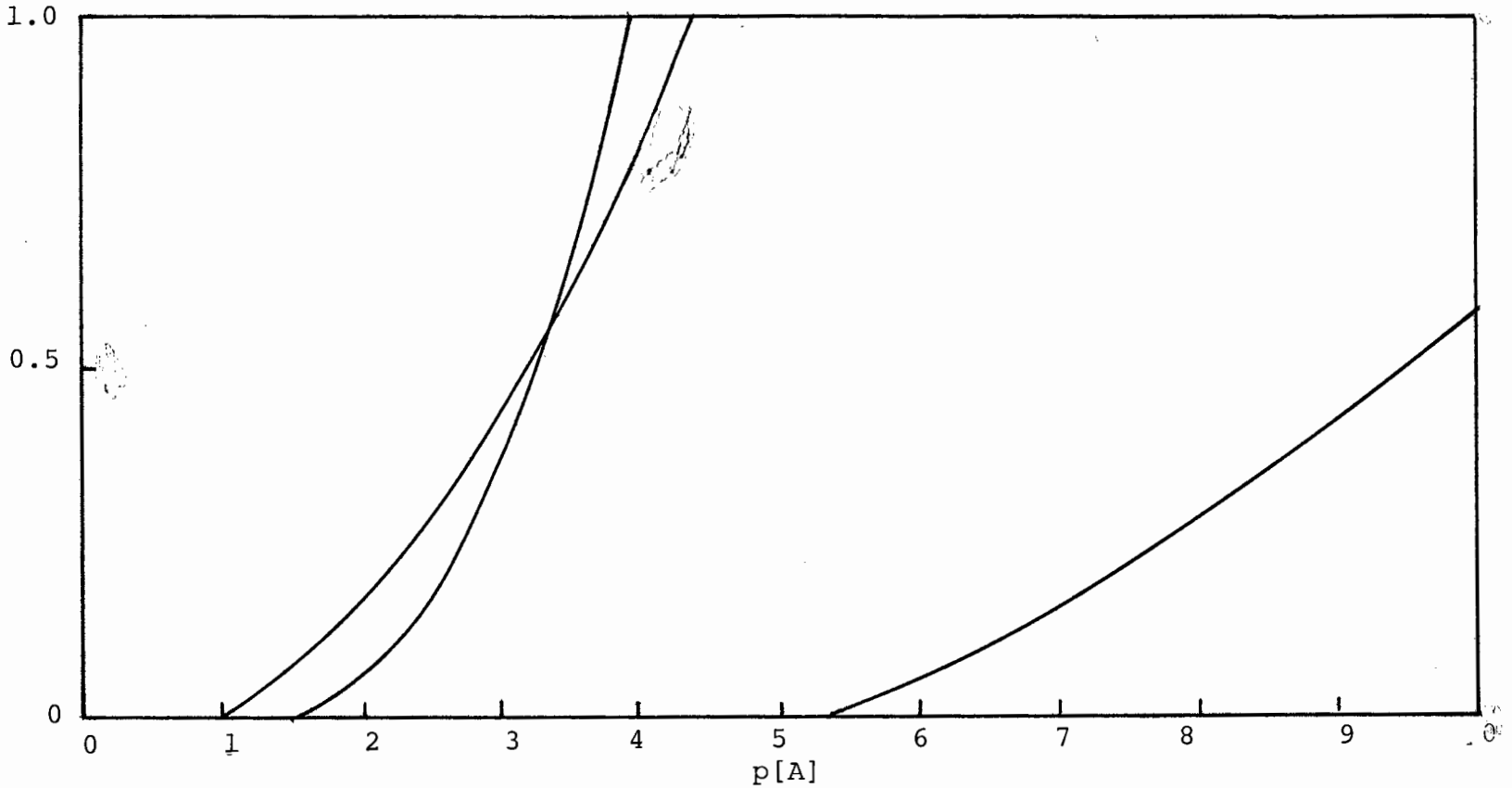

FIGURE 2. PMI curves for the effect of (i) DEO on the low molecular weight fraction of calcium ions and (ii) DMO on the molecular weight fractions of zinc and copper ions. Log PMI plotted against the log of the ratio by which the total ligand concentration (T_L) is increased on scanning.

formation of charged species, in this case the MLH_{-1}, that cannot penetrate the membrane barrier. For DEO the excretion can be expected since the formation constants of Ca-DEO are greater or equal to the Cu-DEO constants. However, the Zn-DMO formation constants are much lower than Cu-DMO constants, about 2.0 log units lower, yet Zn(II) is showing signs that it will be excreted from the plasma. The reason for this is that the free metal ion concentration of Zn(II) is 10^6 times higher than that of Cu(II). Because DMO concentration is so low, 10^{-8} $mol.dm^{-3}$, in the system virtually all of the DMO present is taken up by zinc. This has serious implications concerning zinc, because if the agent DMO is administered into the plasma, it could cause a zinc-deficiency. Zinc is important biologically, especially in tissue repair processes [133] and its deficiency could lead to serious side effects.

At higher concentrations about 10^{-4} $mol.dm^{-3}$ of DMO in the plasma DMO does mobilise copper but that is not the case with DEO. This could suggest that the smaller ligand is the nearly ideal one for copper mobilisation. Tying this observation up with that of the Cu-BSA, it could mean that DMO can compete with the albumin for copper by binding the metal ion directly. It is unlikely that the same modus operandum for D-penicillamine can be applicable to DMO since the oxygen and nitrogen atoms in the ligand can form weak

hydrogen bonds, as compared to the disulfide link formed by D-penicillamine with the albumin.[34, 44]

In order for a drug to be active in the treatment of RA it need not only be a good copper mobiliser but should also have dismutase activity. Superoxide radicals promote connective tissue degradation [12] and are therefore contributing to the chronic state of the disease. In search for an agent that does both, i.e. mobilise copper and also have superoxide dismutase activity, natural amino acids were tested together with the currently used drugs in RA treatment by Roberts and Robinson. [86] They found that histidine and cysteine competed effectively for copper binding and they gave I_{50} values of 4.5 and 12μM respectively. In the plasma, histidine and cysteine are the two predominant low molecular weight ligands that bind the exchangeable copper in plasma. [132]

The ligands in this study have properties similar to the polypeptides in their copper binding properties, and in their dismutase activity they are promising to have antirheumatic action. DEO has an I_{50} value of 6 which is in the region between the two active amino acids, histidine and cysteine. The advantage DEO and DMO have over these amino acids is the ability to form chelates.

With the above observations the conclusion can be arrived at that a polypeptide with a histidine-like structure on one of the side rings could work well in RA treatment. Possibly the structures similar to those studied by Sarkar et al. [61] However the CH_2 groups between the nitrogens would have to be two. This is shown to be effective in the structure-activity relationship depicted in Chapter 5. Finally, DMO is a much better ligand than DEO in mobilising copper in the plasma and the SOD activity is likely to be similar to that of DEO since the elemental structure is similar.

REFERENCES

1. M. Duc Dodon and G.A. Quash
Rheumatol. Int. (1983) 3 : 97-100

2. J. Clot and J. Sany eds
Rheumatology (1975) vol 6 Karger, Basel

3. G.E. Jackson, P.M. May and D.R. Williams
J. inor. nucl. Chem. (1978) 40 : 1189-1194

4. D.A. Gerber
J. Rheumatol. (1975) 2 : 384

5. J.S. Dixon, N.G. Sitton, K.E. Surrall et al.
Rheumatol. Int. (1983) 3 : 145-149

6. G.W. Rafter
Medical Hypotheses (1987) 22 : 245-249

7. R.B. Parekh, R.A. Dwek, B.J. Sutton et al.
Nature (1985) 316 : 452

8. M. Shingu, T. Todoroki and M. Nobunaga
Inflammation (1987) 11(2) : 143-151

9. J.M.C. Gutteridge, C. Hill and D.R. Blake
Clinica Chimica Acta (1984) 139 : 85-90

10. B.M. Babior
N. Eng. J. Med. (1978) 298 : 721

11. J.M. McCord
Science (1974) 185 : 529

12. B. Halliwell
Cell. Biol. Int. Rep. (1982) 6 : 529-542

13. D. Pitt
"Lysosomes and cell function", Longman Group Ltd., N.Y.
1975 Cha. 6 pp.126-146

14. J. Zodrow and S.H. Rogers
Life Science (1984) 34(20) : 1967-1975

15. B. Henderson, E.R. Pettipher and G.A. Higgs
British Med. Bulletin (1987) 43(2) : pp.415-428

16. L. Klareskog, R. Holmdahl, C. Nordling et al.
Acta. Med. Scand. Suppl. 715 (85-91)

17. A. Lorber, L.S. Cutler and C.C. Chang
Arth. Rheum. (1968) 11 : 65

18. W. Niedermeir, W.W. Prillaman and J.H. Griggs
Arth. Rheum. (1971) 14 : 533

19. D.H.Brown, W.W. Buchanan, A.F. El-Ghobarey et al.
Ann. Rheum. Dis. (1979) 38 : 174-176

20. J.R.J. Sorenson
Recueil des Trav. Chim. des Pays-Bas, June/July 1987
106 : 6-7 L-02

21. C.H. Cashin, E.J. Lewis and (late) T. Burden
British J. Rheumatol. (1985) 24 : 137-146

22. P.S. Hallman, D.D. Perrin and A.E. Watt
Biochem. J. (1971) 121 : 549-555

23. D.P. Bajpayee
Ann. Rheum. Dis. (1975) 34 : 162-165

24. M.W. Whitehouse and W.R. Walter
Agents Actions (1978) 8 : 85-90

25. P.Z. Neumann and A. Sass-Kortsak
J. Clin. Invest. (1967) 46(4) : 646-658

26. P.M. May, P.W. Linder and D.R. Williams
J. Chem. Soc. Dalton (1977) 588-595

27. D.I.M. Harris and A. Sass-Kortsak
J.Clin. Invest. (1967) 46(4) : 659-667

28. L.F.Wong, J.C. Cooper and D.W. Margerum
J. Am. Chem. Soc. (1976) 98(23) : 7268-

29. T.P.A. Kruck, S. Lau and B. Sarkar
Can. J. Chem. (1976) 54 : 1300-1308

30. B. Sarkar and Y. Wigfield
Can. J. Biochemistry (1968) 46 : 601-607

31. B. Sarkar
in Transport of Copper, Cha 6 pp.233-281

32. J.A. Bush, J.P. Mahoney, H. Markowitz et al.
J. Clin. Invest. (1955) 34 : 1766

33. S.B. Osborn, C.N. Roberts and J.M. Walshe
Clin. Sci. (1963) 24 : 13

34. P.E. Lipsky
Agents Actions Suppl. (1984) 14 : 181-204

35. L.S. Simon and J.A. Mills
New Engl. J. Med. (1980) 302 : 1179-1185

36. R.A. Sturge, D.B. Yates, D. Gordon et al.
Ann. Rheum. Dis. (1978) 37 : 315-320

37. L.B. Klickstein, C. Shapleigh and E.J. Goetzl
J. Clin. Invest. (1980) 66 : 1166-1170

38. E.M. Davidson, S.A. Roe and M.J.H. Smith
Ann. Rheum. Dis. (1983) 42 : 677-679

39. T. Suwa, H. Urano, Y. Kohno et al.
Agents Actions (1987) 21(1,2) : 167-172

40. M. Dunn
Drugs Suppl. 1 (1987) 33 : 56-66

41. D.S. Goodman
Drugs Suppl. 1 (1987) 33 : 47-55

42. E.P. Abraham, E. Chain, W. Baker and R. Robinson
Nature (1943) 151 : 107

43. M. Freedman
Adv. Exp. Med. Biol. (1976) 86(B) : 649-673

44. M.M. Jones and P.M. May
Inorg. Chim. Acta (1987) 138 : 67-73

45. M. Micheloni, P.M. May and D.R. Williams
J. Inorg. Nucl. Chem. (1978) 40 : 1209-1219

46. M. Martin, N. Sitton, J. Dixon et al. p.631
D.R. Bard, C.G. Knight and D.P. Page-Thomas p.637
Ann. Rheum. Dis. (1982) 41 : 625-642

47. J.R.J. Sorenson
J. Med. Chem. (1976) 19(1) : 135-148

48. E.J. Underwood
"Trace Elements in Human and Animal Nutrition" 3rd Ed.
Academic Press, New York 1971 p.57

49. G.B. West
J. Pharmacol. Meth. (1982) 8 : 33-37

50. D.H. Brown, W.E. Smith, J.W. Teape and A.J. Lewis
J. Med. Chem. (1980) 23 : 729

51. J.R.J. Sorenson
Chemistry in Britain (Dec. 1984) 1110-1113

52. D.O. Harrison, A.E. Underhill, J.K. Fletcher et al.
Polyhedron (1985) 4 : 681

53. R.G. Schlaadt and P.T. Shannon
"Drugs of choice - current perspective on drug use"
Prentice-Hall, Inc. Englewood Cliffs, New Jersey 1982
p.196

54. Multicentre Trial Group
Lancet (1973) 1 : 275

55. W.G.J. Hol
Pure and Appl. Chem. (1987) 59(3) : 431-436

56. G. Arena, G. Kavu and D.R. Williams
J. Inorg. Nucl. Chem. (1978) 40 : 1221-1226

57. L.A. Svensson
Pharm. Weekbld. (1987) 122 : 245-250

58. G.E. Jackson, P.M. May and D.R. Williams
J. Inorg. Nucl. Chem. (1978) 40 : 1227-1234

59. R.Duncan, H.C. Cable, J.B. Lloyd et al.
Makromol. Chem. (1983) 184 : 1997-2008

60. F.M. Belpaire, R.A. Braeckman and M.G. Bogaert
Biochem. Pharmacol. (1984) 33(13) : 2065-2069

61. B. Sarkar, J. Laussac and S. Lau
"Transport Forms of Copper in Human Serum" in
Biological Aspects of Metals and Metal-Related Diseases
ed. by B. Sarkar, Raven Press, New York 1983

62. L. Lambs, M. Brion and G. Berthon
Agents Actions (1984) 14(5,6) : 743-750

63. M.S. Von Wittenau and R. Yeary
J. Amer. Chem. Soc. (1963) 140 : 258

64. T.F. Chin and J.L. Lach
Am. J. Hosp. Pharm. (1975) 32 : 625

65. L.S. Hurley
"Teratogenic Effects of Mn, Zn, and Cu Deficiencies" in
Biological Aspects of Metals and Metal-Related
Diseases. B. Sarkar ed. Raven Press, New York 1983

66. K.S. Rajan and S. Mainer
J. Inorg. Nucl. Chem. (1978) 40 : 2089-2099

67. E. Holtzman
Lysosomes : A Survey. Springer-Verlag, Wien, New York
1976 Cha. IV, pp.153-196

68. M. Kodama and E. Kimura
J. Chem. Soc. Dalton Transactions (1979) 325-329

69. N. Camerman, A. Camerman and B. Sarkar
Can. J. Chem. (1976) 54 : 1309

70. L-W. Wei, M-S. Chao and C-S. Chung
J. Chinese Chem. Soc. (1979) 26 : 145-151

71. M.M. Muir, J.A. Diaz and L. Oyola
Polyhedron (1984) 3(5) : 551-558

72. M.M. Muir and P.R. Rechani
Inorganica Chim. Acta (1974) 11 : 137-142

73. M-C. Lim
Aust. J. Chem. (1982) 35 : 483-488

74. T.D. Smith and A.E. Martell
J. Amer. Chem. Soc. (1972) 94(12) : 4123-4129

75. D.C. Gould and J.S. Mason
Biochemistry (1967) 6(3) : 801

76. K.E. Gilmore and G.K. Pagenkopf
Inorg. Chem. (1985) 24(15) : 2436

77. R.N. Smith, R.J. Motekaitis and A.E. Martell
Inorg. Chem. (1985) 24(8) : 1132-1142

78. L. Fabbrizzi, F. Forlini, A. Peroti and B. Seghi
Inorg. Chem. (1984) 23(7) : 807-813

79. D.C. Weatherburn, E.J. Billo, J.P. Jones and D.W. Margerum
Inorg. Chem. (1970) 9(6) : 1557

80. L. Fabbrizzi, R. Barbucci and P. Paoletti
J. Chem.Soc. Dalton (1972) 1529

81. S-H. Liu and C-S. Chung
Inorg. Chem. (1986) 25(22) : 3890-3896

82. B. Bosnich, R.D. Gillard, E.D. McKenzie and G.A. Webb
J. Chem. Soc. (A) Inorg. Phys. Theor. (1966) : 1331

83. R. Barbucci, L. Fabbrizzi and P. Paoletti
J.Chem.Soc. Dalton (1972) : 745

84. G.E. Jackson, P.M. May and D.R. Williams
J. Inorg. Nucl. Chem. (1981) 43 : 825-829

85. C. Furnival, P.M. May and D.R. Williams
Agents Actions (1981) 8 (Suppl.) : 241-257

86. N.A. Roberts and P.A. Robinson
British J. Rheumatology (1985) 24 : 128-136

87. D. Nicholls
"Complexes and First Row Transition Elements" p.26
The Macmillan Press Ltd., Hong-Kong 1974

88. R.M. Silverstein, C.G. Bassler and T.C. Morrill
"Spectrometric Identification of Organic Compounds" 3rd Edition, John Wiley and Sons, Inc. 1974, USA, p.106

89. L.J. Bellamy
"Advances in Infrared Group Frequencies" Methuen and Co. Ltd., U.K. 1968

90. F.R. Hartley, C. Burgess and R.M. Alcock
"Solution Equilibria", Ellis Horwood Ltd. 1980

91. A. Sabatini, A. Vacca and P. Gans
Talanta 1974, 21 : 53. Inorg. Chim. Acta (1976) 18 : 237

92. I.G. Sayce
Talanta (1968) 15 : 1397

93. K. Murray and P.M. May
"Equilibrium Simulation and Titration Analysis", Version 1.1. Univ. of Wales Institute of Science and Technology, March 1984

94. P.W. Linder, R.G. Torrington and D.R. Williams
"Analysis Using Glass Electrodes", Open University Educational Enterprises, London, 1984

95. J. Bassett, R.C. Denney, G.H. Jeffrey and J. Mendham
"Vogel's Textbook of Quantitative Inorganic Analysis". 4th Edition, Longman, London 1981

96. G. Gran
International Congress on Analytical Chemistry (1952) 77 : 661

97. K. Murray and P.M. May
Talk presented on metal-ligand formation constants by Potentiometric Titrations Compiling Techniques, 5 April 1984 Chelsea College, London

98. C.F. Baes Jr. and R.E. Mesmer
"The Hydrolysis of Cations", John Wiley and Sons, New York 1976

99. J.E. Huheey
"Inorganic Chemistry - Principles of Structure and Reactivity", 2nd Ed., Harper and Row Publishers, New York 1978

100. K. Murray, personal communication

101. L. Sillen and A. Martell
"Stability Constants of Metal-Ion Complexes", Chem. Soc. Spec. Publishers, 1964 and 1971

102. "The Hydrolysis of Cations", ref. 98 p.287

103. H. Irving and R.J.P. Williams
J. Chem. Soc. (1953) 3192

104. H. Sigel and D.B. McCormick
Acc. Chem. Res. (1970) 3 : 201

105. C.F. Bell and K.A.K. Lott
"Modern Approach to Inorganic Chemistry", Butterworth and Co. (Publishers) Ltd., 1966 2nd Ed.

106. J.C. Bailer, H.J. Emeléus et al. (editors)
"Comprehensive Inorganic Chemistry", Vol. 3 Pergamon Press Ltd., 1973, Great Britain

107. P.J. Morris and R.B. Martin
Inorganic Chem. (1971) 10(5) : 964

108. F. Lions and H. Goodwin
J. Amer. Chem. Soc. (1960) 82 : 5013

109. G. Griesser and S. Fallab
Chimia. (1968) 22 : 90

110. R.P. Bohomo, G. Maccarrone, E. Rizzaarelli and M. Vidali
Inorg. Chem. (1987) 26 : 2893-2897

111. Ref. 106, Vol 1

112. R.D. Gillard and H.M. Irving
Chem.Rev. (1965) 65 : 603

113. A.B.P. Lever
"Inorganic Electronic Spectroscopy" 2nd Edition, Elsevier Science Publishers, B.V. Netherlands, 1984 Cha. 6

114. D.W. Urry
Absorption, circular dichroism and optical rotatory dispersion of polypeptides, proteins, prosthetic group and biomembranes. In "Modern Physical Methods in

Biochemistry". A. Neuberger and L.L.M. van Deenen (editors) Elsevier Science Publ. B.V. (Biomedical division) Netherlands, 1985

115. Ref. 113 "Inorganic electronic spectroscopy" Cha. 4

116. B.L. Silver and D. Gertz
J. Chem. Phys. (1974) 61 : 638

117. B. Hathaway, M. Duggan, A. Murphy et al.
Coord. Chem. Reviews (1981) 36 : 267-324

118. F.A. Cotton and G. Wilkonson
Advanced Inorganic Chemistry, Interscience, New York

119. K.E. van Holde
"Physical Biochemistry", Prentice-Hall Inc., New Jersey, 1971 p.161

120. B.J. Hathaway
J. Chem. Soc. Dalton (1976) : 1196

121. D.L. Gardner
"Pathology of Rheumatoid Arthritis" in "Copeman's Textbook of the Rheumatic Diseases", J.T. Scott, Ed. 5th Ed., Churchill Livingstone, Edinburgh, 1979 273-317

122. N. Borregaard, K.S. Johansen and V. Esmann
Biochem. Biophys. Res. Comm. (1979) 90 : 214-219

123. A.L. Lehninger
"Biochemistry", 2nd Edition, Worth Publishers Inc., New York, 1975 p. 503, Cha. 18

124. H.A.O. Hill
"The ambiguous relationship between metals, metalloproteins and dioxygen in biology" in "Biological Aspects of Metal and Metal-related Disease", B. Sarkar (ed), Raven Press, New York, 1983 pp. 15-21

125. R.W. McGilvery and G.W. Goldstein
"Biochemistry - A Functional Approach", W.B. Saunders Co., 1983 Japan, 416-419

126. J.M.C. Gutteridge, S.K. Paterson, A.W. Segal and B. Halliwell
Biochem. J. (1981) 199 : 259-261

127. E.D. Wills
Biochim. Biophys. Acta (1965) 98 : 238-251

128. J.M.C. Gutteridge
Analyt. Biochem. (1977) 82 : 76-82

129 P. Davis
Clinical and Investigative Medicine (1984) 7(1) : 41-44

130 D.D. Perrin and R.P. Agarwal
Multimetal-multiligand equilibrium : a model for biological systems in "Metal ions in biological systems" H. Sigel ed. Marcel Dekker, New York, 1973 Vol 2, pp.167-206

131 M.K. Kim and A.E. Martell
J. Am. Chem. Soc. (1966) 88 : 914

132 G.F. Bryce, R.W. Roeske and F.R.N. Gurd
J. Biol. Chem. (1965) 240 : 3837

133 W.J. Pories, J.H. Henzel, C.G. Rob and W.H. Strain
Lancet (1967) i : 121